

# JCU ePrints

This file is part of the following reference:

**Ann Jacob, Jaiby (2009) *Evolution of the Saxby and Mt. Angelay Igneous Complexes and their role in Cloncurry Fe Oxide-Cu-Au ore genesis*. PhD thesis, James Cook University.**

Access to this file is available from:

<http://eprints.jcu.edu.au/10791>



## Chapter 5: Halogen chemistry of Cloncurry intrusions

### 5.1. Introduction

Volatile elements, in particular fluorine and chlorine, play an important role in magmatic and hydrothermal processes. Minerals that incorporate halogens and crystallize with variable F/Cl ratios are potentially useful indicators of fluid or magma composition if the partitioning behaviour of these elements between minerals and fluids or magmas is known. Halogen variations in hydrous minerals have been used to understand the controls on mineralization in many magmatic or magmatic-hydrothermal systems, most commonly in porphyry environments (e.g., Munoz and Swenson 1981; Selby and Nesbitt 2000) and mafic and ultra mafic complexes (Boudreau et al., 1986; Boudreau 1995).

This chapter discusses the chemistry of hydrous minerals including biotites, amphiboles and apatites and aims to use the halogen abundances and ratios (F/Cl) of minerals from intrusive rocks to determine various magmatic and non magmatic processes that may have influenced the fluid chemistry. Mineral chemical studies are also important to verify the results obtained from field, petrographic and geochemical studies, and are used in comparison with fluid inclusion studies to provide an overall understanding of the role of magmatic fluid evolution and release in IOCG genesis in the Cloncurry District (Chapter 8).

### 5.2. Halogen substitution in minerals

The substitution of halogens into minerals depends on a number of factors including the activity of halogen ion or halogen acid present during crystallization, the cation

population of the mineral structure, the temperature of hydroxyl-halogen exchange, and the effects, if any, of post-crystallization leaching or enrichment due to hydrothermal fluids or groundwater. In igneous intrusions, amphiboles, apatites and micas form the common mineral residences for halogens, especially fluorine and chlorine, by replacing hydroxyl anions.

A model equation of exchange equilibrium between a mineral and either a silicate melt or aqueous fluid phase was presented by Munoz (1984) using micas:



where X stands for either F or Cl.

The equilibrium for the exchange may thus be expressed:

$$\log K = \log (a_X / a_{\text{OH}}) + \log (a_{\text{H}_2\text{O}} / a_{\text{HX}}) \quad (2),$$

where  $a_x$  and  $a_{\text{OH}}$  are the activities of halogen and hydroxyl components present in mica solid solution and  $a_{\text{H}_2\text{O}}$  and  $a_{\text{HX}}$  are the activities of  $\text{H}_2\text{O}$  and HF or HCl present in the magma or fluid.

By assuming a standard state of pure  $\text{H}_2\text{O}$  and HX, respectively at 1 bar and the temperature of interest, the fluid activities may be replaced by fugacities. Then the equilibrium expression is now written as:

$$\log K = \log (X_X / X_{\text{OH}})_{\text{mica}} + \log (a_{\text{H}_2\text{O}} / a_{\text{HX}}) \quad (3),$$

where  $X_X$  and  $X_{OH}$  are mole fractions of F or Cl, and OH. If the equilibrium constant is known, it is possible to use the analysed halogen / hydroxyl ratio in the mica to calculate the fugacity ratio of  $H_2O$  to halogen acid which prevailed during the exchange. It is important to remember that these exchange equations cannot define an absolute activity or fugacity of halogen acid, but only a ratio relative to  $H_2O$ . The equilibrium constant for equation 1 is strongly dependent on the composition of the mica, and especially on the cationic occupancy of the octahedral sheet.

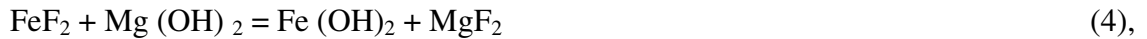
The activities of HF and HCl do not directly reflect the total fluoride and chloride contents of the aqueous fluids: however,  $a_{HF}$  may be a reliable monitor of total fluid F content because, in felsic magmatic systems most of the F present is complexed as HF (speciation calculations of Zhu and Sverjensky 1991; Piccoli et al. 1999). Conversely, Cl speciation in aqueous fluids is much more complex, and  $a_{HCl}$  cannot be equated with total fluid chlorinity. For melts, these activities are also related to magma compositional variation even if the melt is under-saturated with respect to aqueous volatiles. Partition coefficients between melt, minerals and co-existing aqueous phase are poorly known, however, which restricts the level to which the interplay between these can be understood from mineral chemistry alone.

### *5.2.1. Avoidance effects & Intercept values*

The coupled substitution reactions may introduce substantial mineral compositional variations that do not directly reflect fluid chemistry. Hydroxyl bearing ferromagnesian silicate minerals with high Mg/Fe ratios tend to incorporate more F than comparable minerals with lower Mg/Fe ratios. Minerals enriched in Fe show relatively low F contents, commonly referred to as Fe-F avoidance. Similarly minerals with high Mg

contents commonly are poor in Cl ions and this is known as Mg-Cl avoidance. These effects are very common in amphiboles and biotites of varying Mg / Fe ratios.

Ramberg (1952) explained Fe-F avoidance in silicates in terms of the strongly exothermic model reaction:



The equilibrium constant for the reaction is very positive -log k is 9.57 at 298K (Wagman et al., 1982) which attests to the preference of Fe-OH bonds over Fe-F bonds.

F and Cl intercept values were defined by Munoz (1984), which are single numerical values that expresses the relative degree of F and Cl enrichment in a mica. Because of Fe-F and Mg-Cl avoidance, the wt% F and Cl by themselves are inadequate measures of relative enrichment except for micas of very similar Mg / Fe ratio. He defined a fluorine intercept value for biotite as:

$$\text{IV}(\text{F})_{\text{bio}} = 1.52 X_{\text{Mg}} + 0.42 X_{\text{An}} + 0.20 X_{\text{Sid}} - \log(X_{\text{F}} / X_{\text{OH}}) \quad (5),$$

where  $X_{\text{Mg}} = \text{Mg}/(\text{Mg}+\text{Fe})$ ;  $X_{\text{Sid}} = [(3-\text{Si}/\text{Al})/1.75] (1-X_{\text{Mg}})$ ;  $X_{\text{An}} = 1-(X_{\text{Mg}}+X_{\text{Sid}})$ ; and  $X_{\text{F}}$  and  $X_{\text{OH}}$  are mole fractions of F and OH, respectively, on the hydroxyl site.

Because the Cl content in micas is commonly less than the F content, less information is available about Cl=OH exchange. If the model halogen exchange reaction is written in terms of Cl,



and the equilibrium constant calculated from thermodynamic data (Munoz, 1984) is very negative ( $\log k = -10.1$  at 298.15K), indicating that Fe-Cl bonds should be strongly preferred over Mg-Cl bonds. Mg-Cl avoidance has been confirmed in many natural biotite analyses. The Cl intercept value is defined as:

$$IV (Cl) = -5.01 - 1.93 X_{Mg} - \log (X_{Cl} / X_{OH}) \quad (7),$$

and is conceptually similar to IV (F).

The smaller intercept values correlate with higher degrees of F or Cl enrichment in the coexisting fluid, for a given Mg content. The IV (F) of most natural biotites range from about 3.0 to near 0 and IV (Cl) varies from -3 to around -4.5.

The F/Cl intercept value is defined as:

$$IV (F/Cl) = IV (F) - IV (Cl) \quad (8)$$

Because the OH is omitted, calculation of IV (F/Cl) is not affected by uncertainties in OH occupancy, which is difficult to determine for biotite. Thus values of IV (F/Cl) are likely to be more accurate than either IV (F) or IV (Cl). If the temperature of halogen=OH exchange is known, then the IV (F/Cl) intercept values can be used as a quantitative measure of the ratio of halogen acid activity.

Zhu and Sverjensky (1991, 1992) have calculated the HCl/HF activity ratios for biotite and apatite in magmatic volatile-bearing aqueous fluids by assuming ideal mixing of OH-, Cl-, and F-components. This internally consistent thermodynamic database is used in this thesis to determine and isolate the crystal chemical controls, and then to

retrieve information on magmatic or fluid halogen proportions from mineral chemical analyses.

### 5.3. Samples and methodology

A total of 39 alteration-free (chlorite-poor) samples were collected from various parts of the Saxby (SIC) and Mt. Angelay (MAIC) Igneous Complexes, including granites, syenodiorites and gabbros. Polished thin sections were studied in both transmitted and reflected light.

Mineral chemical analyses were carried out at the Advanced Analytical Centre, James Cook University, using a JEOL JXA 8200 electron probe micro-analyzer with wavelength dispersive collector (WDS). Mineral compositions were determined for majority of the minerals, but the analyses were particularly focused on primary amphiboles, biotite and apatite as they have the potential to track halogens. Standard operating conditions included an accelerating potential of 15kV and a beam current of 20nA with 1-5 $\mu$  beam diameter. Single element spectra were used to carry out overlap corrections utilizing mineral and synthetic standards, and were cross checked against international and in-house standards run prior to each session. The standards were different for silicate (amphiboles and biotite) and apatite analyses and the element matrix corrections were made using Armstrong and ZAF Scientific software respectively. The average detection limit for Cl is 100ppm and that of F is 500ppm, however it can vary in each analysis depending on the matrix effects. The structural formulae were calculated assuming all Fe as Fe<sup>2+</sup>.

The fluid activity ratios of Cl and F from biotite compositions were calculated by the thermodynamic database developed by Zhu and Sverjensky (1991, 1992) using the spread sheet developed by Coulson et al. (2001), in which the intrusions were assumed to be emplaced and crystallized at ~2kbar pressure. Three different biotite crystallization temperatures including 850°C, 750°C and 650°C were used for fluid activity calculation; however the results were approximately the same and 850°C was used for the interpretation purpose, on the basis that most hydrous minerals grew towards the end of crystallisation of mafic to intermediate magmas. Crystallization conditions and assumptions used for various calculations and their details are discussed by Coulson et al. (2001), and are similar to (although slightly lower pressure than) conditions of emplacement of Cloncurry intrusions. Halogen contents of amphiboles are controlled by their composition in a more complex manner than biotite (Morrison, 1991) and so the activities of halogens in the fluid in equilibrium with amphiboles could not be calculated in the absence of biotite (Zhu and Sverjensky, 1992). Apatite fluid activity ratios were not calculated, but the chlorine and fluorine contents of apatites mimic the trends in biotite and amphibole (see below).

Halogen contents of whole rocks were determined by Quantitative X-ray Fluorescence Spectrometry (XRF). The pressed powder fillets were prepared from approximately 6.5grams of unignited sample, which was mixed with 4-5 drops of ethyl cellulose. This was then pressed into a pellet in an Aluminium cup of 32mm diameter. The specimens were analysed in a Bruker-AXS S4 Pioneer XRF Spectrometer and the data collected from various scan ranges are processed through Bruker-AXS Spectra-plus Software. The check standard used for halogen analysis is FSL.



## 5.4. Results

### 5.4.1. *Chemistry of minerals*

The halogen content of hydrous minerals varies partly as a function of the coexisting mineral assemblage, so all the main minerals in each intrusive rock were analysed along with the halogen-bearing ones. The common primary mineral phases of the SIC and MAIC include plagioclase, hornblende, biotite, clinopyroxene, alkali feldspar, quartz, apatite and magnetite. These minerals differ in their relative abundances, growth textures and compositions in various rocks. Detailed petrographic descriptions and relationships between minerals in each rock types are provided in Chapter 3. The results of various mineral analyses are tabulated in Appendix 4, in addition to the data and figures presented here.

#### 5.4.1.1. **Plagioclase**

Plagioclase is a major mineral constituent in all the intrusive suits of the SIC and MAIC (see chapter 3). Primary plagioclases from different intrusions show significant variations in chemistry. In felsic and intermediate intrusions, plagioclases show homogenous composition and are exclusively oligoclase ( $An_{12-26}$ ) (Table 5.1; Fig. 5.2A). They mostly contain 2.2-5.7 wt % CaO, 6.8-10.6 wt %  $Na_2O$ , and very low  $K_2O$  (0.1-0.3 wt %). Zoned crystals with Ca-rich cores and Ca-poor rims were rarely observed in intermediate intrusions. In mafic intrusions, the variation in percent anorthite is very large with values ranging from oligoclase to anorthite ( $An_{12}$  to  $An_{100}$ ) and occasional zoned plagioclases were also present. The cores of zoned crystals are commonly andesine and the rims are oligoclase. In altered rocks, the secondary plagioclase is albite ( $An_{0-10}$ ) (Fig. 5.2B) and many minerals show albite replacement. Representative analyses of plagioclases are provided in Table 5.1.

<i>Location</i>	SIC	SIC	SIC	MAIC	MAIC	MAIC
<i>Rock type</i>	Mafic	Intermediate	Felsic	Mafic	Intermediate	Intermediate
<i>Sample</i>	JB 12	JB 82C	JB 81	JB 63	JB 6C	JB 60C
<i>Origin</i>	Primary	Primary	Primary	Primary	Primary	Secondary
<i>Plag type</i>	Anorthite	Oligoclase	Oligoclase	Andesine	Oligoclase	Albite
<i>No.</i>	36	7	59	83	126	91
<i>Oxide wt%</i>						
<i>SiO<sub>2</sub></i>	43.90	66.43	66.91	61.15	66.27	74.16
<i>TiO<sub>2</sub></i>	0.10	0.00	0.00	0.05	0.09	0.01
<i>Al<sub>2</sub>O<sub>3</sub></i>	22.08	23.63	22.70	25.73	22.97	20.80
<i>FeO</i>	2.64	0.08	0.08	0.09	0.07	0.05
<i>MnO</i>	0.01	0.02	0.00	0.02	0.00	0.00
<i>MgO</i>	0.02	0.02	0.00	0.00	0.00	0.00
<i>CaO</i>	26.28	4.62	3.44	7.16	3.94	0.10
<i>Na<sub>2</sub>O</i>	0.04	8.16	10.02	7.55	9.28	10.63
<i>K<sub>2</sub>O</i>	0.02	0.10	0.10	0.26	0.21	0.05
<i>Cl</i>	0.02	0.00	0.00	0.00	0.00	0.00
<i>F</i>	0.00	0.00	0.05	0.00	0.00	0.04
<i>Total</i>	95.11	103.05	103.30	102.01	102.83	105.84
<i>Cations based on 32 Oxygens</i>						
<i>Si</i>	8.92	11.33	11.42	10.69	11.36	12.13
<i>Ti</i>	0.02	0.00	0.00	0.01	0.01	0.00
<i>Al</i>	5.29	4.75	4.57	5.30	4.64	4.01
<i>Fe</i>	0.45	0.01	0.01	0.01	0.01	0.01
<i>Mn</i>	0.00	0.00	0.00	0.00	0.00	0.00
<i>Mg</i>	0.01	0.00	0.00	0.00	0.00	0.00
<i>Ca</i>	5.72	0.84	0.63	1.34	0.72	0.02
<i>Na</i>	0.02	2.70	3.32	2.56	3.08	3.37
<i>K</i>	0.01	0.02	0.02	0.06	0.05	0.01
<i>Cl</i>	0.01	0.00	0.00	0.00	0.00	0.00
<i>F</i>	0.00	0.00	0.03	0.00	0.00	0.02
<i>Total</i>	20.43	19.66	19.97	19.96	19.87	19.55
<i>Ab</i>	0.26	75.72	83.58	64.67	80.01	99.22
<i>An</i>	99.63	23.69	15.86	33.89	18.77	0.50
<i>Or</i>	0.11	0.59	0.56	1.45	1.21	0.28

*Table 5.1: Representative plagioclase analyses from various intrusions of the Saxby and Mt. Angelay Igneous Complexes. The whole data is in Appendix 4.4.*

#### **5.4.1.2. Pyroxene**

Petrographically, pyroxene was typically the earliest ferromagnesian silicate to crystallize and is commonly observed in rocks with < 64 wt % SiO<sub>2</sub> (see chapter 3) (Fig. 5.2A). Pyroxene compositional fields of the SIC and MAIC intrusions are shown in Fig.5.3A and representative analyses are listed in Table 5.2. All pyroxenes are augite and/or diopsidic augite. In most analyses, the CaO contents of clinopyroxenes range from 20 to 23 wt% and the X<sub>Mg</sub> values vary from 0.71 to 0.79. The halogen (F and Cl) contents of clinopyroxenes are negligible, varying from 0 to 0.01wt%, and do not show any significant variation relative to other ferromagnesian minerals like hornblende and biotite.

#### **5.4.1.3. Amphibole**

Amphibole is present in most of the SIC and MAIC intrusions (see chapter 3) and is divided into magnesio-hornblende and tschermakite according to the classification of Leake et al (1997) (Fig.5.3B & Table 5.3). Tschermakite is typically observed in the gabbros and magnesio-hornblende in the more evolved intrusions (Fig. 5.2C). The X<sub>Mg</sub> values of amphiboles within the SIC and MAIC rocks commonly range from 0.53 to 0.78. Secondary amphiboles are also observed in many intrusions, especially those from the mixing-mingling zones (SIC) and magmatic-hydrothermal transition zones (MAIC), and are typically actinolite (Fig. 5.2D & E; 5.3B). Fluorine and chlorine contents of primary amphiboles vary from 0.1 to 1.1 wt% and they show several different trends (see below).

<i>Location</i>	SIC	SIC	SIC	MAIC	MAIC
<i>Rock type</i>	Mafic	Mafic	Mafic	Mafic	Mafic
<i>Sample</i>	JB 1	JB 12B	JB 35F	JB 60A	JB 60B
<i>No.</i>	5	24	27	7	85
<i>Oxide wt%</i>					
<i>SiO<sub>2</sub></i>	55.74	54.23	52.88	53.73	53.5
<i>TiO<sub>2</sub></i>	0.0429	0.0953	0.0853	0.1115	0.0074
<i>Al<sub>2</sub>O<sub>3</sub></i>	0.6595	0.4199	1.0221	0.8555	0.8273
<i>FeO</i>	6.86	8.33	8.24	9	7.46
<i>MnO</i>	0.3317	0.4206	0.3892	0.3603	0.2584
<i>MgO</i>	14.15	13.97	13.51	14.2	13.93
<i>CaO</i>	22.48	23.08	23.14	21.75	23.59
<i>Na<sub>2</sub>O</i>	0.5716	0.3839	0.5691	0.5076	0.598
<i>K<sub>2</sub>O</i>	0.0958	0	0.0067	0.0127	0.0109
<i>Cl</i>	0.0108	0.0036	0.0055	0	0.0089
<i>F</i>	0	0	0	0.0234	0.042
<i>Total</i>	100.942	100.933	99.848	100.550	100.233
<i>Cations based on 6 oxygens</i>					
<i>Si</i>	2.03	2.00	1.98	1.99	1.99
<i>Ti</i>	0.00	0.00	0.00	0.00	0.00
<i>Al</i>	0.03	0.02	0.05	0.04	0.04
<i>Fe</i>	0.21	0.26	0.26	0.28	0.23
<i>Mn</i>	0.01	0.01	0.01	0.01	0.01
<i>Mg</i>	0.77	0.77	0.75	0.78	0.77
<i>Ca</i>	0.88	0.91	0.93	0.86	0.94
<i>Na</i>	0.04	0.03	0.04	0.04	0.04
<i>K</i>	0.00	0.00	0.00	0.00	0.00
<i>Cl</i>	0.00	0.00	0.00	0.00	0.00
<i>F</i>	0.00	0.00	0.00	0.00	0.00
<i>Total</i>	3.97	4.00	4.02	4.01	4.02
<i>Mg#</i>	0.79	0.75	0.75	0.74	0.77

*Table 5.2: Representative clinopyroxene analyses from various intrusions of the Saxby and Mt. Angelay Igneous Complexes. The whole data is in Appendix 4.5.*

<i>Location</i>	SIC	SIC	SIC	SIC	MAIC	MAIC
<i>Rock type</i>	Mafic	Mafic	Intermediate	Felsic	Mafic	Intermediate
<i>Sample</i>	JB 81	JB 82A	JB 1	JB 35F	JB 63	JB 8B
<i>No.</i>	48	201	1	1	1	1
<i>Oxide wt%</i>						
<i>SiO<sub>2</sub></i>	47.80	45.80	42.01	43.84	44.81	44.37
<i>TiO<sub>2</sub></i>	0.30	0.19	3.05	1.09	2.11	1.17
<i>Al<sub>2</sub>O<sub>3</sub></i>	6.66	8.15	10.84	9.00	8.35	7.87
<i>FeO</i>	15.82	17.66	14.33	16.91	18.52	20.61
<i>MnO</i>	0.21	0.15	0.17	0.29	0.34	0.29
<i>MgO</i>	12.63	11.42	12.17	12.01	10.48	9.01
<i>CaO</i>	11.65	11.78	11.26	10.81	11.48	11.00
<i>Na<sub>2</sub>O</i>	1.52	1.54	2.55	1.08	2.03	2.11
<i>K<sub>2</sub>O</i>	0.40	1.06	1.41	1.13	1.15	1.22
<i>Cl</i>	0.19	0.23	0.42	0.66	0.48	0.45
<i>F</i>	0.60	0.31	0.22	0.10	0.17	0.30
<i>Total</i>	97.78	98.30	98.43	96.92	99.92	98.41
<i>Cations based on 23 Oxygens</i>						
<i>Si</i>	7.06	6.81	6.24	6.56	6.64	6.74
<i>Ti</i>	0.03	0.02	0.34	0.12	0.24	0.13
<i>Al</i>	1.16	1.43	1.90	1.59	1.46	1.41
<i>Fe<sup>3+</sup></i>	0.39	0.45	0.28	0.65	0.28	0.30
<i>Fe<sup>2+</sup></i>	1.56	1.75	1.50	1.47	2.02	2.32
<i>Mn</i>	0.03	0.02	0.02	0.04	0.04	0.04
<i>Mg</i>	2.78	2.53	2.70	2.68	2.31	2.04
<i>Ca</i>	1.84	1.88	1.79	1.73	1.82	1.79
<i>Na</i>	0.44	0.44	0.73	0.31	0.58	0.62
<i>K</i>	0.08	0.20	0.27	0.22	0.22	0.24
<i>Cl</i>	0.05	0.06	0.11	0.17	0.12	0.12
<i>F</i>	0.28	0.15	0.10	0.05	0.08	0.14
<i>Total</i>	15.70	15.73	15.99	15.59	15.80	15.90
<i>XMg</i>	0.64	0.59	0.64	0.65	0.53	0.47
<i>XFe</i>	0.36	0.41	0.36	0.35	0.47	0.53

*Table 5.3: Representative amphibole analyses from various intrusions of the Saxby and Mt. Angelay Igneous Complexes. The whole data is in Appendix 4.1.*

#### **5.4.1.4. Biotite**

Biotite occurs as a mid to late-stage crystallization product in the intrusive rocks of the SIC and MAIC, forming discrete grains, but also commonly as a replacement of amphibole (see chapter 3) (Fig. 5.1A & B). They were analysed from a variety of rock types including mafic, felsic and intermediate intrusive rocks, and some metasediments. The  $X_{Mg}$  values of biotites from intrusive rocks range from 0.55 to 0.71 (Table 5.4) with the highest values being typically associated with the gabbros. The  $Al_2O_3$  contents of biotite are enriched with progressive magma evolution towards felsic compositions, and the  $TiO_2$  and  $MgO$  contents are depleted (Table 5.4). Biotite halogen contents also show variation with magma evolution in which the Cl decreases and F increases with increasing rock silica content. Representative biotite analyses from various rock types are listed in Table 5.4.

#### **5.4.1.5. Apatite**

Apatite is commonly observed as inclusions in amphibole and biotite from the mafic and intermediate intrusions, but is also seen associated with late crystallizing phases such as quartz (see chapter 3) (Fig.5.2C; 5.1C). Representative apatite analyses are tabulated in Table 5.5. Both zoned and unzoned apatite grains were observed. All apatites analysed are fluorapatite ( $F / (F+Cl) > 0.5$ ) (see below), which is typical of igneous apatite (Nash, 1984). Of the minor elements in apatite,  $Na_2O$ ,  $FeO$  and  $MnO$  range from 0 to 0.5 wt% and  $SrO$  ranges up to 0.2 wt%.  $As_2O_5$  contents are mostly between 0 and 0.06 wt% and  $SO_3$  values from 0.02 to 0.9 wt%.

<i>Location</i>	SIC	SIC	SIC	SIC	MAIC	MAIC
<i>Rock type</i>	Mafic	Mafic	Intermediate	Felsic	Mafic	Intermediate
<i>Sample</i>	JB 1	JB 35F	JB 82A	JB 15	JB 63	JB 8B
<i>No.</i>	1	1	199	1	1	1
<i>Oxide wt%</i>						
<i>SiO<sub>2</sub></i>	38.18	36.58	38.19	34.10	9.74	9.73
<i>TiO<sub>2</sub></i>	3.54	3.96	0.59	1.68	4.31	1.71
<i>Al<sub>2</sub>O<sub>3</sub></i>	13.47	13.42	13.78	16.33	0.04	0.03
<i>FeO</i>	14.01	17.02	18.41	27.93	37.24	37.41
<i>MnO</i>	0.08	0.12	0.10	0.26	13.51	12.62
<i>MgO</i>	16.25	13.27	12.58	3.74	0.16	0.06
<i>CaO</i>	0.01	0.01	0.09	0.07	0.13	0.12
<i>Na<sub>2</sub>O</i>	0.19	0.10	0.09	0.07	18.49	18.75
<i>K<sub>2</sub>O</i>	9.77	9.87	9.73	8.11	12.80	12.60
<i>Cl</i>	0.51	0.74	0.32	0.43	0.81	0.54
<i>F</i>	0.42	0.38	0.56	0.05	0.23	1.08
<i>Total</i>	96.43	95.46	94.43	92.78	97.46	94.65
<i>Cations based on 11 oxygens</i>						
<i>Si</i>	2.83	2.79	2.95	2.79	2.79	2.92
<i>Ti</i>	0.20	0.23	0.03	0.10	0.24	0.10
<i>Al</i>	1.18	1.21	1.25	1.57	1.19	1.16
<i>Fe</i>	0.87	1.09	1.19	1.91	1.16	1.22
<i>Mn</i>	0.01	0.01	0.01	0.02	0.01	0.00
<i>Mg</i>	1.80	1.51	1.45	0.46	1.43	1.47
<i>Ca</i>	0.00	0.00	0.01	0.01	0.00	0.00
<i>Na</i>	0.03	0.02	0.01	0.01	0.02	0.02
<i>K</i>	0.92	0.96	0.96	0.85	0.93	0.97
<i>Cl</i>	0.06	0.10	0.04	0.06	0.10	0.07
<i>F</i>	0.10	0.09	0.14	0.01	0.05	0.27
<i>Total</i>	7.89	7.91	7.90	7.78	7.89	7.93
<i>XMg</i>	0.67	0.58	0.55	0.19	0.55	0.55
<i>XFe</i>	0.33	0.42	0.45	0.81	0.45	0.45

*Table 5.4: Representative biotite analyses from various intrusions of the Saxby and Mt. Angelay Igneous Complexes. The whole data is in Appendix 4.2.*

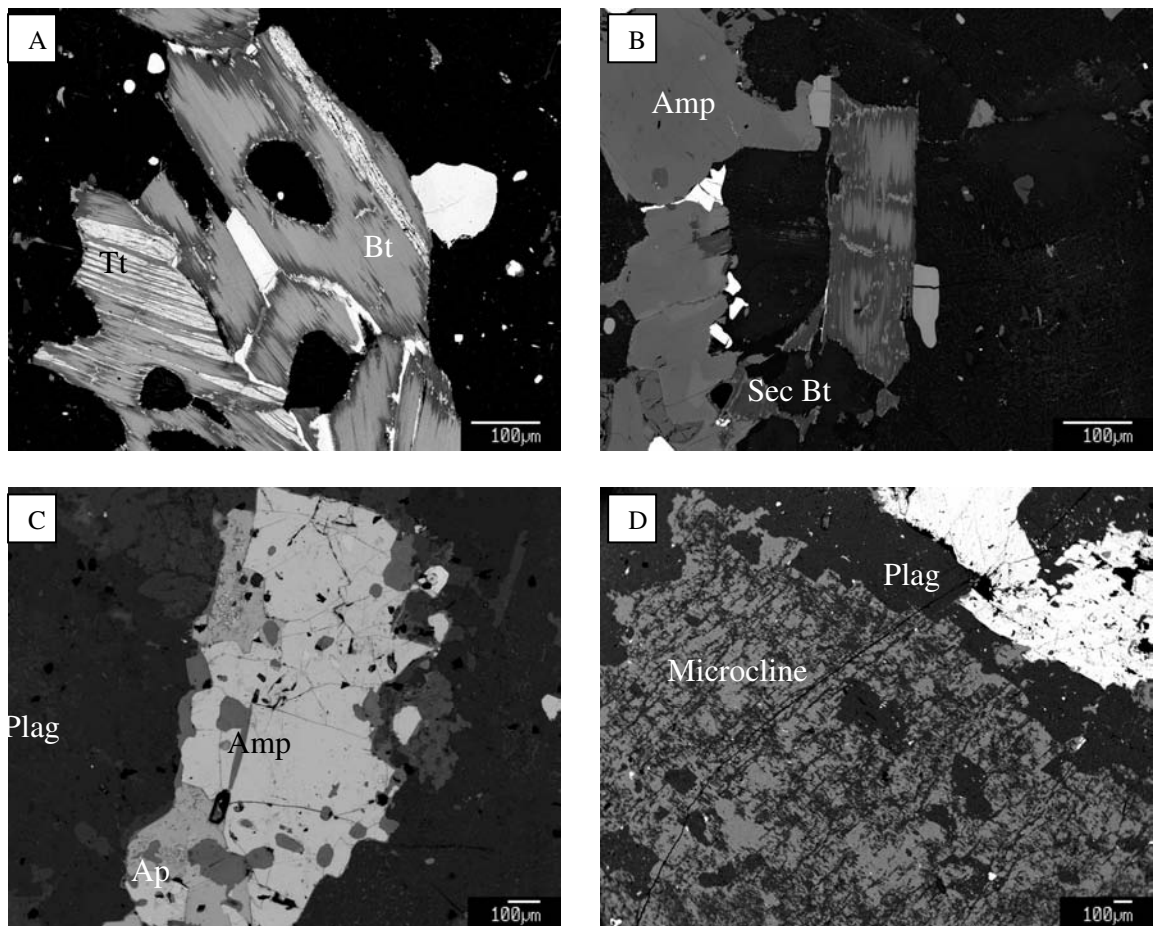
<i>Location</i>	SIC	SIC	SIC	MAIC	MAIC
<i>Rock type</i>	Mafic	Mafic	Intermediate	Intermediate	Intermediate
<i>Sample</i>	JB 1	JB 35F	JB 82C	JB 8B	JB 60C
<i>No.</i>	5	97	45	13	90
<b>Oxide wt%</b>					
<i>P2O5</i>	38.147	40.161	41.011	38.173	37.21
<i>CaO</i>	54.854	56.308	57.137	55.599	52.572
<i>SiO2</i>	0.171	0.269	0.112	0.299	0.238
<i>SrO</i>	0.128	0.073	0.051	0.06	0.022
<i>Ce2O3</i>	0.551	0.097	0.097	0.404	0.432
<i>FeO</i>	0.164	0.058	0.147	0.144	0.143
<i>MnO</i>	0.071	0.043	0.064	0.037	0.064
<i>SO3</i>	0.119	0.192	0.114	0.068	0.003
<i>As2O5</i>	0.019	0.015	0	0	0
<i>Na2O</i>	0.117	0	0	0	0
<i>Cl</i>	2.254	0.434	0.186	0.205	0.531
<i>F</i>	2.412	3.403	3.741	4.061	3.988
<b>Total</b>	97.482	99.522	101.043	97.294	93.404
<b>Cations based on 25 oxygens</b>					
<i>P</i>	6.281	6.359	6.383	6.221	6.280
<i>Ca</i>	8.922	8.807	8.784	8.950	8.765
<i>Si</i>	0.033	0.050	0.021	0.058	0.047
<i>Sr</i>	0.014	0.008	0.005	0.007	0.003
<i>Ce</i>	0.039	0.007	0.007	0.028	0.032
<i>Fe</i>	0.034	0.012	0.029	0.030	0.031
<i>Mn</i>	0.012	0.007	0.010	0.006	0.011
<i>S</i>	0.017	0.027	0.016	0.010	0.000
<i>As</i>	0.002	0.001	0	0	0
<i>Na</i>	0.018	0	0	0	0
<i>Cl</i>	0.743	0.138	0.058	0.067	0.179
<i>F</i>	1.484	2.013	2.175	2.472	2.514
<b>Total</b>	17.601	17.427	17.487	17.847	17.862

**Table 5.5:** Representative apatite analyses from various intrusions of the Saxby and Mt. Angelay Igneous Complexes. The whole data is in Appendix 4.3.

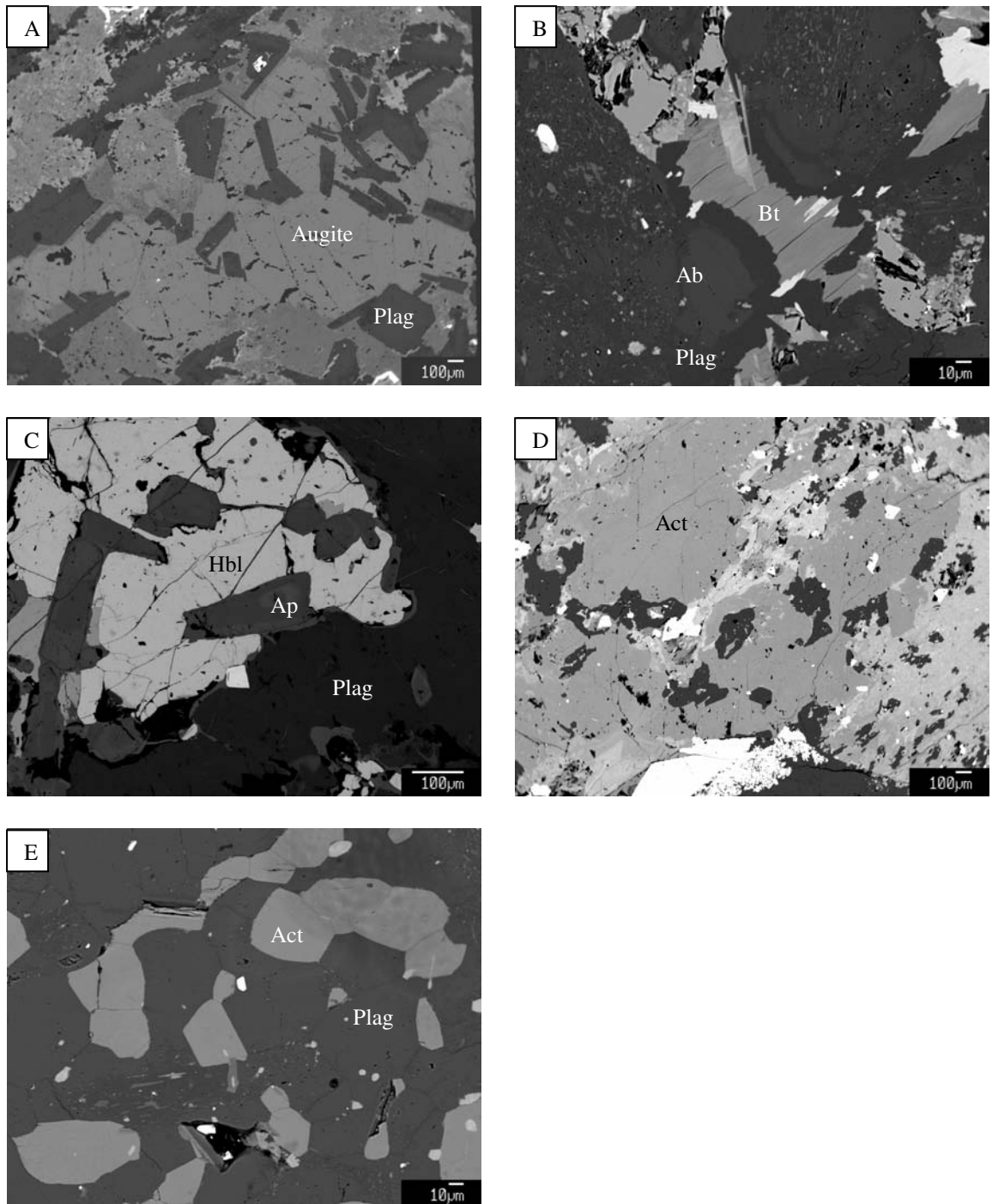


#### 5.4.1.6. Other minerals

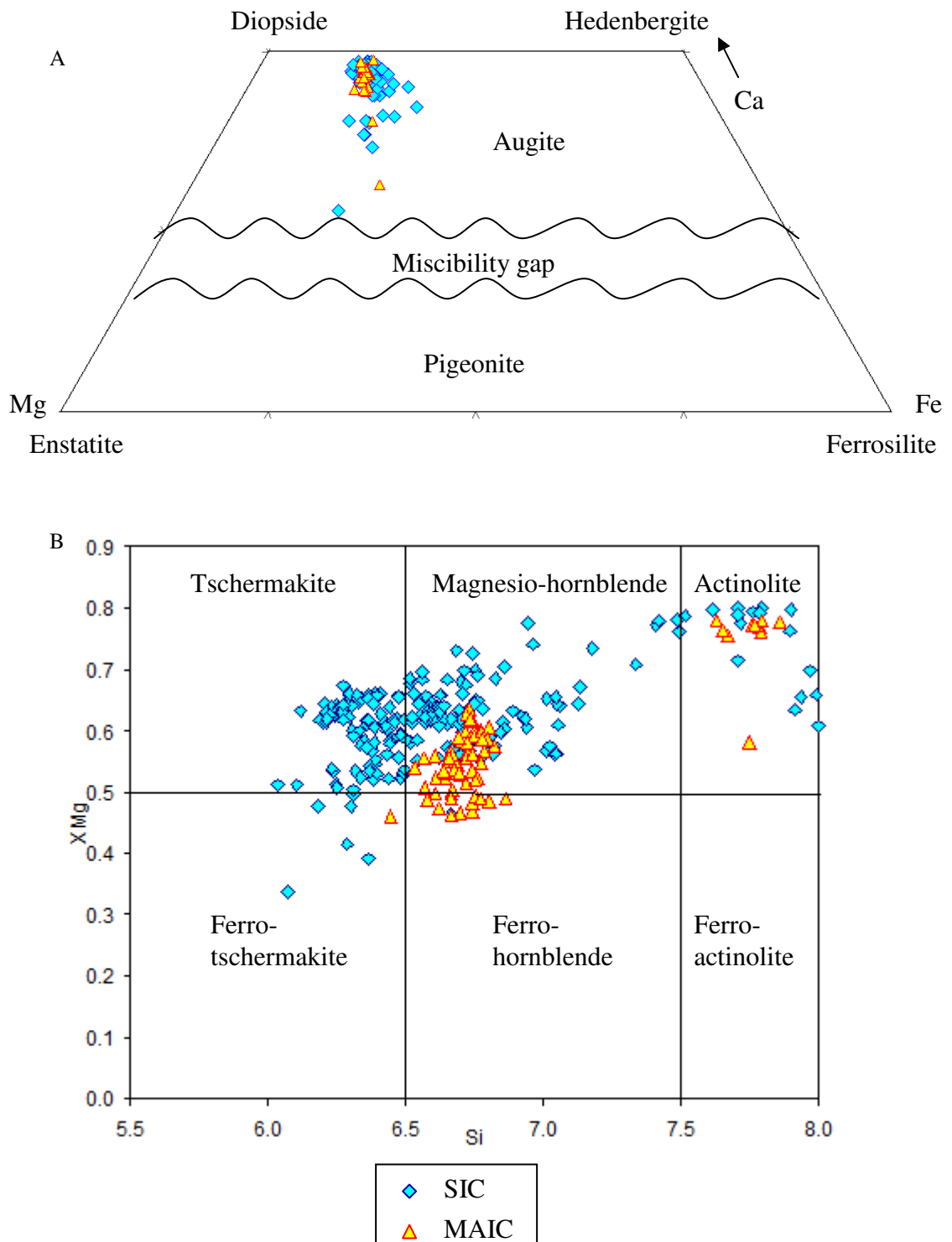
A number of other minerals including K-feldspar, quartz, magnetite, titanite and chlorite were also analysed, K-feldspar and quartz being abundant in felsic intrusions (see chapter 3). The  $Al_2O_3$  and  $K_2O$  contents of feldspars vary from 18 to 19 wt% and 14 to 17 wt% respectively. K-feldspar analyses show compositions including both microcline and orthoclase; however the most abundant feldspar is microcline (Fig. 5.1D). Quartz contains no detectable impurities using the electron microprobe.



**Figure 5.1A:** Back-scattered electron (BSE) photomicrograph of primary biotite-Sample JB 37D; **5.1B:** Back-scattered electron (BSE) photomicrograph of biotite alteration in amphibole-Sample JB 37D; **5.1C:** Back-scattered electron (BSE) photomicrograph of apatite inclusions in amphibole-Sample JB 6C; **5.1D:** Back-scattered electron (BSE) photomicrograph of Microcline-Sample JB 60C.



**Figure 5.2A:** Back-scattered electron (BSE) photomicrograph of primary plagioclases showing ophitic intergrowth with augite-Sample JB 68; **5.2B:** Back-scattered electron (BSE) photomicrograph of secondary albite replacement-Sample JB 37B; **5.2C:** Back-scattered electron (BSE) photomicrograph of primary amphibole grain with zoned apatites in it-Sample-JB 6C; **5.2D:** Back-scattered electron (BSE) photomicrograph of secondary actinolite of hydrothermal origin-Sample JB 64B; **5.2E:** Back-scattered electron (BSE) photomicrograph of actinolite with recrystallized boundaries. Sample collected from magma mixing-mingling zone, SIC-Sample JB 37C/M.



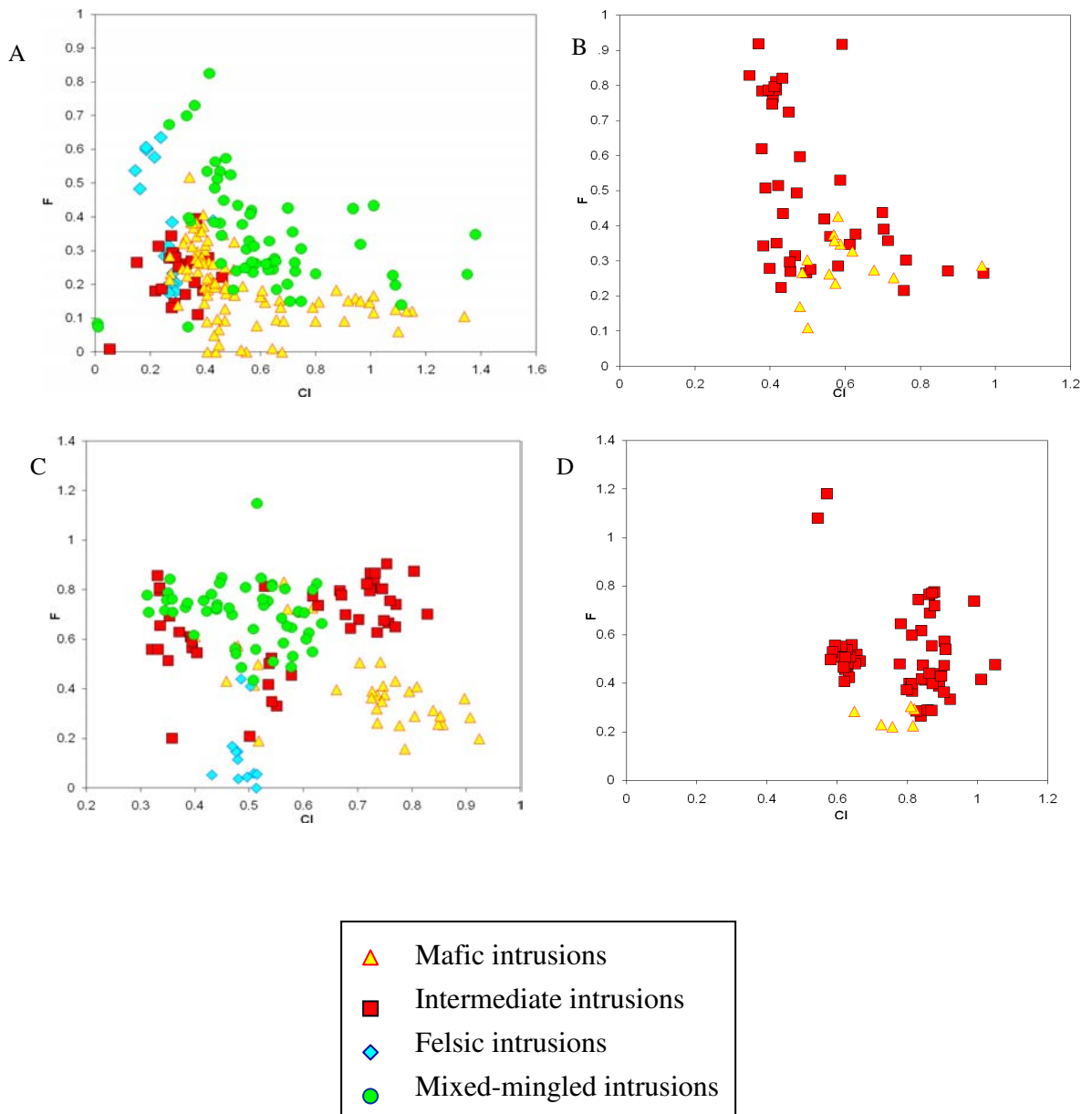
**Figure 5.3A:** Pyroxene compositions for the mafic and intermediate samples from the SIC and MAIC plotted on the pyroxene quadrilateral with respect to Ca-Mg-Fe. The pyroxene compositions vary from augite to diopsidic augite; **5.3B:** Variation in the amphibole compositions for the SIC and MAIC intrusions (Leake et al., 1997). Primary amphiboles are Magnesian-hornblende and Tschermakite, and secondary amphiboles are actinolite. The whole data sets are available at Appendix 4.1 & 4.5.

#### *5.4.2. Halogen variations in minerals of Saxby and Mt. Angelay intrusions*

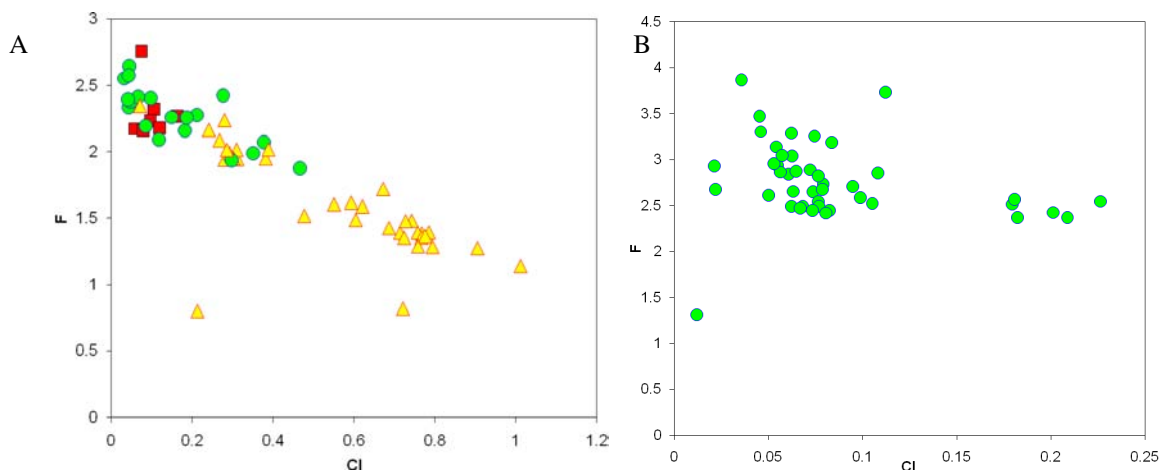
Fluorine and chlorine contents of primary amphiboles, biotites and apatites vary in a systematic manner, and biotite and amphibole F-and Cl-contents tend to be uniformly lower than apatites. The amphiboles display a range in F (0 to 0.9 wt %) and Cl (0.1 to 1.3 wt %), with high Cl (0.3 to 1.3 wt %) and low F (0 to 0.5 wt %) contents in mafic rocks (Fig: 5.4A & B). The intermediate rocks show amphibole Cl values ranging from 0.3 to 1 wt% and F from 0.2 to 0.9 wt%. Amphiboles from felsic rocks show distinct Cl (0.1 to 0.2 wt %) and F (0.5 to 0.6 wt %) values, with F/Cl ratios apparently different from the mafic and intermediate trends (Fig. 5.4A). Scattered patterns of F versus Cl in amphibole are obtained from the magma mixed-mingled rocks of the SIC (Fig. 5.4A), which show large variations in the F and Cl contents.

Chlorine concentrations of biotites in mafic rocks show values ranging from approximately 0.4 to 0.9 wt % and fluorine values vary between 0.2 and 0.8 wt % (Fig.5.4C & D). Similar to trends shown by amphibole and apatite halogen contents (see below), the Cl in biotites decreases and F increases from mafic to intermediate rocks. Felsic intrusions show strictly different trends from mafic and intermediate rocks with a large variation in biotite F (0-0.4 wt %) for approximately fixed Cl (0.4-0.5 wt %). The halogen patterns in biotites from mixed-mingled rocks are scattered.

Unlike amphiboles and biotites, apatites show more restricted halogen trends which commonly follow a linear pattern with respect to amphiboles and biotites. In apatites from mafic intrusions, the Cl and F contents are mostly similar with values ranging from 2 to 3.5 wt% (Fig.5.5A & B). Apatite analyses from single mafic rocks commonly show similar F-Cl contents. Less commonly, however, different grains in a sample may

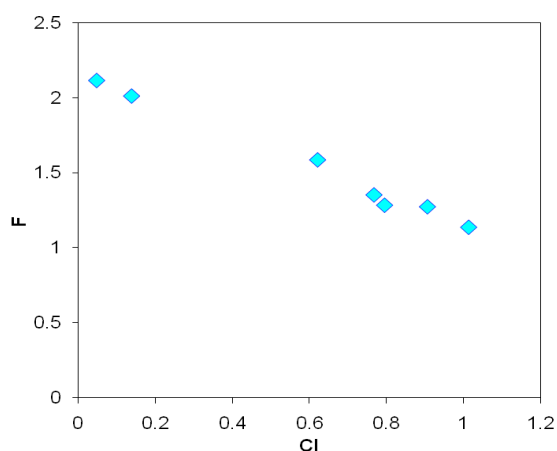


**Figure 5.4:** Fluorine and chlorine variations in primary ferro-magnesian minerals; **5.4A:** Amphibole from the intrusive rocks of the SIC; **5.4B:** Amphibole from the intrusives of the MAIC; **5.4C:** Biotite from the intrusive rocks of the SIC; **5.4D:** Biotite from the intrusive rocks of the MAIC. Crystal chemical controls have strong influence in the amphibole and biotite halogen data, which makes the trends scattered. The whole data sets are available in Appendix 4.1 & 4.2.



**Figure 5.5:** Fluorine and chlorine variations in primary apatites. **5.5A:** SIC rocks; **5.5B:** MAIC rocks. In all the minerals, the Cl content decreases, and F increases with magma evolution. Symbols are same as figure 5.4. The whole data is in Appendix 4.3.

show a range in composition and an extreme example is shown in Fig.5.6. With magma evolution (increasing silica), the Cl contents of apatite decreases and F increases, consistent with amphibole and biotite F/Cl ratios. Apatite data on felsic intrusions could not be collected due to their scarcity. In intermediate rocks, the F concentrations range up to 6.5 wt% and Cl is lower, ranging up to 0.03 wt%. Similar to the amphibole and biotite data, the mixed-mingled rocks show large halogen ranges for apatite, overlapping with the data from separate mafic and intermediate rocks.

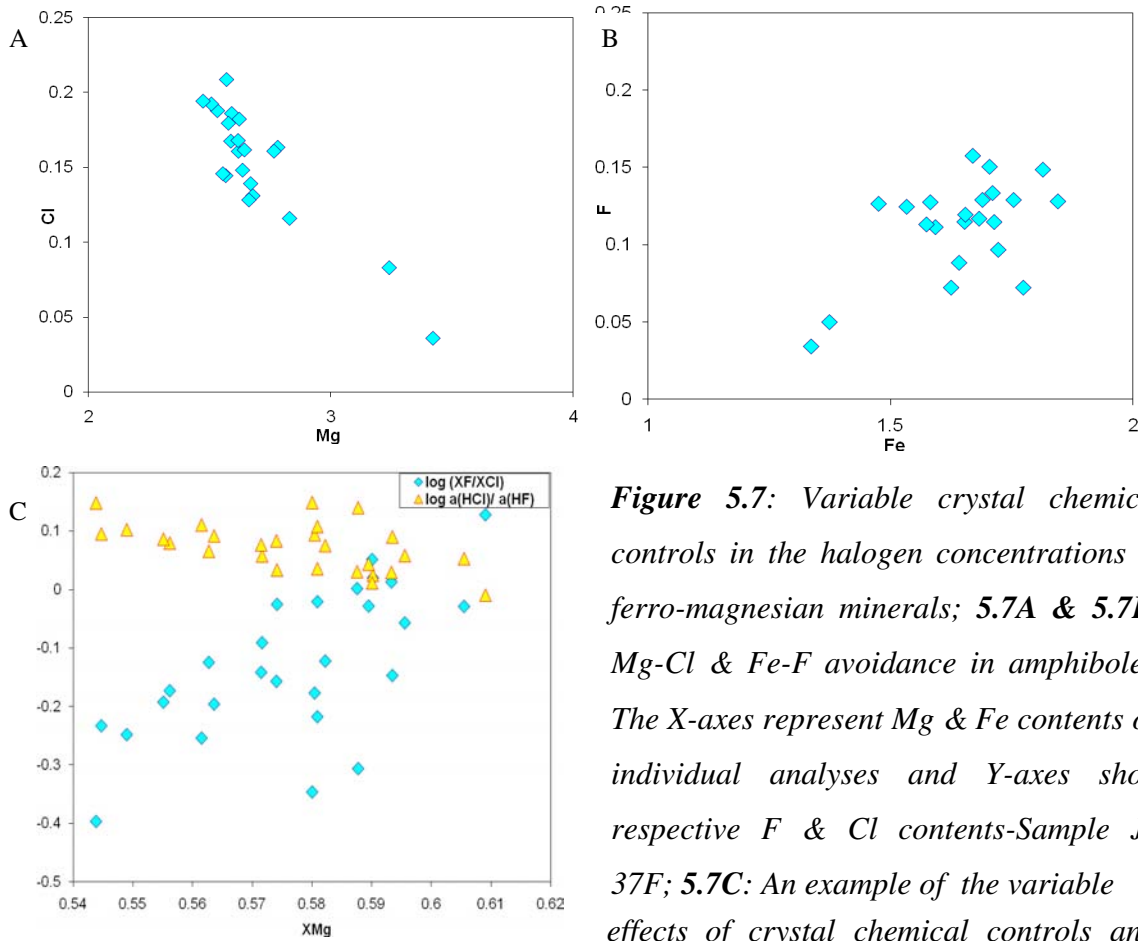


**Figure 5.6:** Fluorine and chlorine contents show wide ranges in a single rock-Sample JB 35F.

### *5.4.3. Halogen variations in coexisting fluid*

Here, no distinction is made between the halogen content of magma and that of coexisting aqueous fluid, largely because of insufficient data in the literature concerning partitioning of halogens between these (at least in terms of deriving such information from mineral compositions). The simplest assumption made here is that the composition of the minerals reflects the halogen content of volatile under-saturated magma, and the term 'fluid' is used here in that context. Uncertainties with this assumption are considered in the Discussion.

The halogen trends of the ferro-magnesian minerals are variably controlled by bulk rock and mineral Mg and Fe abundance (Munoz, 1984, see above). In the SIC and MAIC rocks, the Mg-Cl avoidance trends appear to be stronger than Fe-F avoidance (Fig. 5.7A & B). Because of the differences in crystal chemical controls, the F and Cl contents of amphiboles and biotites cannot be used alone to infer halogen activities in the associated fluid. With the thermodynamic data base developed by Zhu and Sverjensky (1991, 1992), the mineral chemical controls in the F/Cl substitution on biotite structure are isolated and the final results represent the halogen compositions of the fluid, which is in equilibrium with biotite. An ideal example is shown in Fig. 5.7C, in which the flat trend of triangles represents calculated halogen fluid chemistry (accounting for Mg-Cl avoidance) whereas the blue diamonds represent the total halogen content of biotite. The F and Cl contents of biotite grains from all the intrusions of the SIC and MAIC are treated with this thermodynamic data base and the results are provided in Appendix 4.2.



**Figure 5.7:** Variable crystal chemical controls in the halogen concentrations of ferro-magnesian minerals; 5.7A & 5.7B: Mg-Cl & Fe-F avoidance in amphiboles. The X-axes represent Mg & Fe contents on individual analyses and Y-axes show respective F & Cl contents-Sample JB 37F; 5.7C: An example of the variable effects of crystal chemical controls and

calculated fluid chemistry from biotite analyses in the mafic rocks of SIC-Samples JB 12B & 35F. X-axis represents biotite  $X_{Mg}$  values. Much of the variation in F and Cl contents relative to  $X_{Mg}$  is due to avoidance -separation of these crystal chemical controls gives flatter trends, representing the exact fluid chemistry.

Representative calculated F and Cl activity ratios of fluid in equilibrium with biotite from the various intrusions of the SIC and MAIC are tabulated in Table 5.6. These fluid halogen compositions are shown plotted with respect to biotite  $X_{Mg}$  in Fig. 5.8 A & B and in Fig. 5.8C both SIC and MAIC rocks are plotted together. The results show a compositional distinction between the biotites of felsic and mafic-intermediate intrusions. The biotites in the mafic intrusions show the highest  $X_{Mg}$  values followed by intermediate intrusions; however the biotite  $X_{Mg}$  values of felsic intrusions are relatively very low.



<i>Location</i>	SIC	SIC	SIC	SIC	MAIC	MAIC
<i>Rock type</i>	Mafic	Mafic	Intermediate	Felsic	Mafic	Intermediate
<i>Sample</i>	JB 1	JB 35F	JB 82A	JB 15	JB 63	JB 8B
<i>No.</i>	1	1	1	1	3	1
<i>XMg</i>	0.67	0.58	0.51	0.17	0.57	0.53
<i>XFe</i>	0.33	0.42	0.49	0.83	0.43	0.47
<i>XF</i>	0.05	0.05	0.07	0.01	0.03	0.13
<i>XCl</i>	0.03	0.05	0.02	0.03	0.05	0.04
<i>XOH</i>	0.92	0.91	0.91	0.96	0.91	0.83
<i>XF/XCl</i>	1.52	0.95	3.26	0.23	0.67	3.71
<i>log (XF/XCl)</i>	0.18	-0.02	0.51	-0.64	-0.17	0.57
<i>log (X<sub>Cl</sub>/X<sub>OH</sub>)<sub>bt</sub></i>	-1.46	-1.28	-1.64	-1.51	-1.24	-1.36
<i>log a(HCl)<sub>fluid</sub></i>	-1.29	-1.15	-1.54	-1.58	-1.12	-1.26
<i>log (X<sub>F</sub>/X<sub>OH</sub>)<sub>bt</sub></i>	-1.28	-1.30	-1.13	-2.15	-1.42	-0.80
<i>log a(HF)<sub>fluid</sub></i>	-2.30	-2.24	-1.99	-2.68	-2.34	-1.68
<i>a(HCl)/a(HF)</i>	1.02	1.09	0.45	1.10	1.22	0.42
<i>log a(HCl)/a(HF)</i>	0.01	0.04	-0.35	0.04	0.09	-0.38

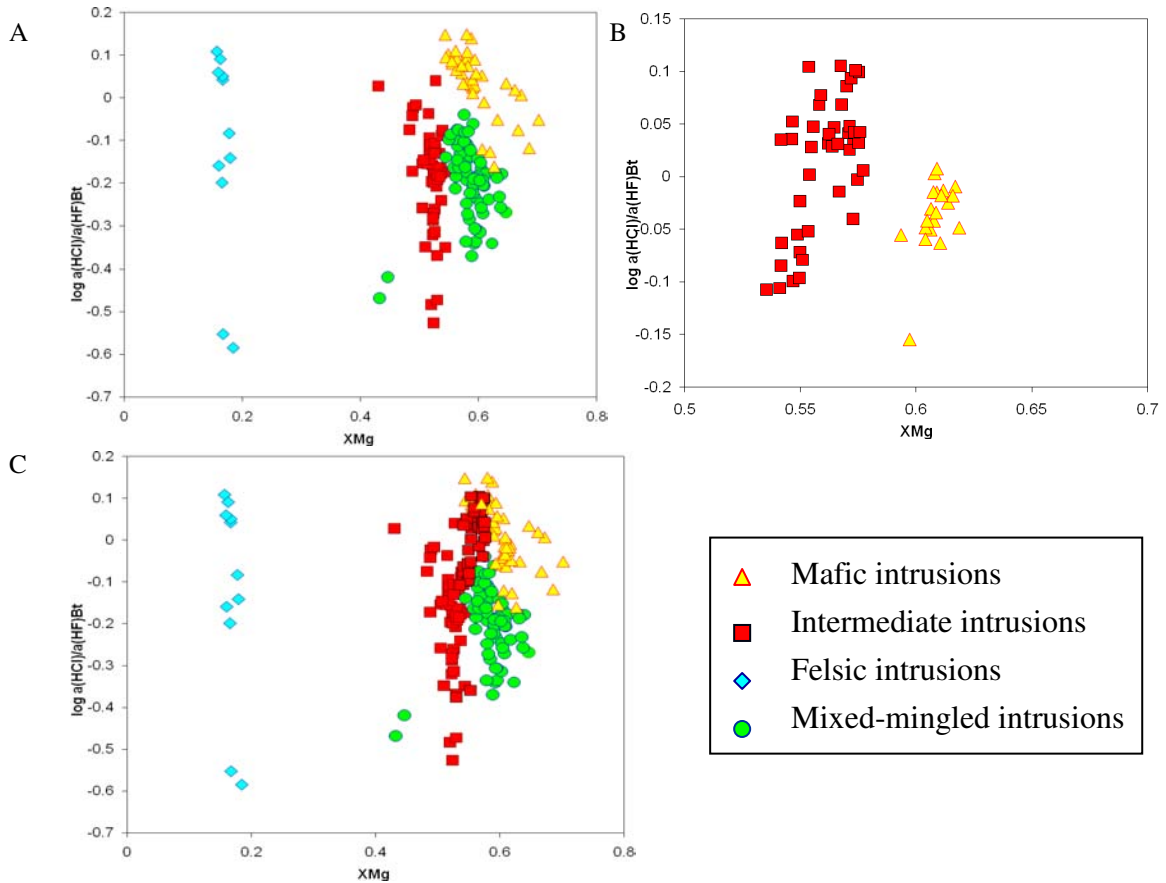
**Table 5.6:** Representative halogen activities of magmatic fluid in equilibrium with biotites calculated from various intrusions of the Saxby and Mt. Angelay Igneous Complexes. The whole data is in Appendix 4.2.

Similarly, in felsic intrusions, the halogen activities of the fluid in equilibrium with biotite show large variations, but that of the mafic intrusions are high and restricted. The halogens in the intermediate intrusions also vary widely.

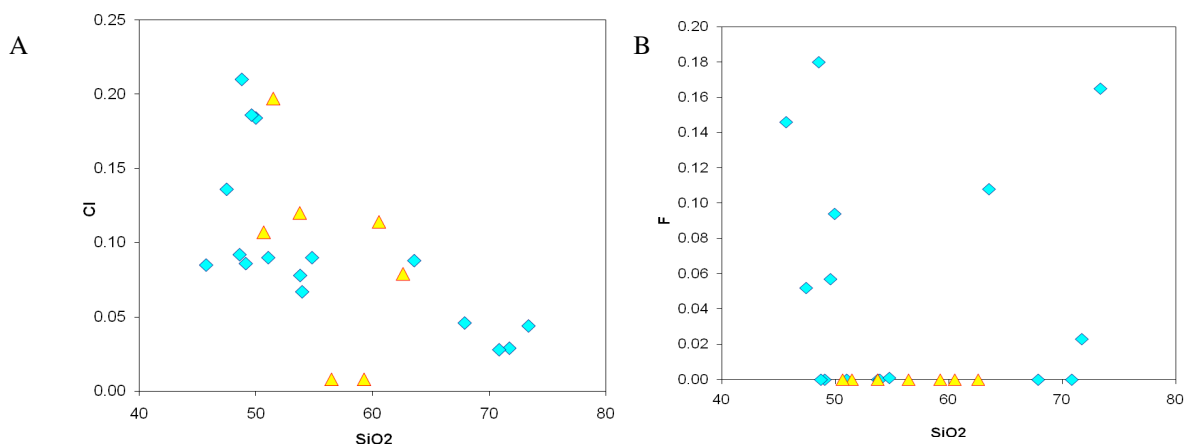
#### 5.4.4. Halogens in whole rocks

The whole rock halogen contents were determined by X-ray Fluorescent Spectrometry (XRF) from a number of intrusions to compare with the mineral halogen data. The halogen analyses of whole rocks show high Cl in mafic intrusions and progressive depletion with increasing magma silica content (Fig.5.9A). This is consistent with the

mineral Cl data. The F contents of whole rocks are mostly below detection and the available data is not enough to constrain the variations (Fig.5.9B).



**Figure 5.8:** Calculated halogen activity ratios of fluid in equilibrium with biotite from various rock types. X-axis represents biotite  $X_{Mg}$  values and Y-axis shows calculated halogen activity ratios in coexisting fluid. **5.8A:** SIC rocks; **5.8B:** MAIC rocks; **5.8C:** SIC and MAIC rocks together.



**Figure 5.9:** Halogen variations in whole rocks; **5.9A:** Chlorine variations in whole rocks; **5.9B:** Fluorine variations in whole rocks. Symbols are same as figure 5.2. The Cl concentration of magma decreases with fractionation, similar to mineral halogen trends. However, most of the F values are below detection. The whole data is in Appendix 3.2.

## 5.5. Discussion

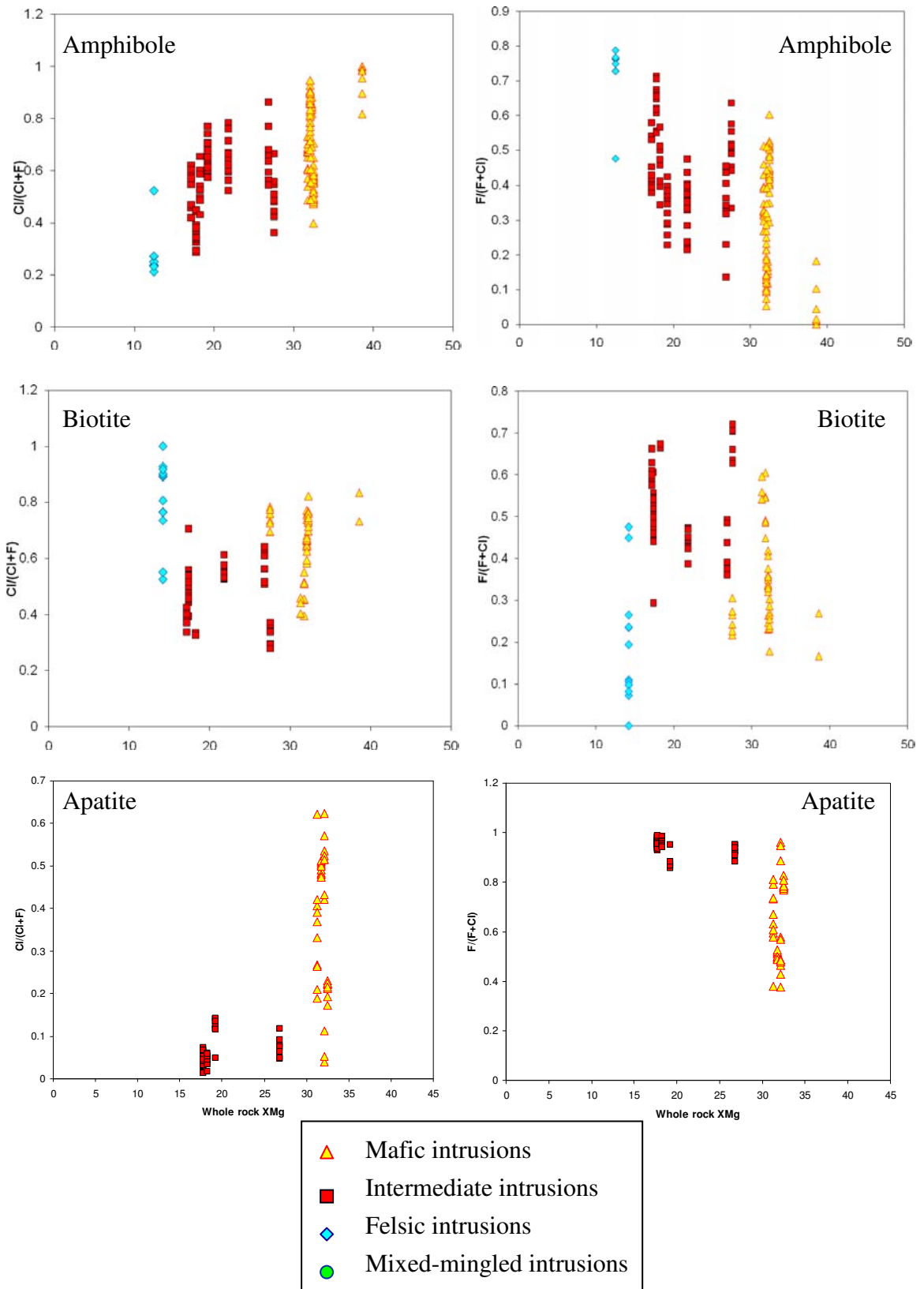
### 5.5.1. F and Cl volatile evolution in the SIC and MAIC

The F-Cl volatile evolution of the SIC and MAIC rocks can be influenced by various factors including whole rock geochemistry, variation in mineral abundances, and halogen partitioning between minerals and fluids. Fig. 5.10 displays a comparison of the chemical variation in fluorine and chlorine for various halogen bearing minerals in different intrusions with respect to magma evolution. Whole rock  $X_{Mg}$  values were used as a tool to track the magma evolution. These figures illustrate that there are broad similarities in the halogen trends of these minerals in which the Cl decreases and F increases from mafic to intermediate rocks with the felsic rocks showing a different trend. The intake of halogens into minerals can be controlled by a number of factors including the magma composition and mineral site vacancy, and so the halogen contents can vary in each mineral. However, the consistency of the trends relative to

magma composition suggests that they track the compositional evolution of the magma (and/or aqueous fluid in equilibrium with the magma). In Fig 5.11A & B the halogen activity ratios of fluid in equilibrium with biotites of different intrusions in the SIC and MAIC are compared, which also follow the same pattern.

The partitioning of halogens in an intrusion probably relates to the abundance of minerals and ultimately to the primary melt composition. For example, if the parent magma is mafic in composition, then a number of minerals including olivine, pyroxene, amphibole and biotite can host the volatiles. If the halogens are compatible, then progressive crystallization will leave the residual melt depleted in these components as they accumulate in the minerals. The trend of decreasing biotite and amphibole halogen contents from mafic to intermediate rocks is consistent with compatible behaviour of the halogens. In a granitic melt, the abundance of ferromagnesian minerals is less than for more mafic rocks. If the magma was halogen-rich initially, these minerals can show high halogen contents and the residual melt may be enriched in halogens, to the point that an exsolved aqueous fluid is also enriched.

In the SIC and MAIC rocks, the whole rock  $Mg/(Mg+Fe)$  has a strong control on the formation of various mineral assemblages (Fig 5.11C). The mafic intrusions commonly contain a variety of halogen-bearing minerals including clinopyroxene, amphibole, biotite and apatite. In intermediate intrusions, the clinopyroxene is completely absent and the most evolved phases are devoid of both clinopyroxene and apatite, and contain only amphibole and/or biotite. An example of the mineral assemblage control on halogen partitioning is shown in Fig. 5.11D. Rocks that contain only one halogen-bearing mineral (e.g., either amphibole or biotite) show wider ranges of F/Cl ratio, and



**Figure 5.10:** Variation in chlorine and fluorine vs. whole rock  $X_{Mg}$  for amphibole, biotite and apatite for the SIC and MAIC intrusions. In all the minerals, the Cl decreases and F increases with magma evolution.

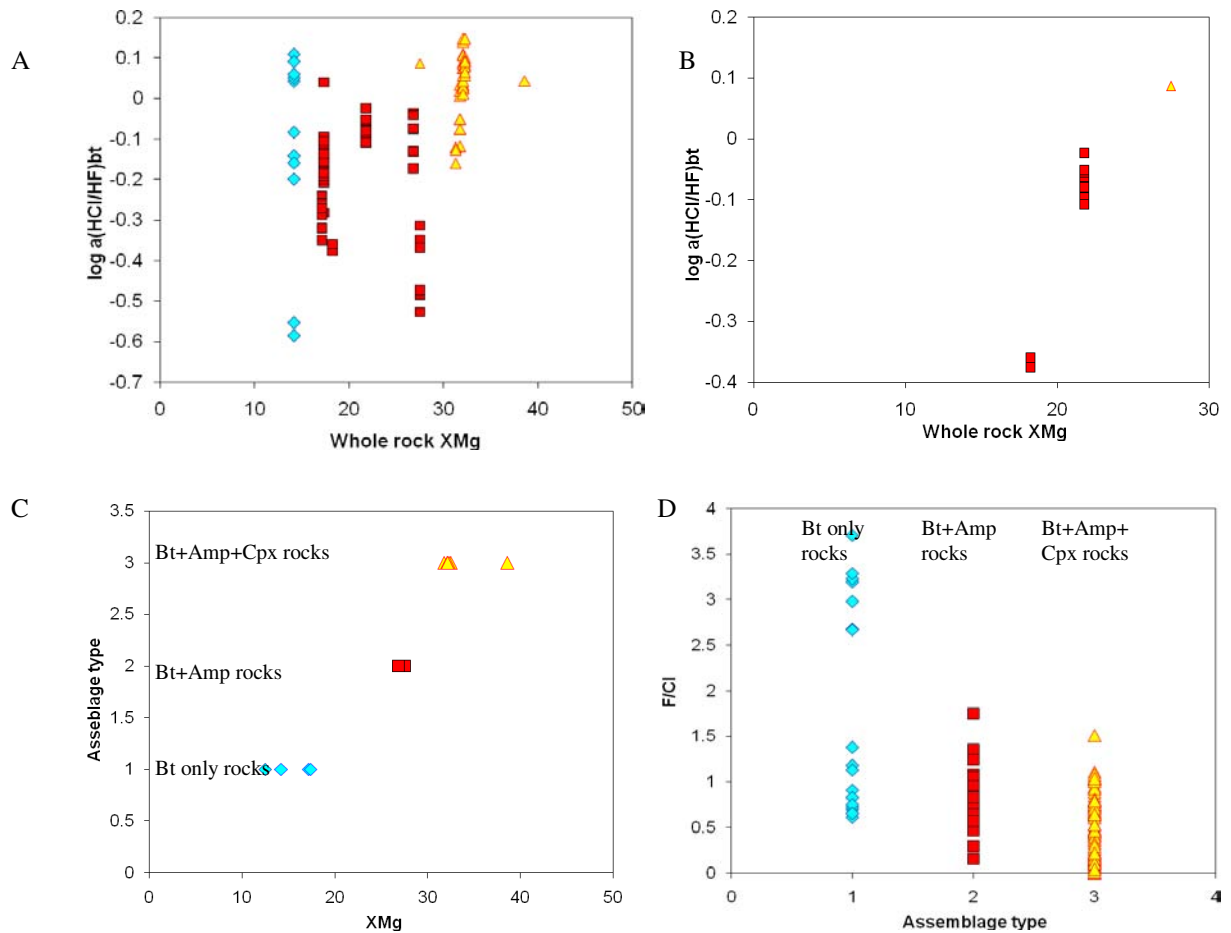
with an increased number of minerals, the range gets narrower. These trends suggest continuous halogen partitioning between minerals and magmatic fluid. The mixed-mingled rocks of the SIC show abnormal ratios, which may have resulted from the complex geochemical changes during mixing and mingling, or fundamentally different halogen contents and ratios of the two magmas.

Figure 5.12A show F-Cl partitioning between ferro-magnesian minerals in various intrusive suites of the SIC and MAIC. In mafic and intermediate intrusive rocks, biotite either crystallizes before amphibole, or they formed approximately simultaneously (Chapter 3). The partitioning between amphibole and biotite shows linear trends, suggesting few fluctuations in the fluid chemistry during their crystallisation. For amphibole-biotite pairs, halogen ratios of amphiboles are also compared with the halogen ratios of the calculated fluid in equilibrium with biotite in Fig.5.12B.

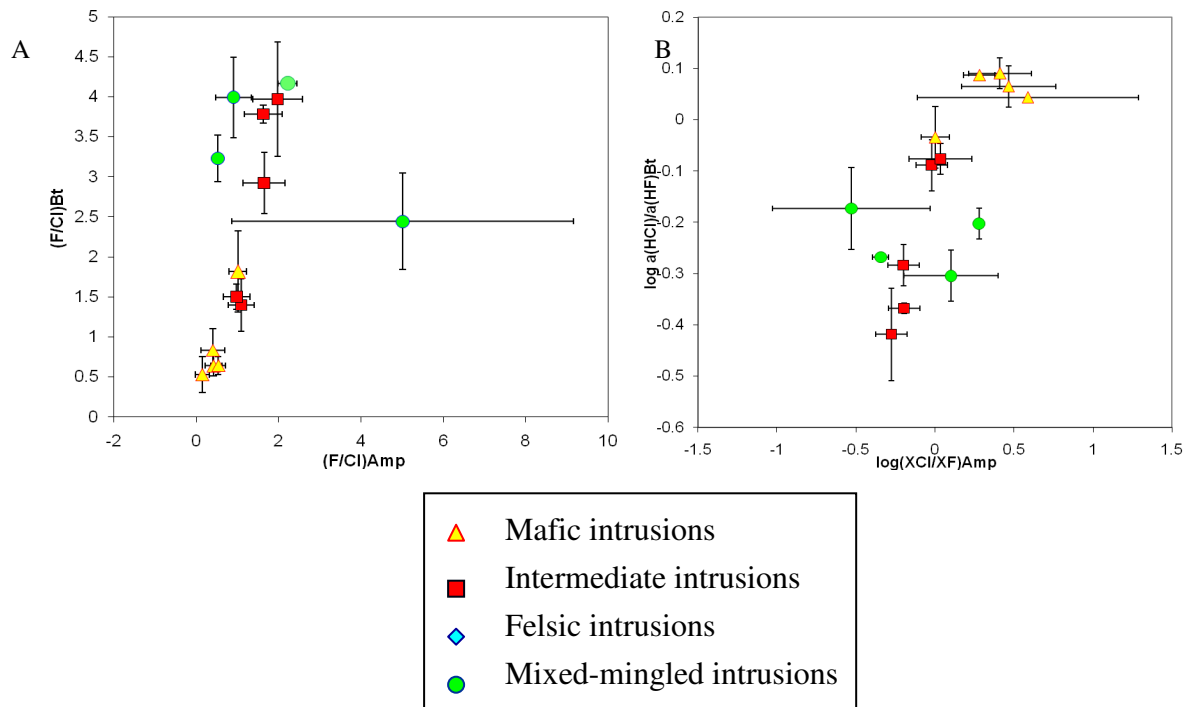
Even though the crystal chemical effects in amphiboles are not separated out, the trends show linear patterns. The F-Cl values from the Saxby mixed-mingled rocks are displaced from the linear trend observed in the other rocks, indicating complexity in halogen partitioning between minerals and fluid in the process of mixing.

The halogen partitioning between apatite and both amphibole and biotite shows apparently very poor correlation. This may reflect that the ideal halogen substitution in apatite at high temperatures into the OH site (e.g., Volfinger et al., 1985; Tacker and Stormer, 1989) was not influenced by magma compositional variation in the same way that biotite and amphibole were. However, in Fig. 5.5A & B it is clear that the halogen substitution in apatites did change with magma evolution. So the simplest explanation

might be that Fe-Mg variations that controlled amphibole and biotite compositions to some extent did not influence apatite crystallization or chemistry.



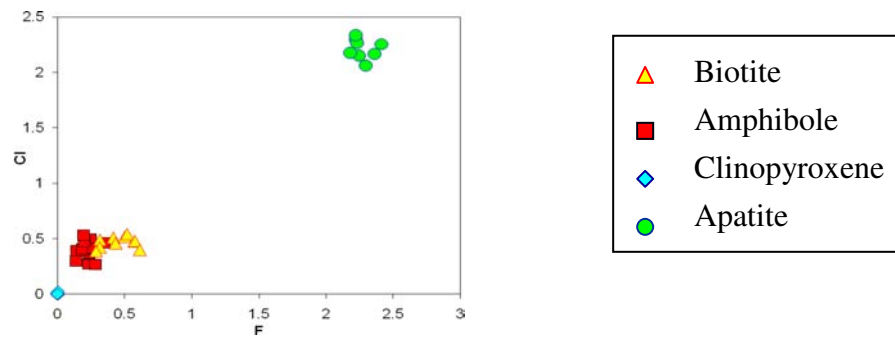
**Figure 5.11:** Variation in chlorine and fluorine activities of residual fluid in equilibrium with biotite vs. whole rock  $X_{Mg}$ . **5.11A:** SIC intrusions, **5.11B:** MAIC intrusions; **5.9C:** Whole rock  $X_{Mg}$  vs. mineral assemblages. The plot shows a strong control of  $X_{Mg}$  in the formation of various minerals; **5.11D:** Amphibole F/Cl ratios vs. different mineral assemblages. The F/Cl ratio is tightly constrain for mafic intrusions but gets broader for more felsic varieties. Symbols are same as figure 5.10.



**Figure 5.12A:** Chlorine and fluorine partitioning between amphibole and biotite in different intrusions of the SIC and MAIC; **5.12B:** Chlorine and fluorine contents of amphibole compared with calculated halogen activities of fluid in equilibrium with biotite. Both plots show linear trends, suggesting the partitioning is consistent. The values were taken from samples with both amphibole and biotite analyses. The error bars represent  $2\sigma$  standard deviations derived from averaging, with the numbers of samples averaged presented in Appendix 4.1 and 4.2.

The F-Cl abundance in different minerals within the same rock appeared to follow a constant pattern with pyroxenes containing the least and apatites containing the highest halogen enrichment (Fig. 5.13). However, the partitioning of halogens between different minerals in the same intrusions may be similar or different. For example, Fig 5.14A-C shows the F and Cl contents of hornblendes, biotites and apatites from a gabbro. The F partitioning between hornblende and biotite appears to be similar, but the Cl is highly partitioned in the hornblende compared to biotite. In apatites, the partitioning of both F and Cl is very high compared to biotite and hornblende.





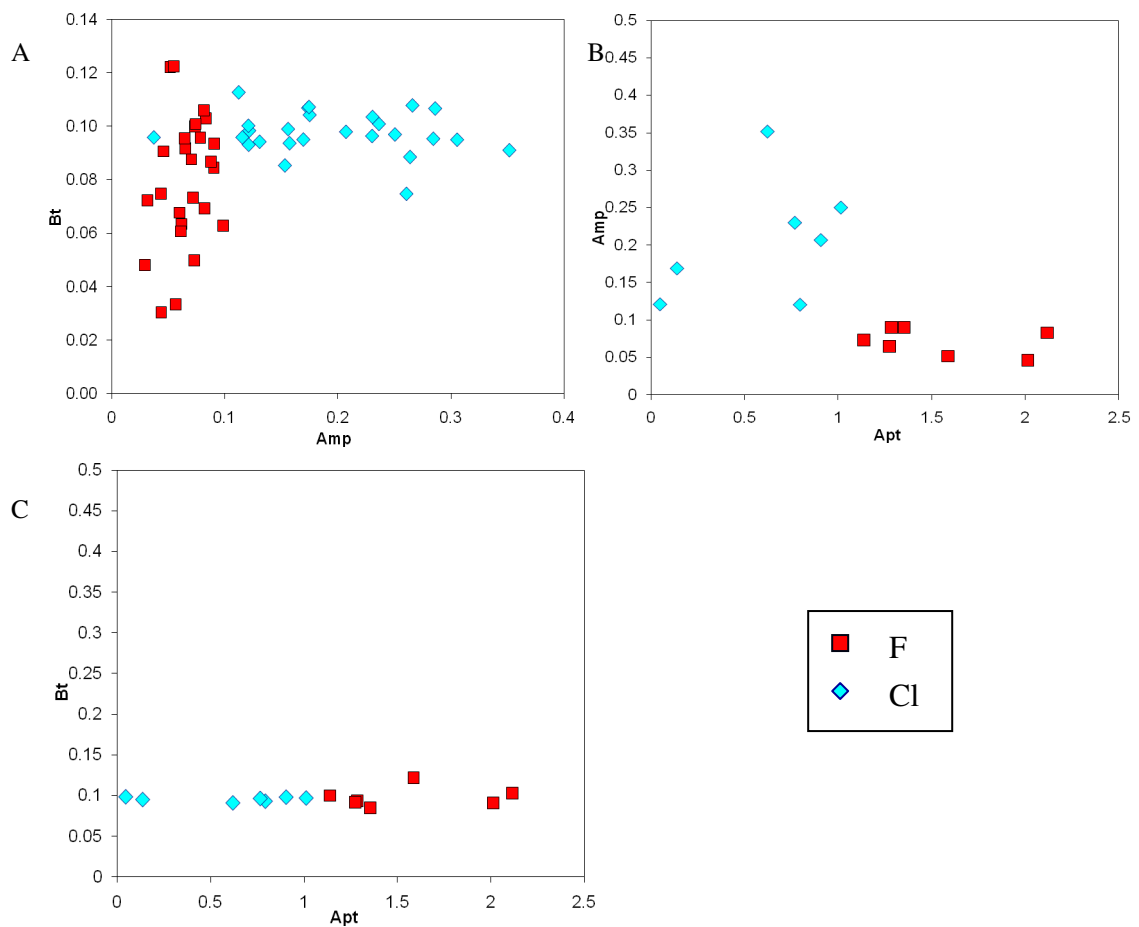
**Figure 5.13:** Halogen abundances in different minerals within the same intrusion-Sample JB 1. The apatite shows highest halogen content and clinopyroxene shows the lowest.

Sub-solidus alteration in amphiboles and biotites has apparently created some variation in the halogen data (see also Nash, 1976; Munoz and Swenson, 1981; Dilles, 1987). In many intrusions, the primary amphiboles show biotite alteration (Chapter 3; Fig. 5.1B) and the F and Cl contents of these secondary biotites show similar halogen contents to those of the amphiboles they are replacing. However, the halogen contents of coexisting primary amphiboles and biotites are clearly distinct. Also, the microprobe results from the core and rim of a single primary amphibole or biotite grain do not show any significant halogen variations. Thus, although changes occur between rocks of different bulk composition, during the crystallisation of minerals within one rock, equilibrium was fully established between the magma composition, the minerals and any coexisting aqueous fluid (Fig. 15A).

### 5.5.2. Possible causes of halogen variation

Halogen variations in magmatic fluids can be caused by a number of factors including changes in bulk rock chemistry, P-T conditions, magma degassing, wall rock interaction and coupled substitution reactions in minerals. In the SIC and MAIC

intrusions, coupled substitution reactions in ferro-magnesian minerals played a major role in the halogen abundance of amphibole and biotite, and these minerals show strong Mg-Cl avoidance compared to Fe-F avoidance (Fig 5.7A & B). The high whole rock Mg content compare to Fe may also have preferentially distributed F into the minerals, rather than Cl.



**Figure 5.14:** Halogen partitioning between different minerals in the same intrusion **5.14A:** Halogen partitioning between amphibole and biotite; **5.14B:** Halogen partitioning between amphibole and apatite; **5.14C:** Halogen partitioning between biotite and apatite –All the analyses are from sample JB 35F. The results show variable effects in different minerals.

Although these effects have produced somewhat scattered trends in amphibole and biotite F-Cl plots (Fig 5.4), they appear to indicate two different halogen evolution histories primarily related to different magma sources, compositions or processes. The relatively continuous variation in the F and Cl of halogen bearing minerals (Fig 5.4, 5.5A & B & 5.10) from the mafic and intermediate intrusions together with whole rock halogen variations suggests that they were controlled by progressive fractional crystallisation of a fairly homogeneous parental magma composition (also see Chapter 4), without any impact from the incursion of metamorphic or meteoritic fluids, or from sudden vapour saturation.

The calculated  $\log a_{\text{(HCl)}} / a_{\text{(HF)}}$  values of magmatic fluid in equilibrium with biotite show a decrease from mafic to intermediate intrusions (Fig 5.11A), which may correspond to a fractional crystallization history (Loferski and Ayuso, 1995). However, this trend could result from two possibilities; an increase in  $a_{\text{HF}}$  through time at constant  $a_{\text{HCl}}$  or a decrease in  $a_{\text{HCl}}$  at constant  $a_{\text{HF}}$ . It is also possible that this trend could also result from a simultaneous increase in magma F content (through residual enrichment) and loss of Cl through progressive release of a chlorine bearing volatile phase, capable of transporting and scavenging copper and gold and other metals (e.g. Piccoli and Candela, 1994). Such a situation suggests the chances of magma degassing. However, there are no breaks in the relationships between mineral halogen data and bulk composition that might point to a particular episode of volatile saturation in these rocks, so such a process would have to occur repeatedly and relatively continuously to explain the data. Most likely, the halogens in these minerals in mafic to intermediate magmas reflect closed-system exchange between magma and minerals during progressive, continuous, fractional crystallization. Such a conclusion, however, is not particularly

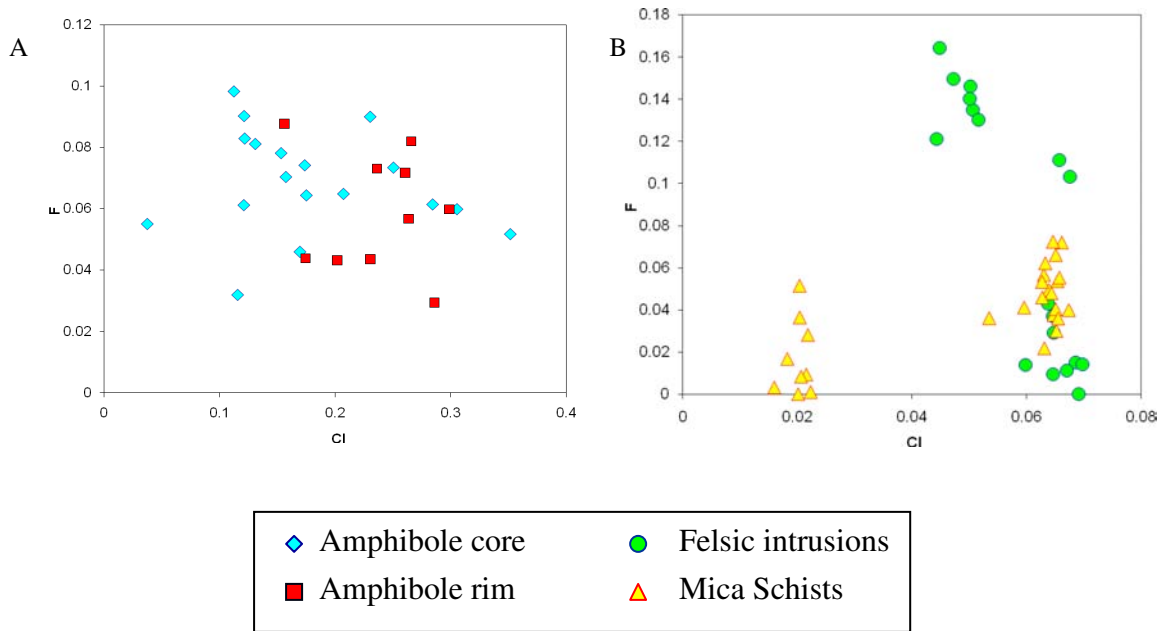
consistent with inferences made from comparing fluid inclusion behaviour and magmatic-hydrothermal crystallization products of the SIC and MAIC (Chapter 6). This problem is discussed further in Chapter 8.

The halogen patterns of minerals in the felsic intrusions are different to the other magmas and highly variable, suggesting different source and/or crystallization history (Fig 5.4A & C, 5.8D & F, 5.10 & 5.11A). A distinctive magmatic origin for the abundant felsic intrusions of the SIC and MAIC was suggested in the previous chapters (chapters 2 & 4), as also reflected by the different halogen signatures of the minerals in these intrusions. The felsic rocks have lower bulk halogen content but wide variation in Cl/F ratios of individual minerals and calculated fluid HCl/HF values. The variability of the mineral halogen data in the relatively compositionally homogeneous felsic magmas suggest that degassing or wall rock interaction may have been more pronounced in the felsic intrusions than in the mafic and intermediate ones. A possible involvement of external halogen involvement cannot be discarded, due to similarities in the F and Cl values of felsic intrusions and country rocks (e.g. schists; Fig 5.15B), although the amount of data collected from intrusion/wallrock contacts was insufficient to clearly determine this.

A magmatic source for halogens in the primary minerals can also be understood by comparing them to secondary minerals that relate to alteration (especially sodic-calcic alteration and later chloritisation). The secondary biotites replacing igneous amphiboles often have same Cl and F as the amphibole they replace. This similarity suggests that the local diffusion of halogens from amphibole into secondary biotite was the likely cause rather than the effect of external saline fluids. Furthermore, the high halogen

concentrations of apatite inclusions within the ferro-magnesian minerals of mafic rocks suggest high F-Cl concentration in the less fractionated, primary magma (Fig 5.5A, B & 5.10). In the SIC and MAIC rocks, apatites are mostly observed as inclusions in amphiboles and biotites, suggesting their crystallization at high temperatures. Apatite is commonly less prone to subsolidus alteration and they record, early, high temperature magmatic conditions (Roegge et al., 1974; Parry and Jacobs 1975; Tacker and Stormer 1989; Munoz 1990; Piccoli and Candela 1994; Coulson and Chambers 1996; Piccoli et al., 1999). Fractionation caused a continuous decrease in chlorine and increase in fluorine with magma evolution, which is consistently recorded by all halogen bearing minerals (Fig 5.10).

The rocks from the magma mixed-mingled zones of the SIC show large variations in halogen chemistry of amphiboles and biotites, but apatite halogen values are fairly tightly constrained. This suggests that although the magma mixing has re-equilibrated the volatile contents of ferro-magnesian minerals, the consistent apatite chemistry may indicate that the mafic magmas (with more apatite) contributed the majority of the halogens to the mixed magmas. Subsequent crystallisation of amphibole and biotite may have caused variable halogen contents in these minerals because Fe and Mg were shared between the two magmas types whereas the halogens were primarily derived from the mafic component.



**Figure 5.15A:** Amphibole analyses showing similar rim and core compositions-Sample JB 35F. The analyses do not show any variation between core and rim; **5.15B:** Halogen contents of felsic intrusions vs country rocks. Large variations in the F contents of felsic intrusions are sometimes similar to that of country rocks.

### 5.5.3. Magma volatile evolution and IOCG deposits

The continuous variation in calculated HCl/HF ratios of magmatic fluid in equilibrium with biotites, together with systematic amphibole and apatite F and Cl variations with increasing degree of fractionation in the mafic to intermediate trend is consistent with a gradual F depletion due to removal in halogen-bearing minerals. The apparent correlation with enrichment in chlorine confirms that Cl behaves more incompatibly than F during fractionation.

The potential of magmatic-derived Cl to transport ore components and form ore deposits is proposed by many workers (Crerar & Barnes 1976; Mutschler et al. 1981; Boudreau et al. 1986; Brookins 1989; Coulson et al 2001) and in the SIC and MAIC mafic and intermediate intrusions, the halogen variations suggest the presence of a

chlorine bearing fluid at the final stages of fractionation. The presence of Cl in the final magmatic fluids is suggested from the increase in Cl incompatibility with fractional crystallization and such a fluid may have contributed to the formation of ore deposits in Cloncurry (Chapter 8). Evidence for the highly metalliferous nature of these magmatic fluids is obtained from fluid inclusion studies, which will be discussed in chapters 6 & 7.

## 5.6. Conclusions

The common primary minerals observed in the intrusive rocks of the SIC and MAIC include oligoclase, augite, hornblende, biotite, apatite, microcline, orthoclase, quartz and magnetite. Albite, titanite, actinolite and chlorite were also observed, but are secondary.

The halogen contents of hornblende, biotite and apatite were studied in detail and it is suggested that the felsic and mafic-intermediate intrusions of the SIC and MAIC are distinct in terms of mineral chemistry. The halogen compositions in mafic and intermediate intrusions provide the best indication of how fractional crystallization proceeded in closed system conditions, which are consistent with the fractionation of a tholeiitic magma. With magma evolution, the halogen bearing minerals of amphibole, biotite and apatite show a continuous increase in F and decrease in Cl contents. The Cl variations in whole rocks follow the same mineral Cl trends, but the F contents are very low or not detectable. The temporal variation in calculated HCl/HF activity ratios of residual fluid in equilibrium with biotite also show highest  $\log a(\text{HCl}/\text{HF})$  values associated with mafic intrusions, followed by intermediate intrusions. The felsic intrusions show very low whole rock Cl values with highly variable mineral halogen

contents, suggesting the possibility of magma degassing and/or wall rock interaction for their halogen contents.

The mineral halogen studies together with field and geochemical studies give new suggestions for the magmatic volatile evolution of the Cloncurry intrusions. The continuous loss of Cl from the minerals during fractional crystallization suggests Cl enrichment in the final fluid phase, which may have contributed to ore genesis. These results also help to interpret the fluid inclusion observations and to explore the connection between intrusions and IOCG deposits in the following chapters.



## Chapter 6: Fluid chemistry and evolution of Cloncurry intrusions

### 6.1. Introduction

Like mineral and whole rock chemistry, fluid inclusions can provide vital information about magmatic evolution and hydrothermal processes. Rocks may contain multiple generations of fluid inclusions that represent different geological settings. Petrographic analysis can distinguish different fluid types and their paragenesis, and microthermometric data can provide information about their chemistry and trapping conditions. The main aim of this study is to recognize various fluid types in the Saxby Igneous Complex (SIC) and the Mt. Angelay Igneous Complex (MAIC). The conventional fluid inclusion results obtained from this study will be compared with fluid inclusion micro-analytical results (Chapter 7) and field, petrographic, mineral chemical and whole rock geochemical observations (Chapter 2, 3, 4 & 5) to determine the role of fluids in magmatic evolution, alteration and IOCG ore genesis. This chapter describes the petrographic and microthermometric results of fluid inclusion analysis from various rocks of the SIC and the MAIC.

### 6.2. Fluid inclusions studies in Cloncurry District

Most fluid inclusion studies in the Cloncurry area have concentrated on ore deposits and regional hydrothermal systems. Abundant multi-solid and aqueous fluid inclusions have been reported from the IOCG deposits as have carbonic and aqueous-carbonic inclusions (Beardsmore, 1992; Krcmarov, 1995; Adshead, 1995; Dong, 1995 & 1996; Rotherham, 1997a&b; Baker, 1998; Rotherham et. al., 1998; Mark et. al., 1999; Perring et. al., 2000; Williams et. al., 2001; Kendrick et. al., 2007; Fisher and Kendrick, 2008). Fluid inclusion types in hydrothermally altered rocks and veins are mostly aqueous and carbonic (e.g.

Oliver, 1995; De Jong & Williams, 1995; Xu, 2000; Bertelli, 2007; Kendrick et. al., 2008). Limited fluid inclusion studies on granites have recognized abundant multisolid, aqueous and carbonic inclusions (Perring et. al., 2000; Mark et. al., 2004a; Mustard et. al., 2005; Bertelli, 2007; Baker et. al., 2008).

CO<sub>2</sub>-rich fluid inclusions are common in granites, ore deposits and alteration-related rocks, but the multi-solid inclusions are abundant in IOCG deposits and granitic environments, and are comparatively absent in the Na-Ca alteration zones (e.g. Baker et. al., 2008). Studies suggest that the hypersaline brines responsible for the regional sodic-calcic alteration are derived from magmas (e.g. Marshall & Oliver 2006) or from dissolution of evaporitic chlorides during or after regional metamorphism (Oliver, 1995; De Jong & Williams, 1995) or from bittern brines and basement fluids (e.g. Kendrick et. al., 2007).

Evidence for both fluid mixing and unmixing have been observed in the Cloncurry rocks and are implicated as potential ore precipitation mechanisms (Adshead, 1995; Rotherham, 1997b; Baker, 1998; Perring et. al., 2000; Williams et. al., 2001; Fu et. al., 2003; Mustard et. al., 2004 & 2005; Kendrick et. al., 2007; Baker et. al., 2008; Fisher, 2008). The coexistence of both CO<sub>2</sub>-only inclusions and hypersaline brine inclusions in the IOCG deposits and some magmatic-hydrothermal transition zones are interpreted to be the evidence of liquid-vapour immiscibility in the Cloncurry district (e.g. Perring et. al., 2000). Pollard (2001) proposed that this coexistence is due to the unmixing of an original H<sub>2</sub>O-CO<sub>2</sub>-NaCl ± CaCl<sub>2</sub> fluid, probably derived from magma. The latest studies in fluid inclusions (Fu et. al., 2003; Mustard et. al., 2005; Baker et. al., 2008) argue that the presence of mixed CO<sub>2</sub>-H<sub>2</sub>O-halite±other solids inclusions and the occurrence of

carbonate (calcite, siderite etc) daughter minerals in many other hypersaline brine inclusions indicate the possibility of fluid mixing in the Cloncurry area. PIXE data on individual fluid inclusions shows varying Br/Cl ratios in primary multisolid inclusions (Williams et. al., 2001) that support the possibility of mixing between high salinity magmatic fluids and low salinity Na-Ca fluids. Fluid inclusion studies on the Ernest Henry deposit show a contribution of magmatic and/or mantle-derived fluids to the halogen and noble gas signals of ore-related fluid inclusions, as well as other signals from halite dissolution (Kendrick et. al., 2007).

Fluid inclusion studies on Cloncurry intrusions are restricted to limited work in the rocks of the Williams Batholith (Perring et. al., 2000; Mark and Foster, 2000, Mustard et. al., 2005). These studies note the presence of primary multisolid inclusions in the granitoids of Cloncurry. The first fluid inclusion work reported on granites was on Mt. Angelay Granites by Tolman (1998), who identified four inclusion types: liquid-vapour (LV), liquid-vapour-halite (LVH), liquid-vapour-halite multisolid brines with up to 6 daughter minerals (LVHSn<sub>2to6</sub>) and possible vapour or liquid CO<sub>2</sub> inclusions. Mark & Foster (2000) documented complex magmatic-hydrothermal transition textures containing highly saline fluid inclusions, indicating the interaction of crystallizing magmas with highly saline fluids of regional metamorphic origin. The occurrence of high salinity, multi-solid brine inclusions and halite-bearing liquid CO<sub>2</sub> inclusions supports a fluid unmixing model (Mustard et. al., 2005), although mixing models must also be considered. Their preliminary PIXE data indicated the presence of magnetite and chalcopyrite as daughter minerals in the fluids.

### 6.3. Sample Selection and Description

As the main objective of the research is to constrain the fluid evolution of the intrusive phases of the Cloncurry area, the sampling included mostly igneous rocks. The samples were from granites, magma mixed-mingled rocks, brain rocks, pegmatites, aplites and quartz veins. Quartz contains clusters and trails of fluid inclusions that represent different stages of the fluid evolution. Samples selected for fluid inclusion analyses are summarized in Table 6.1.

**Granites:** Four samples of granite from the Mt. Angelay and Saxby Granites were gathered. These are subhedral, medium to coarse grained, biotite±hornblende-bearing granites, which show typical plutonic textures (Fig.6.1A). Major minerals include quartz, microcline, orthoclase and albite with accessory mafics. The quartz content of these rocks varies from 30% to 50%. Perthite and myrmekite are common intergrowth textures in granites.

**Mixed-mingled rocks:** Three samples were collected from the mixing-mingling zones of mafic and felsic magmas in the SIC (Fig.6.1B; also see Chapter 2). These are subhedral, fine to coarse grained rocks with biotite and hornblende as mafic minerals. The rocks are mainly composed of quartz and microcline with plagioclase. The quartz content is 35 to 45%, but most of the quartz grains are recrystallized. The mixing and mingling of magmas resulted in the recrystallization of minerals and so the primary fluid inclusions from these rocks are inferred to represent at least part of the recrystallization history. Triple junctions, developed during recrystallization, are very common along the mineral boundaries.

Sample No	Location	Rock type	Mineralogy	Host Mineral	Petrography	Microthermometry	PIX E	LA-ICP-MS	No of samples analyzed
<b>JB 4</b> <b>JB 59</b>	Mt. Angelay	Granite	Biotite- hornblende- albite- orthoclase- microcline- quartz with minor sericite	Quartz	√	√	√	√	2
<b>JB 61</b> <b>JB 64A</b>	Mt. Angelay	Brain rock	Spherulitic intergrowth of albite and quartz with magnetite-hematite rims	Quartz	√	√	√	√	2
<b>JB 6D</b> <b>JB 7</b>	Mt. Angelay	Pegmatite	Biotite- quartz- albite- microcline	Quartz	√	√	√		2
<b>JB 81</b> <b>JB 88B</b>	Saxby	Granite	Biotite- hornblende- albite- orthoclase- microcline- quartz with minor sericite	Quartz	√	√	√	√	2
<b>JB 37C/F</b> <b>JB 79B</b> <b>JB 82B</b>	Saxby	Mixed-mingled rock	Biotite- hornblende- albite- quartz- microcline- orthoclase- magnetite with signs of recrystallization	Quartz	√	√	√		3
<b>JB 37A1</b> <b>JB 35E</b>	Saxby	Pegmatite	Biotite- quartz- albite- microcline	Quartz	√	√	√		2
<b>JB 88D</b>	Saxby	Aplite	Fine grained quartz, albite and microcline with rare Fe- oxides	Quartz	√	√		√	1
<b>JB 88C</b>	Saxby	Quartz vein	Quartz	Quartz	√	√	√	√	1

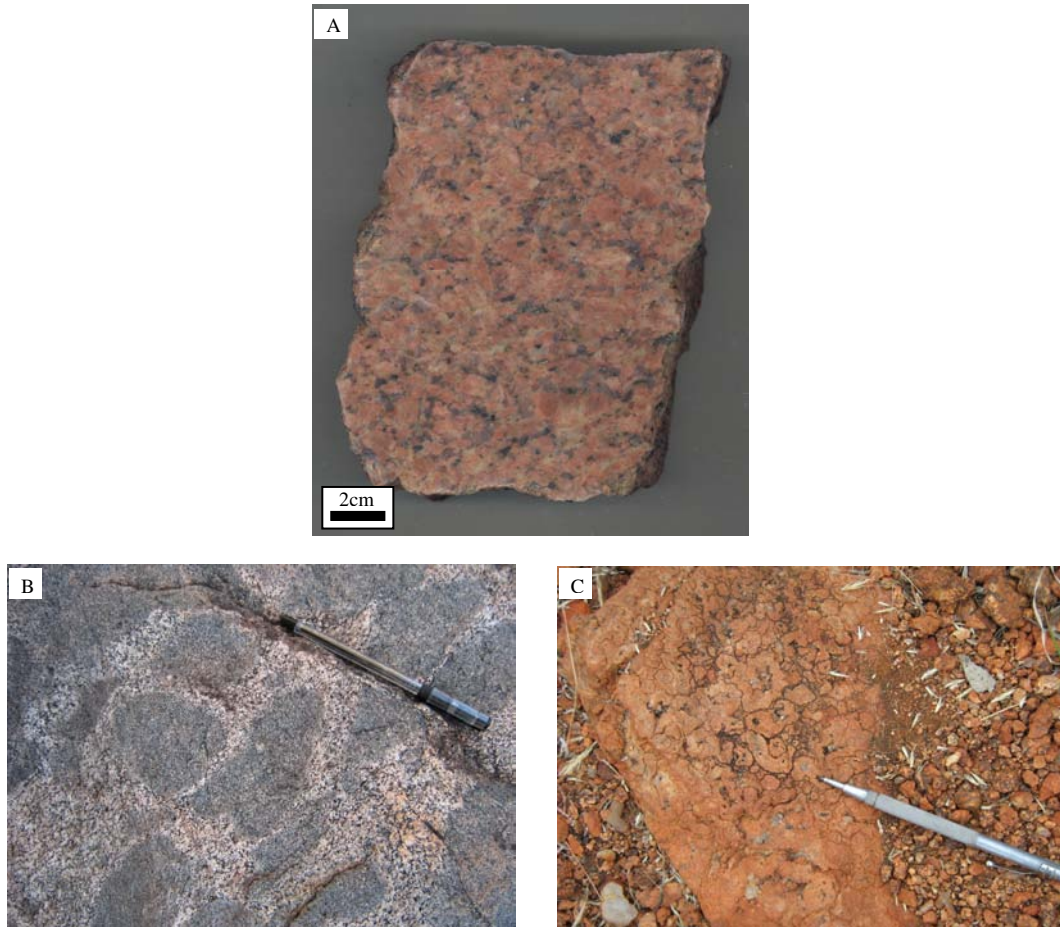
*Table 6.1: Description of samples selected for the fluid inclusion study and analyses undertaken on each sample*

**Brain rocks:** Brain rocks are principally composed of quartz, albite, and magnetite (see Chapter 3; Tolman, 1998; Mark and Foster, 2000). They are observed at the top of an intrusion, which is part of the MAIC. This area contains a number of veins with magmatic and hydrothermal minerals and is described as magmatic-hydrothermal transition zone by Mark and Foster (2000). The rocks display a variety of textures including equigranular, spherulitic, granophyric and graphic intergrowths between quartz and albite (Fig.6.1C). The texture contains fine and transparent needles of albite and quartz, which appear to coarsen inwards and commonly end in miarolitic cavities. These cavities were later filled with quartz, and the spaces between polygonal structures with magnetite. Fluid inclusions were analysed from two samples of brain rocks in this study.

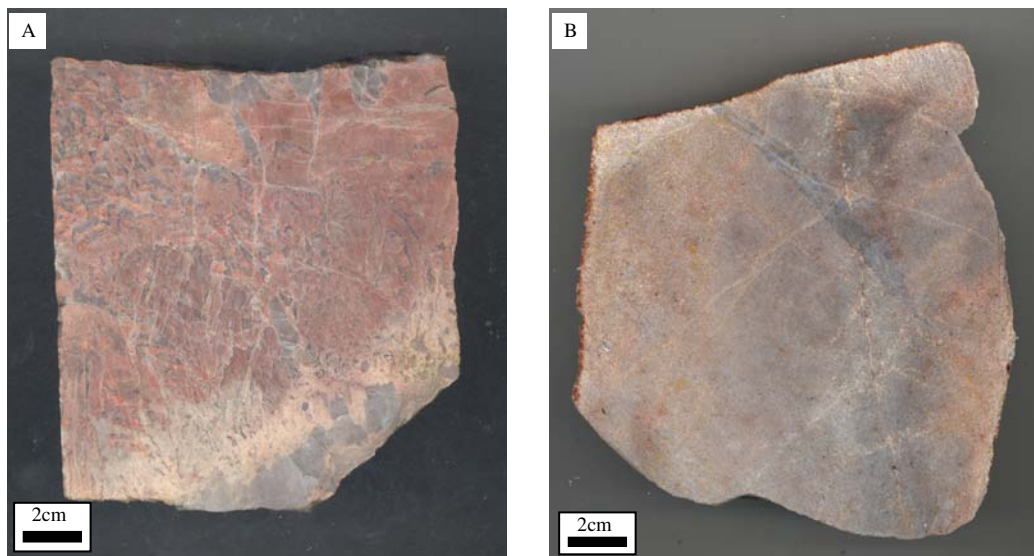
**Pegmatites:** Fluid inclusions from four different pegmatite samples were studied, including two from the SIC and two from the MAIC. Primary quartz, albite and microcline are the major minerals in all the pegmatites with traces of magnetite/hematite and mafic minerals (Fig.6.2A).

**Aplite:** An aplite sample was collected from the SIC (Fig.6.2B). The rock has fine grained equigranular primary quartz and albite with microcline and rare Fe-oxides.

**Quartz Vein:** One sample of quartz vein was studied from the SIC. The vein consists of large subhedral quartz grains with abundant fluid inclusions and the vein cuts the granite.



**Figure 6.1:** Representative igneous rocks analysed for fluid inclusions. **6.1A:** Mt. Angelay granite-Sample JB 4 (WPT 020); **6.1B:** Mixed-mingled rock from SIC- WPT 098 (Magma mingling outcrop 1- Chapter 2- Fig. 2.3); **6.1C:** Brain rocks of MAIC- WPT 134.



**Figure 6.2A:** Pegmatite from the SIC-Sample JB 36 (WPT 097); **6.2B:** Aplite with cross cutting quartz vein from the SIC-Sample JB 88D (WPT 142).

## 6.4. Methodology

### *6.4.1. Petrography & Microthermometry*

Petrography and microthermometric analyses of fluid inclusions were carried out in the School of Earth & Environmental Sciences, James Cook University. The microthermometric analyses were undertaken on a Linkam MDS600 heating-freezing stage with liquid nitrogen as the cooling agent. The stage is coupled to a BX51 Olympus polarizing microscope and to a PC which performs all stage operations with Linksys software. The thermocouple was calibrated regularly between temperatures of  $-56.6^{\circ}\text{C}$  and  $374.1^{\circ}\text{C}$  using synthetic  $\text{CO}_2$  and pure  $\text{H}_2\text{O}$  standards. The precision of the temperatures for both  $\text{CO}_2$  and  $\text{H}_2\text{O}$  was better than  $\pm 0.1^{\circ}\text{C}$  at heating rates of  $0.5^{\circ}\text{C}/\text{minute}$ . In total, 216 fluid inclusions were analysed and the data are tabulated in appendix 5.

The microthermometric interpretations of fluid inclusions are based on three assumptions: 1) a homogenous fluid composition at the time of fluid entrapment; 2) no addition or loss of material from the inclusion after the entrapment; and 3) no change in volume of the inclusion after fluid trapping. The analysis includes heating and freezing of fluid inclusions with observations of phase changes. The temperatures for various phase changes provide information about the fluid composition, salinity, density and P-T conditions at the time of fluid entrapment. To avoid decrepitation problems, freezing experiments were performed first on all the inclusions followed by heating.

Fluid inclusion groups were initially classified based on the phases present at room temperature (Shepherd et. al., 1985). This preliminary sorting is followed by the paragenetic classification of Roedder (1984) for primary, pseudo-secondary and



secondary inclusions. Primary fluid inclusions are entrapped during the growth of a crystal and they appear as clusters or along the growth zones of a mineral. These inclusions represent the actual composition of the fluid from which the host mineral is formed. Secondary inclusions develop after the growth of a crystal and are generally observed as healed fractures or trails which cross cut the boundaries of the host mineral. Pseudo-secondary fluid inclusions also form along healed fractures, but before the crystal growth has terminated. These inclusions can be identified as trails within the host mineral that do not cross the mineral boundary.

#### *6.4.2 Estimation of salinity, density and P-T conditions*

Microthermometric results of fluid inclusions were used to calculate the salinity, density and chemical composition of two phase (L+V), three phase (L+V+S) and multisolid fluid inclusions using the following programs;

1. ***Calcicbrine***-designed for fluids in the H<sub>2</sub>O-NaCl-CaCl<sub>2</sub> system (Naden, 1996), and
2. ***BULK***-designed for various fluids and salts in complex fluid systems (Bakker, 2003).

Fluid inclusions with eutectic values  $\leq -55^{\circ}\text{C}$  have both NaCl and CaCl<sub>2</sub> and the salinities of these inclusions were calculated with Calcicbrine. This program allows the calculation of NaCl and CaCl<sub>2</sub> concentration individually and the salinity is expressed as their sum in wt%. For the salinity calculation of two phase (L+V) inclusions, the program requires ice melting and hydrohalite melting temperatures, but hydrohalite dissolution was not observed in the majority of the two phase inclusions, likely resulting from its metastability. In this case, a value of 0.1 was used, which is the maximum stability limit of hydrohalite. The salinities of three phase (L+V+S) and multisolid inclusions were

calculated with ice melting and halite melting temperatures. *CalcicBrine* was developed using concepts and experimental data presented in Bodnar et al., 1989, Oakes et al., 1990, Vanko et al., 1988 and Yanatieva, 1964.



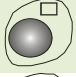




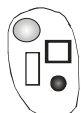
The program BULK calculates salinities of fluid inclusions with eutectic values  $> -55$  °C. In this case, NaCl was assumed as the only salt present in the system and calculations were made based on ice melting temperature and total homogenization temperature. The equations of state used in this calculation are described in Zhang & Frantz, 1987, Wagner & Pruss, 1993, Krumgalz et al., 1996 and Bodnar 1993. The program also allows the calculation of density and molar volume of fluid inclusions. The eutectic temperatures and micro-analytical techniques (see next Chapter) show the presence of a number of other salts (KCl, MgCl<sub>2</sub>, FeCl<sub>2</sub>), but with microthermometry, the exact estimation of these salts is not possible. A large number of two phase (L+V) fluid inclusions are treated by this method and the salinities are expressed as NaCl wt%, even though the fluids represent a more complex system than H<sub>2</sub>O-NaCl. The densities of CO<sub>2</sub>-bearing fluid inclusions were also calculated with BULK, which requires the total homogenization temperature of CO<sub>2</sub>, and the equations of state are described by Span & Wagner, 1996 and Duschek et al., 1990.

The isochores were calculated using ISOC program, which is designed for isochore calculation in fluid systems (Bakker, 2003) and the results were compared with independent geothermometers (see below) to understand the entrapment conditions. The equations of state for the calculation of isochores are described by Span & Wagner, 1996.

## 6.5. Results

### 6.5.1. Classification of fluid inclusions

Based on the composition of the fluid, number of phases present at room temperature and paragenesis, fluid inclusions are classified into four major groups (tables 6.2 & 6.3).

Type		Phases	Origin	Size ( $\mu\text{m}$ )	Fluid inclusion
<b>Type I</b> <b>CO<sub>2</sub> bearing</b>	Type I a	CO <sub>2</sub> (L)	P & PS	<5 – 15	
	Type I b	CO <sub>2</sub> +H <sub>2</sub> O	P & PS	<5 – 25	
	Type I c	CO <sub>2</sub> + H <sub>2</sub> O+S	P & PS	<10 – 30	
<b>Type II</b> <b>Two phase</b>	Type II a	L+V	P	<5 – 20	
	Type II b	L+V	S	<5 – 20	
<b>Type III</b> <b>Three phase</b>	Type IIIa	L+V+S	P	<5 – 30	
	Type IIIb	L+V+S	S	<5 – 40	
<b>Type IV</b> <b>Multisolid</b>	Type IV	L+V+MS	P & PS	<5 – 30	

**Table 6.2:** Summary and classification of different fluid inclusion types observed in the SIC and MAIC rocks. This grouping was made based on petrographic and microthermometric observations. Abbreviations: P-Primary; S-Secondary; PS-Pseudo-secondary; L-Liquid; V-Vapour; S-Solid; MS-Multi-solid.

	Mt. Angelay granites	Mt. Angelay brain rocks	Mt. Angelay pegmatites	Saxby granites	Saxby mixed-mingled rocks	Saxby pegmatites	Saxby aplite	Saxby quartz vein
<b>Type I a</b>	Common	Common	Common	Common	Common	Common	Common	Common
<b>Type I b</b>	-	Rare	-	-	Rare	-	Rare	Rare
<b>Type I c</b>	Rare	Rare	-	-	-	-	-	Rare
<b>Type II a</b>	-	Rare	-	-	-	-	-	Rare
<b>Type II b</b>	Common	Common	Common	Common	Common	Common	Common	Common
<b>Type IIIa</b>	-	Rare	-	-	-	-	-	-
<b>Type IIIb</b>	Abundant	Abundant	Abundant	Abundant	Abundant	Abundant	Abundant	Abundant
<b>Type IV</b>	-	Abundant	-	Rare	-	-	-	-

*Table 6.3: Relative abundance of fluid inclusions in various rock types from the SIC and MAIC.*

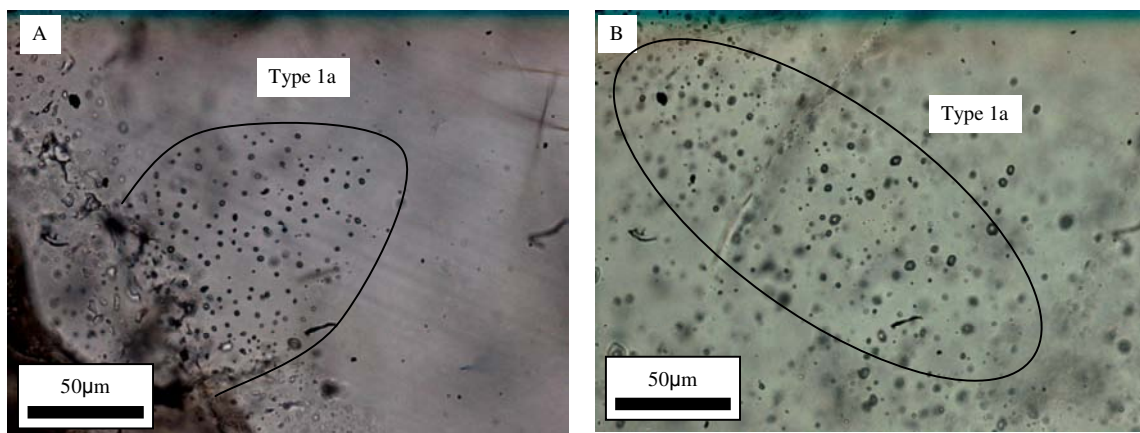
#### **6.5.1.1. Type 1: CO<sub>2</sub>-bearing fluid inclusions**

CO<sub>2</sub>-bearing fluid inclusions are primary in origin and sub classified into CO<sub>2</sub>-only inclusions (1a), mixed CO<sub>2</sub>-H<sub>2</sub>O inclusions (1b) and mixed CO<sub>2</sub>-H<sub>2</sub>O brine inclusions (1c). The CO<sub>2</sub>-only inclusions are common in all the samples where as the latter two inclusion types are present exclusively in brain rocks and are comparatively rare. Type 1a, 1b and 1c fluid inclusions are individually observed along pseudosecondary trails, but in many instances, they occur together at three dimensional spaces. They are generally oval or square in shape, but variable in sizes.

##### ***a. Type 1a-CO<sub>2</sub> only inclusions***

Type 1a inclusions are the most common primary fluid inclusion type in all the rock samples (Fig.6.3A & B). At room temperature most of them contain a single CO<sub>2</sub>-bearing liquid phase with a vapour bubble nucleating upon cooling, but those inclusions which recorded a homogenization temperature  $\geq 30^{\circ}\text{C}$  (see below) contain a CO<sub>2</sub> bubble at room temperature. The inclusions are normally  $\leq 15\mu\text{m}$  in size and commonly occur in isolated primary clusters and along rare pseudo-secondary trails. A total of 41 type 1a inclusions are analysed from various rock types.

The CO<sub>2</sub> melting temperatures of type 1a inclusions vary from  $-52.8$  to  $-58.8^{\circ}\text{C}$  (Fig. 6.4A). The inclusions homogenized by the disappearance of CO<sub>2</sub> vapour bubble to the liquid CO<sub>2</sub> phase. The total homogenization temperatures of primary CO<sub>2</sub>-only inclusions (Fig. 6.4B) from Mt. Angelay range from  $-10.5$  to  $18.2^{\circ}\text{C}$  which correspond to high densities from  $0.98$  to  $0.79$  g/cc. The CO<sub>2</sub>-only inclusions from brain rocks



**Figure 6.3A:** Type 1a fluid inclusions in a quartz crystal in Saxby granite-Sample JB 79B; **6.3B:** Cluster of type 1a fluid inclusions in Mt. Angelay Granite-Sample JB 4.

homogenize from 22.4 to 30.1 and have densities between 0.75 and 0.59 g/cc. Pegmatites from the MAIC have type 1a fluid inclusions with homogenization temperatures and densities varying between the above two rock types. The CO<sub>2</sub>-only fluid inclusions from pegmatites and quartz veins of the SIC also show values similar to those from Mt. Angelay. No type 1a inclusions were studied from Saxby granite because of their small size.

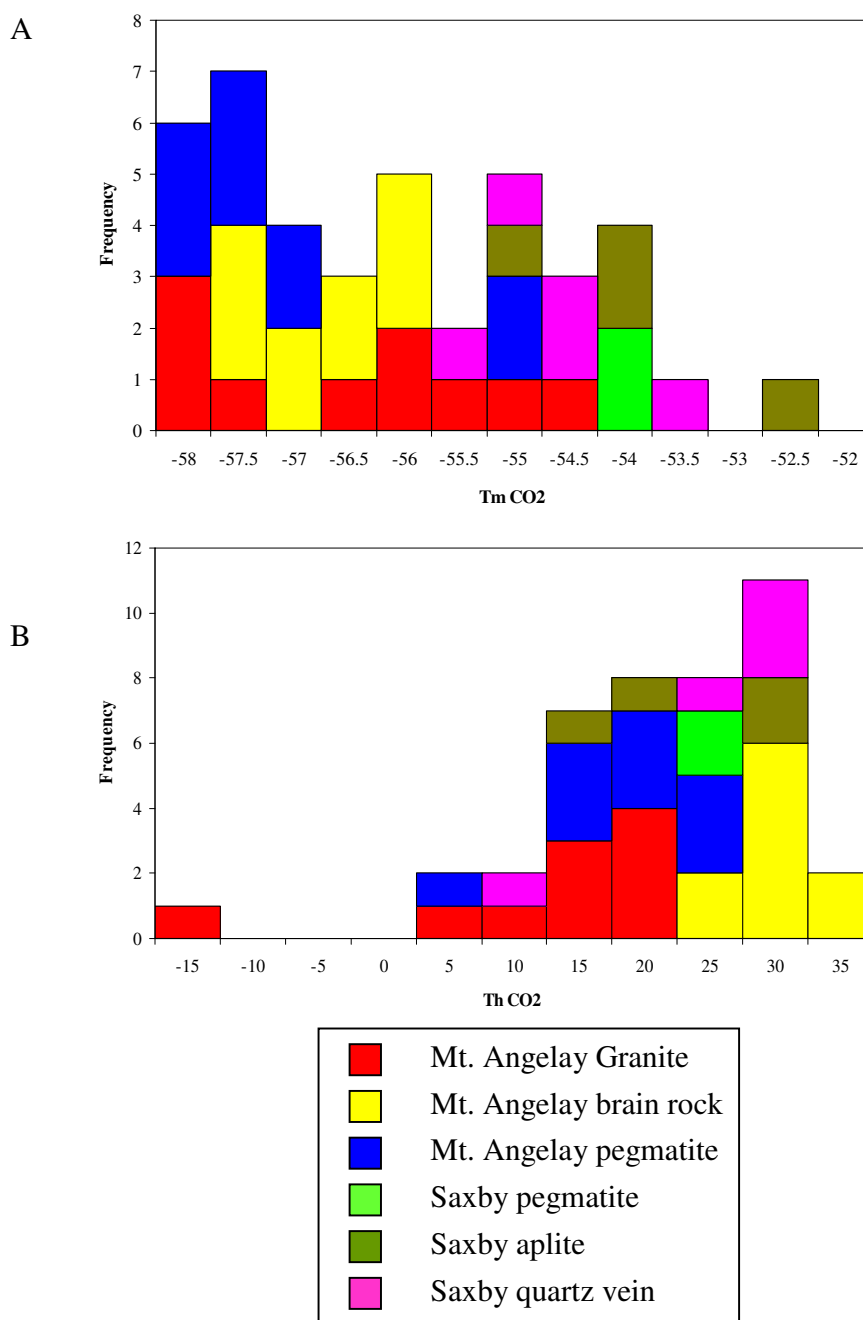
***b. Type 1b-Mixed CO<sub>2</sub>-H<sub>2</sub>O inclusions***

Type 1b fluid inclusions are two phase at room temperature with CO<sub>2</sub> liquid (a CO<sub>2</sub> vapour bubble develops upon cooling) and H<sub>2</sub>O liquid phases. The inclusion size varies from <5 to 25µm and the bubble size commonly ranges from 80 to 90%. These inclusions are observed along pseudo-secondary trails and in three dimensional clusters with type 1a inclusions (Fig. 6.5A, B, C & D).

The microthermometric data from type 1b are restricted because they are rare and commonly decrepitate at temperatures between 350 and 450°C. Only three mixed CO<sub>2</sub>-H<sub>2</sub>O inclusions were analysed and they show CO<sub>2</sub> melting temperatures of -56.4, -55.7 and -55.9°C, and CO<sub>2</sub> homogenization temperatures of 26.9, 27.1 and 27.6°C respectively (Fig. 6.6A & B). The CO<sub>2</sub> homogenization occurred by the disappearance of vapour bubble into the CO<sub>2</sub> liquid phase. Most of the mixed CO<sub>2</sub>-H<sub>2</sub>O inclusions have about 80-90% CO<sub>2</sub> and so the observation of first melting temperatures and the formation of clathrates are extremely difficult during microthermometry. First melting of the aqueous phase was observed in only one inclusion and was -51.3°C, which suggests the presence of cations besides Na<sup>+</sup> (e.g. Ca<sup>+</sup>). One inclusion homogenized to the CO<sub>2</sub> liquid phase at temperature 256.7°C. The decrepitation temperatures of the other two inclusions were 363.7 and 426.8°C. Salinity estimations are not possible without clathrate melting temperatures, which were not observed.

***c. Type 1c: Mixed H<sub>2</sub>O-CO<sub>2</sub>-brine inclusions***

CO<sub>2</sub> bearing brine inclusions consist of two immiscible liquids and a solid phase at room temperature. The immiscible liquids are CO<sub>2</sub> (a CO<sub>2</sub> vapour bubble develops upon cooling) and H<sub>2</sub>O, and the solid phase appears to be halite. Type 1c fluid inclusions range in size from <10 to 30µm and found in three dimensional groups with type 1a and 1b fluid inclusions (Fig. 6.5E). They are also observed along pseudo-secondary trails by themselves.



**Figure 6.4A:** CO<sub>2</sub> melting temperatures of type 1a fluid inclusions. The rock types do not show much variation in CO<sub>2</sub> melting temperatures; **6.4B:** CO<sub>2</sub> homogenization temperatures of type 1a fluid inclusions. Homogenization was to the liquid phase in all cases. The graph shows that the brain rock inclusions homogenized at high temperatures compared to Mt. Angelay granite. The other rocks span over wide ranges.



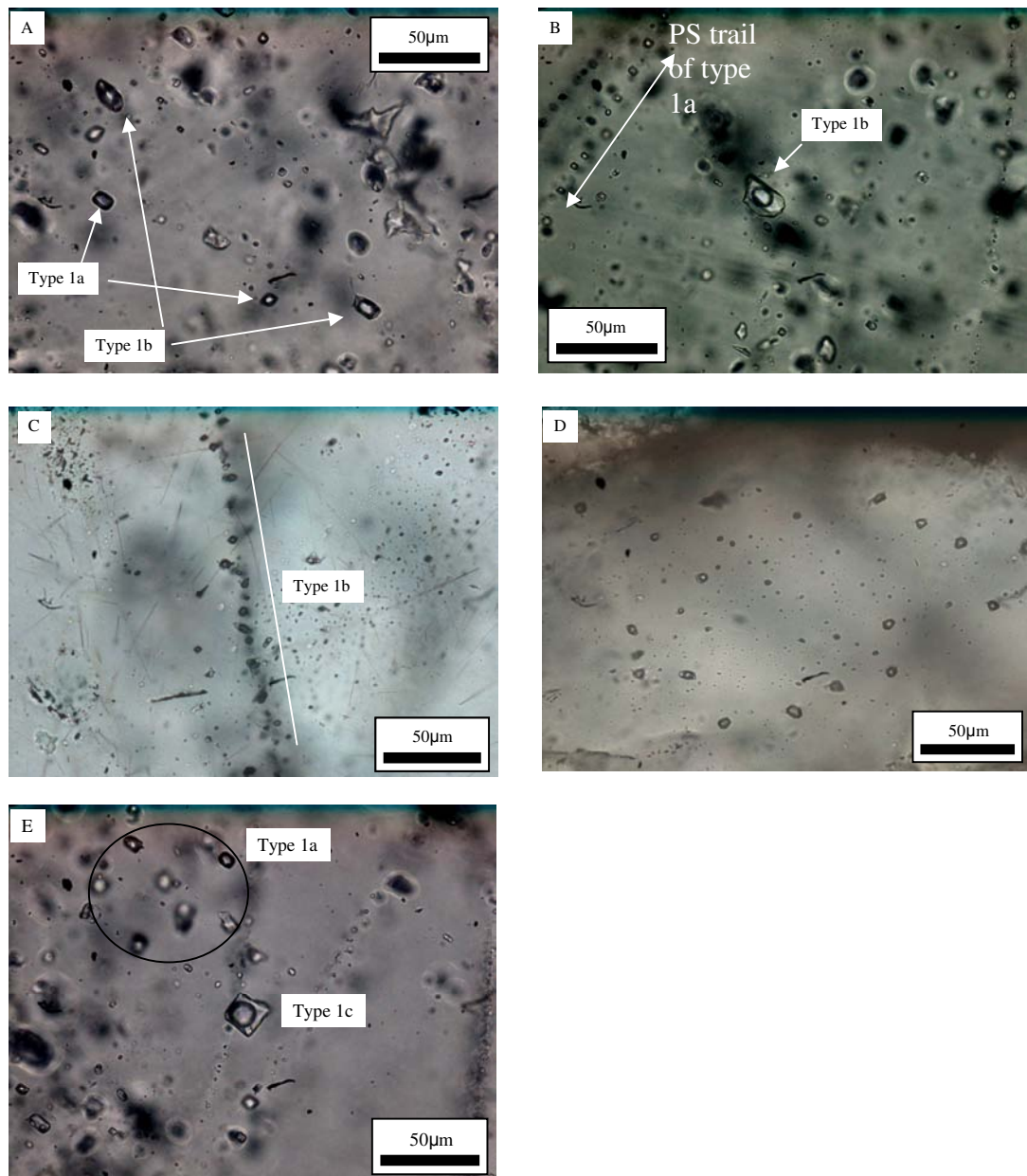
Like type 1b fluid inclusions, the microthermometric data from type 1c inclusions are also limited because of their scarcity. The microthermometric results of type 1c inclusions include four fluid inclusions only with CO<sub>2</sub> melting between -54.7 and -57.8°C (Fig. 6.6A). First melting temperatures were recorded from two fluid inclusions and are -52.5 and -36.2°C. Similarly two of the inclusions show clathrate melting temperatures at -8.2 and -12.3°C. All the four inclusions have shown metastable hydrohalite melting temperatures ranging from -8.7 to 8.3°C. The melting of hydrohalite at temperatures  $\geq 0.1$  may be due to the presence of additional salts in the system. The CO<sub>2</sub> homogenization occurred via disappearance of the CO<sub>2</sub> vapour into the CO<sub>2</sub> liquid phase at temperatures ranging from 27.1 to 29.2°C (Fig. 6.6B). The total homogenization temperatures for the type 1c inclusions were not observed as most decrepitated before homogenizing, but one inclusion homogenized at 235°C by halite homogenization. The low eutectic temperatures from some of the type 1c inclusions indicate the presence of CaCl<sub>2</sub>.

#### **6.5.1.2. Type 2-Two phase (L+V) fluid inclusions**

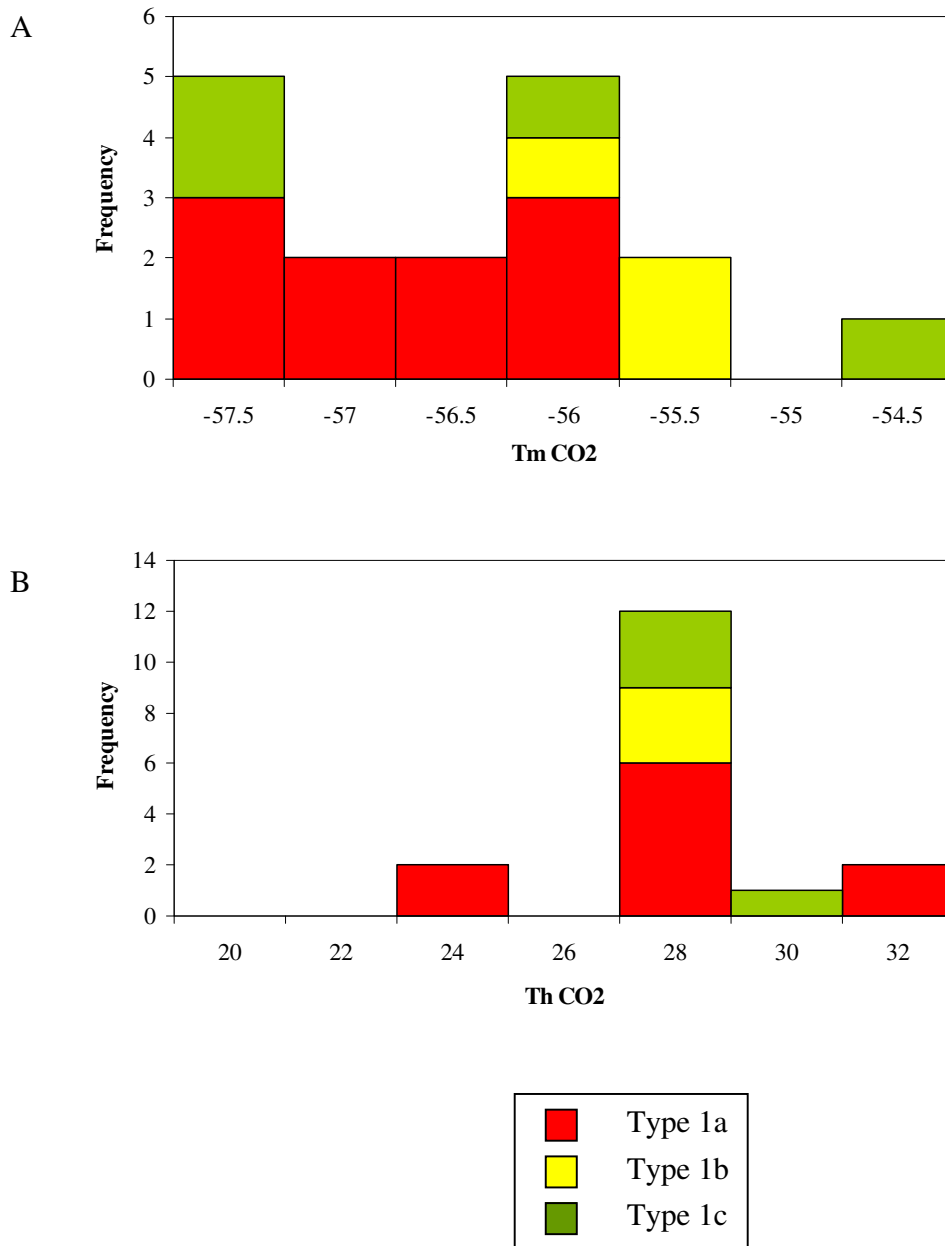
##### ***a. Type 2a-Primary two phase (L+V) inclusions***

Two phase primary fluid inclusions (type 2a) are rare and display higher homogenization temperatures than type 2b inclusions. They occur in random isolated groups and as isolated inclusions within the quartz grains of brain rocks. The vapour bubbles of these inclusions occupy 5-10% of the total inclusion in type 2a, whereas in type 2b vapour occupies closer to 15-20%. The liquid-vapour ratio and higher

homogenization temperatures of type 2a inclusions distinguish them from type 2b inclusions.



**Figure 6.5A:** Assemblage of type 1a and type 1b fluid inclusions in brain rocks-Sample JB 61; **6.5B:** A typical type 1b fluid inclusion from brain rock-Sample JB 64; **6.5C:** Pseudo secondary trail of type 1b fluid inclusions-Sample JB 88D; **6.5D:** Cluster of type 1b fluid Inclusions-JB 79B; **6.5E:** Co existence of type 1a and type 1c fluid inclusions in Mt. Angelay brain rocks-Sample JB 61.



**Figure 6.6A:** CO<sub>2</sub> melting temperatures of type 1a, 1b & 1c fluid inclusions from brain rocks; **6.6B:** CO<sub>2</sub> homogenization temperatures of type 1a, 1b & 1c fluid inclusions from brain rocks.

Type 2a inclusions have eutectic temperatures between  $-30$  and  $-25.3^{\circ}\text{C}$  (Fig.6.9) and final ice melting temperatures from  $-6.8$  to  $-1^{\circ}\text{C}$  (Fig.6.10A). Hydrohalite melting was not observed in these inclusions. The total homogenization of these inclusions occurred by the disappearance of the vapour bubble into the liquid phase at temperatures ranging from  $245$  to  $325^{\circ}\text{C}$  (Fig.6.11A & B). These inclusions have low salinities between  $1.7$  and  $10.2$  wt% NaCl equiv.

***b. Type 2b: Secondary two phase (L+V) inclusions***

Type 2b fluid inclusions are inferred to be the last phase of fluid activity in the study area as they crosscut all other inclusion types and mineral boundaries (Fig. 6.7A & B). They are clearly secondary in origin and common in all the samples. The inclusion size varies from  $<5$  to  $20\mu\text{m}$ .

The first melting of type 2b fluid inclusions spanned over a broad range of temperatures ranging from  $-76.8$  to  $-7.9^{\circ}\text{C}$  (Fig.6.9). Type 2b inclusions with very low eutectic temperatures display a brown colour and granular appearance during cooling, confirming the presence of  $\text{CaCl}_2$  and other divalent salts. The final ice melting temperatures are between  $-38.9$  and  $-0.2^{\circ}\text{C}$  (Fig.6.10A). During heating, the formation of metastable hydrohalite is observed in inclusions with very low eutectic temperatures. The melting of hydrohalite was recorded in between  $2.4$  and  $8.5^{\circ}\text{C}$  (Fig.6.10B) and the total homogenization is from  $100$  to  $225^{\circ}\text{C}$  (average of  $140$  to  $175^{\circ}\text{C}$ ) (Fig.6.11A & B). Salinities of type 2b inclusions with low eutectic temperatures range from  $25.9$  to

30.8 wt% NaCl+CaCl<sub>2</sub> equiv. For fluid inclusions with higher eutectic values, salinities range from 2.7 to 23.1 wt % NaCl equiv.

### **6.5.1.3. Type 3: Halite bearing three phase (L+V+S) fluid inclusions**

#### ***a. Type 3a Primary three phase inclusions***

Primary halite bearing fluid inclusions are rarely observed and are exclusively present in brain rocks. They display variable sizes and L-V-S ratios, and are observed in isolated groups or with primary multisolid inclusions (Fig. 6.7C).

The first melting temperatures of type 3a fluid inclusions range between -69 and -53.2 °C (Fig.6.9) and indicate the presence of CaCl<sub>2</sub> in addition to NaCl. The formation of brown ice and the granular appearance during cooling confirm the presence of CaCl<sub>2</sub> in the fluid. The final ice melting temperatures range from -33.8 to -21.9 °C (Fig.6.10A) with metastable hydrohalite melting close to 12 °C (Fig.6.10B). Upon heating most of the type 3a inclusions decrepitated before total homogenization. The decrepitation temperatures range from 375 to 495 °C. The vapour bubble consistently disappears before the dissolution of halite. The vapour homogenization temperatures range from 145 to 165 °C (Fig.6.11A) with halite dissolution between 310 and 390 °C (Fig.6.11B). Calculated salinities of these inclusions vary from 41.5 to 46.1 wt% NaCl+CaCl<sub>2</sub> equiv with NaCl ranging from 32.5 to 45.1 wt% equiv. and CaCl<sub>2</sub> from 1.1 to 12.3 wt% equiv.

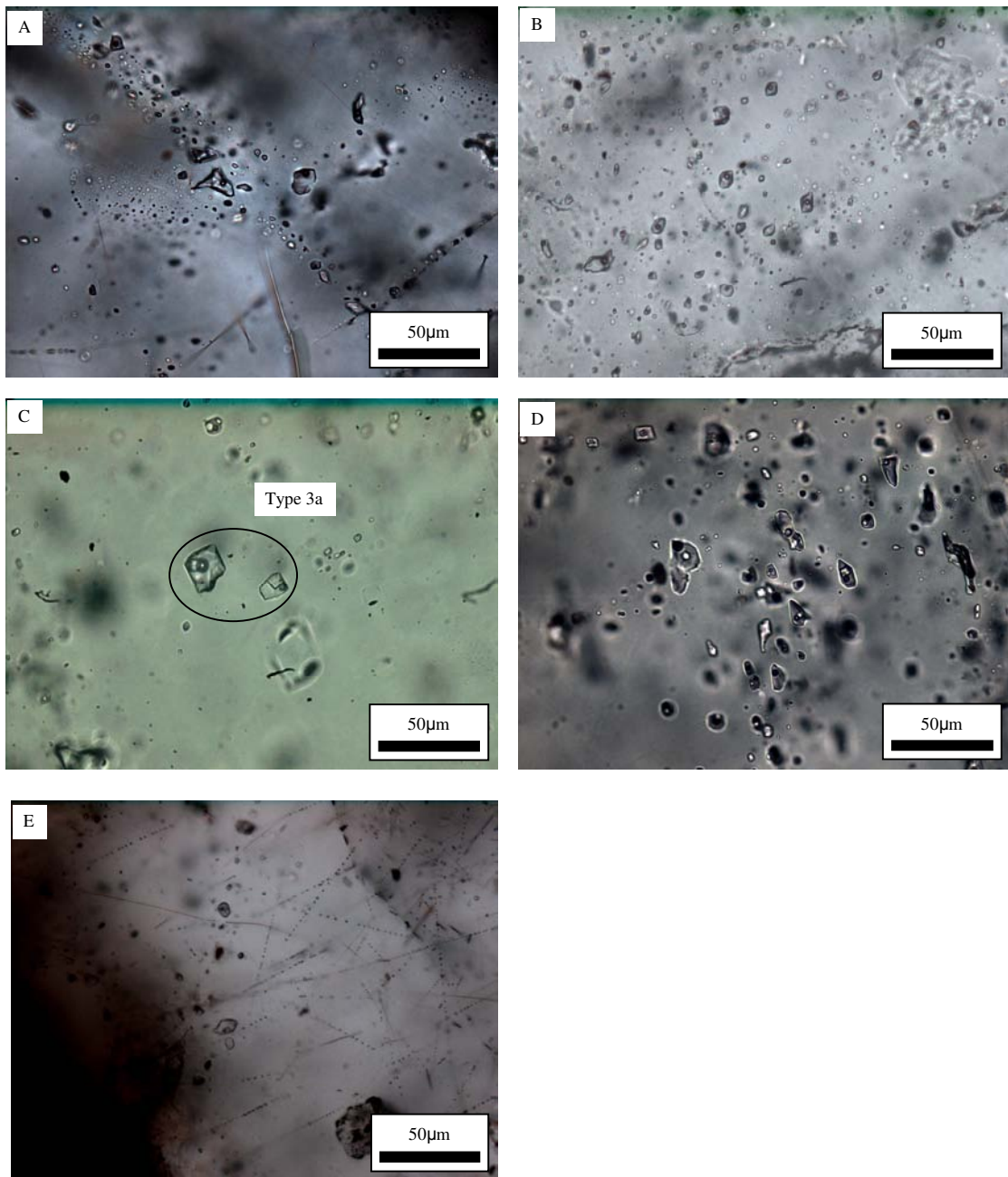
***b. Type 3b Secondary three phase inclusions***

Type 3b inclusions are the most abundant fluid inclusion type in all the samples. They generally occur as trails which cross cut multiple mineral grains (Fig. 6.7D & E), but are cut by Type 2b (L + V) inclusion trails. These inclusions are interpreted as secondary and show a similar L: V: S ratio in all the rocks. The inclusions range from <5 to 30  $\mu\text{m}$  and are oval, elliptical, and occasionally are irregular.

Type 3b inclusions display a wide range of eutectic temperatures. The eutectic temperatures of type 3b fluid inclusions vary from -86.9 to -25.9  $^{\circ}\text{C}$  with the majority between -62 and -73  $^{\circ}\text{C}$  (Fig.6.9). Again, such low eutectic temperatures reflect the presence of  $\text{CaCl}_2$  in addition to  $\text{NaCl}$ . The final ice melting temperatures range from -44.6 to -0.3  $^{\circ}\text{C}$  with an average between -21 and -33  $^{\circ}\text{C}$  (Fig.6.10A). Hydrohalite was metastable in all the inclusions with melting temperatures from 1.9 to 29.3  $^{\circ}\text{C}$  (average between 6 and 13 $^{\circ}\text{C}$ ) (Fig.6.10B). Total homogenization was through halite dissolution in all the inclusions. Vapour homogenization ranges from 120 to 185  $^{\circ}\text{C}$  (Fig.6.11A) and halite dissolution occurs between 140 and 275  $^{\circ}\text{C}$  (average between 180-230  $^{\circ}\text{C}$ ) (Fig.6.11B). Calculated salinities range from 29.1 to 42.7 wt%  $\text{NaCl} + \text{CaCl}_2$  equiv. with  $\text{NaCl}$  values vary from 16.7 to 32.2 wt% equiv. and  $\text{CaCl}_2$  from 2.1 to 18.4 wt% equiv.

**6.5.1.4. Type 4-Multisolid fluid inclusions**

Multisolid fluid inclusions are between <5 and 30  $\mu\text{m}$  in size and consist of a liquid phase, a vapour bubble and up to eight solid phases at room temperature. Halite is

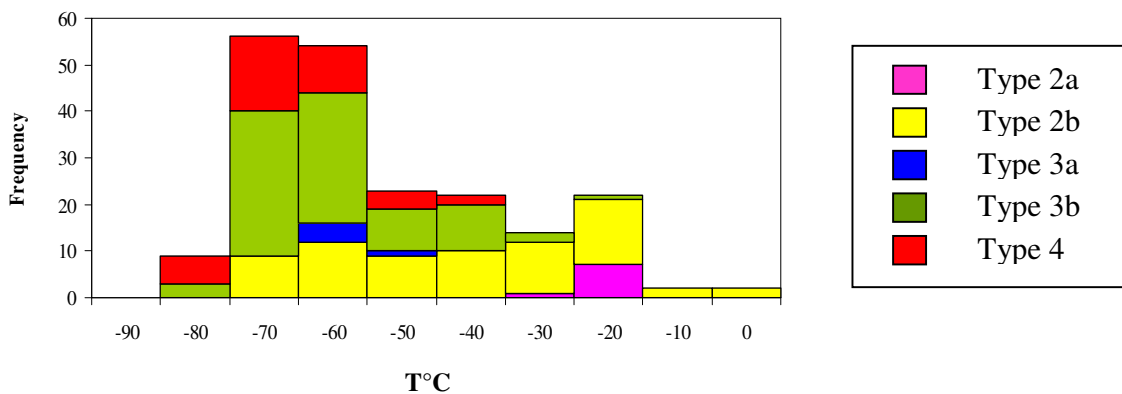
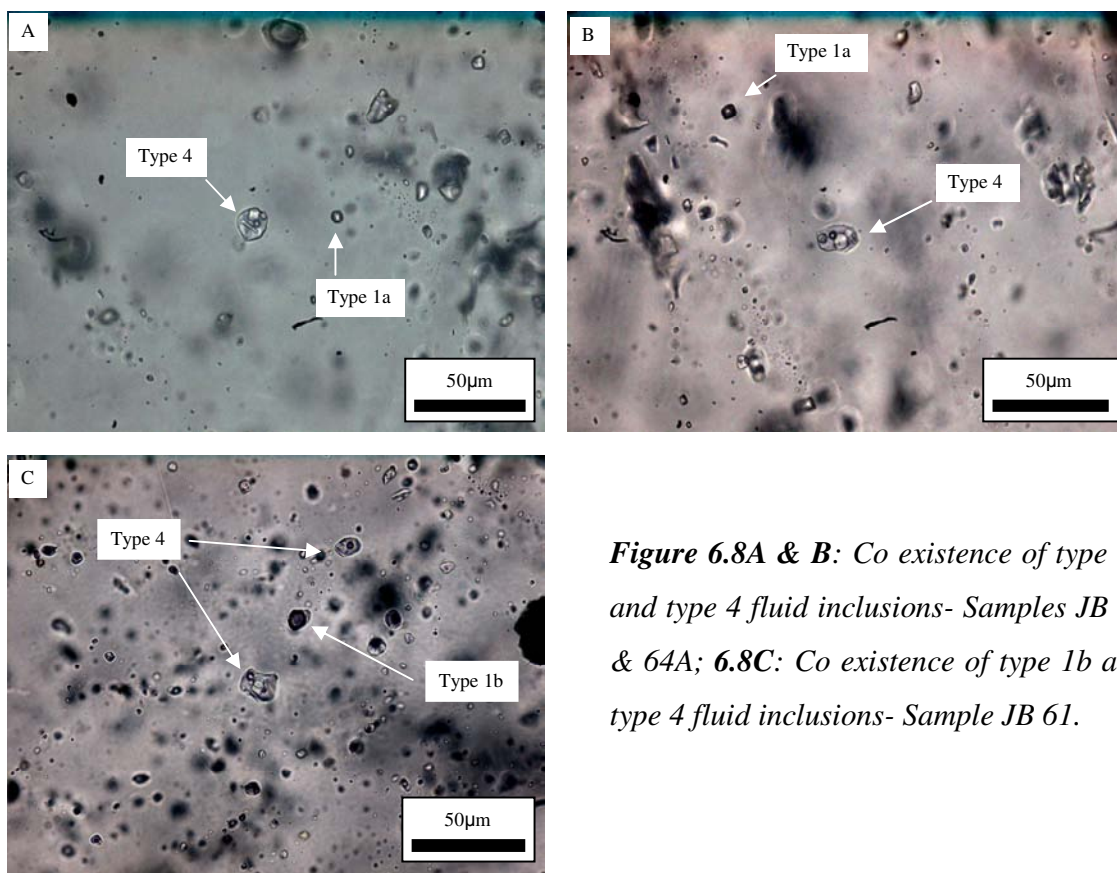


**Figure 6.7A & B:** Secondary L+V inclusion trails which cross cut the entire crystal-Samples JB 37A1 and JB 6D; **6.7C:** Type 3a fluid inclusions with different L+V+S ratios. These are different from abundant secondary L+V+S inclusions and typically observed in brain rocks-Sample JB 61; **6.7D:** Secondary cluster of L+V+S inclusion-Sample JB 64A; **6.7E:** Secondary trail of L+V+S inclusions-Sample JB 37A1.

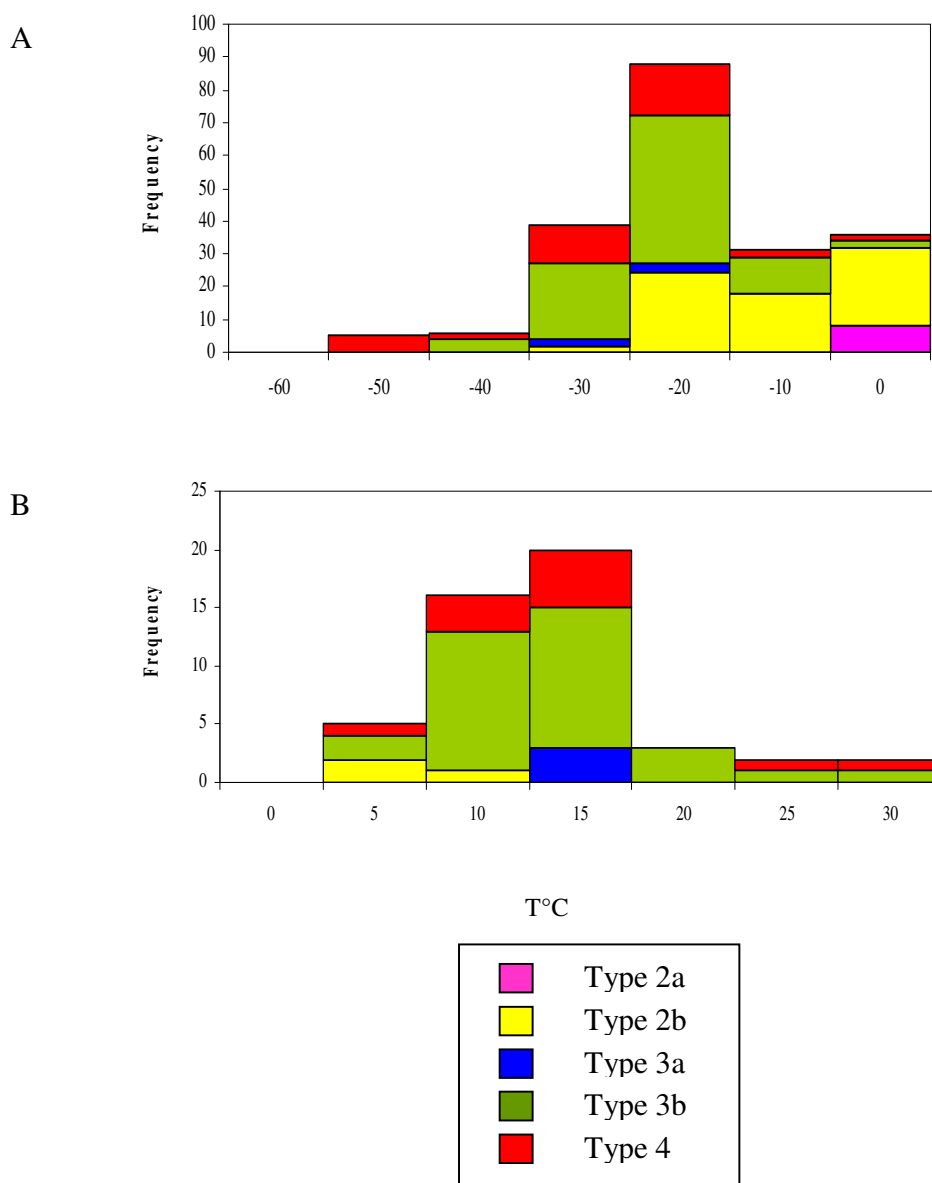
always present and frequently occupies up to 50% of the total inclusion volume. Other common daughter phases include sylvite and calcite, identified by their habit and relief. In all multisolid inclusions, 80% of the total inclusion volume is occupied by solids and the vapour bubble is 10-15%. The multisolid inclusions are commonly interpreted as primary and rarely as pseudo-secondary and are generally observed as clusters or groups and along pseudo-secondary trails. They often found associated with type 1 fluid inclusions (Fig. 6.8A, B & C). Type 4 fluid inclusions are abundant in Mt. Angelay brain rocks and are rare in the Saxby and Mt. Angelay granites.

Type 4 fluid inclusions have low eutectic temperatures ranging from -72 to -88.1 °C (Fig.6.9), which indicates the presence of salts other than CaCl<sub>2</sub> and NaCl. The final ice melting temperatures of these inclusions are between -24.9 and -53.9 °C (Fig.6.10A) with metastable hydrohalite melting from 3.6 to 21.4 °C (Fig.6.10B). These inclusions homogenize by halite dissolution but the majority of inclusions decrepitated before total homogenization. Decrepitation temperatures range from 450 to 575 °C. Vapour homogenization temperatures are between 135 and 180 °C (Fig.6.11A) and halite dissolution temperatures are from 260 to 495 °C (Fig.6.11B). Salinities of multisolid inclusions are expressed as a sum of NaCl and CaCl<sub>2</sub> wt% equiv and the values range from 38.8 to 60.7, with NaCl concentrations from 22.1 to 59.9 wt% equiv. and CaCl<sub>2</sub> from 0.9 to 16.7 wt% equiv.

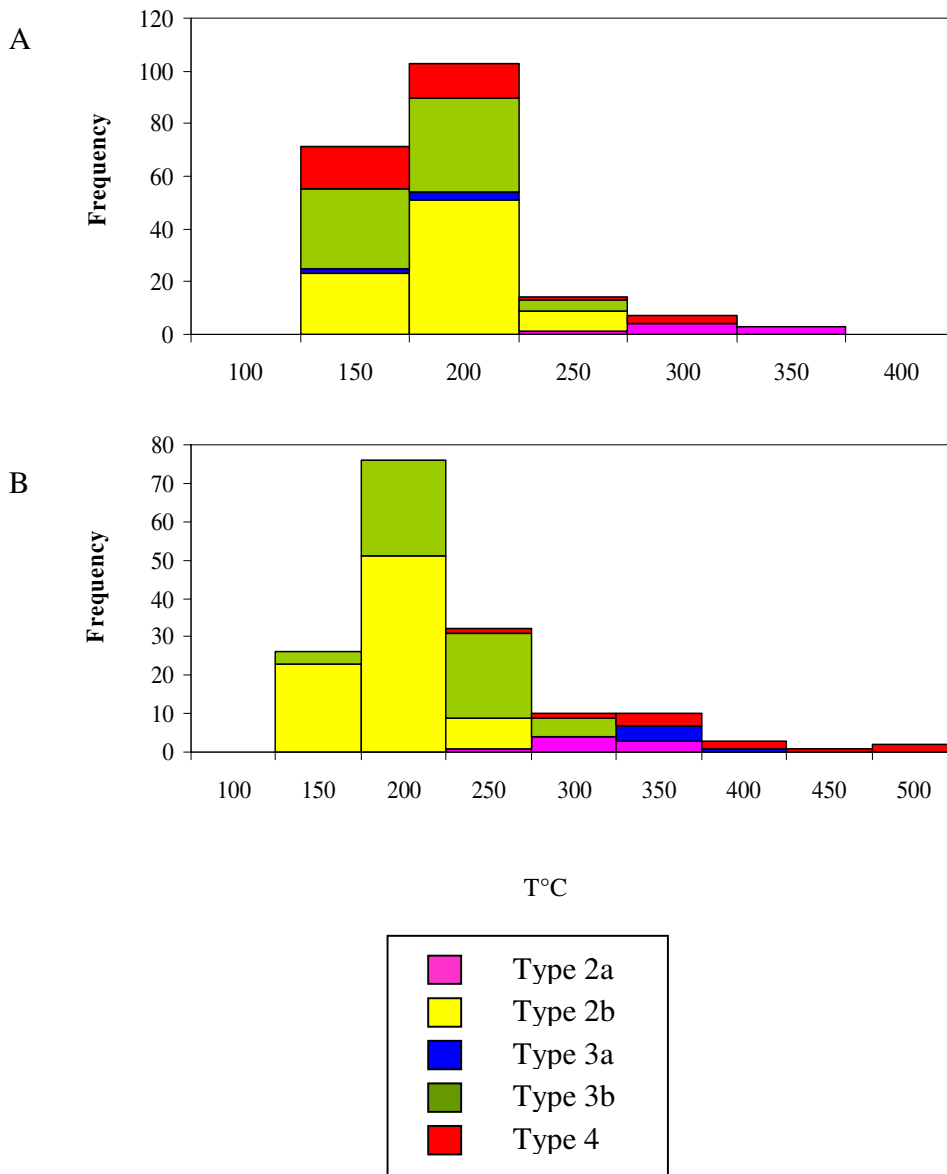




**Figure 6.9:** Eutectic temperatures of different fluid inclusions. Multisolid inclusions and halite bearing inclusions show very low eutectic temperatures compared to L+V inclusions.



**Figure 6.10A:** Final ice melting temperatures of different fluid inclusions; **6.10B:** Hydrohalite melting temperatures of different fluid inclusions. Majority of hydrohalite is reported from type 3b & 4 inclusions and the values show large ranges.



**Figure 6.11A:** Vapour homogenization temperatures of different fluid inclusion types; **6.11B:** Total homogenization temperatures of different fluid inclusion types. All the inclusions homogenized into liquid and type 3a & 4 inclusions show highest homogenization temperatures compare to secondary inclusions. Symbols as same as 6.9.

## 6.6. Discussion

The information on the compositional data and the physical conditions under which the various fluid inclusion generations were trapped are summarized in table 6. 4.






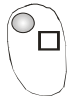
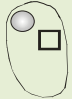
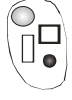
### *6.6.1. Estimation of pressure and trapping conditions*

Type 1a fluid inclusions represent the primary fluid types, which are widespread in all the rock types of the SIC or MAIC, and are used to calculate isochores and to estimate the pressure and temperature conditions at which the inclusions were trapped.

#### *a. Type 1a fluid inclusions*

Here, the data on CO<sub>2</sub> bearing fluid inclusions from Mt. Angelay granite, brain rocks and Mt. Angelay pegmatites are compared. Data on CO<sub>2</sub>-bearing inclusions from the SIC is limited because the CO<sub>2</sub>-bearing fluid inclusions from Saxby granite and mixed-mingled Saxby rocks were not large enough for microthermometry.

In this study, three independent geothermometers were used to constrain the trapping pressure estimates of type 1a fluid inclusions in different rock types, and the calculated isochores are plotted in figures 6.12A-D. The CO<sub>2</sub>-only fluid inclusions from granites were compared with geothermometry and geobarometry calculated by Rubenach et al. (2008) from the northwestern contact aureole of Saxby granite and with the maximum temperature determined for type 4 fluid inclusions (495°C). Rubenach et al. (2008) estimated a temperature of 670°C at 3 kbar pressure from the observed mineral assemblage K-feldspar-sillimanite-andalusite. This is the only available P-T estimation

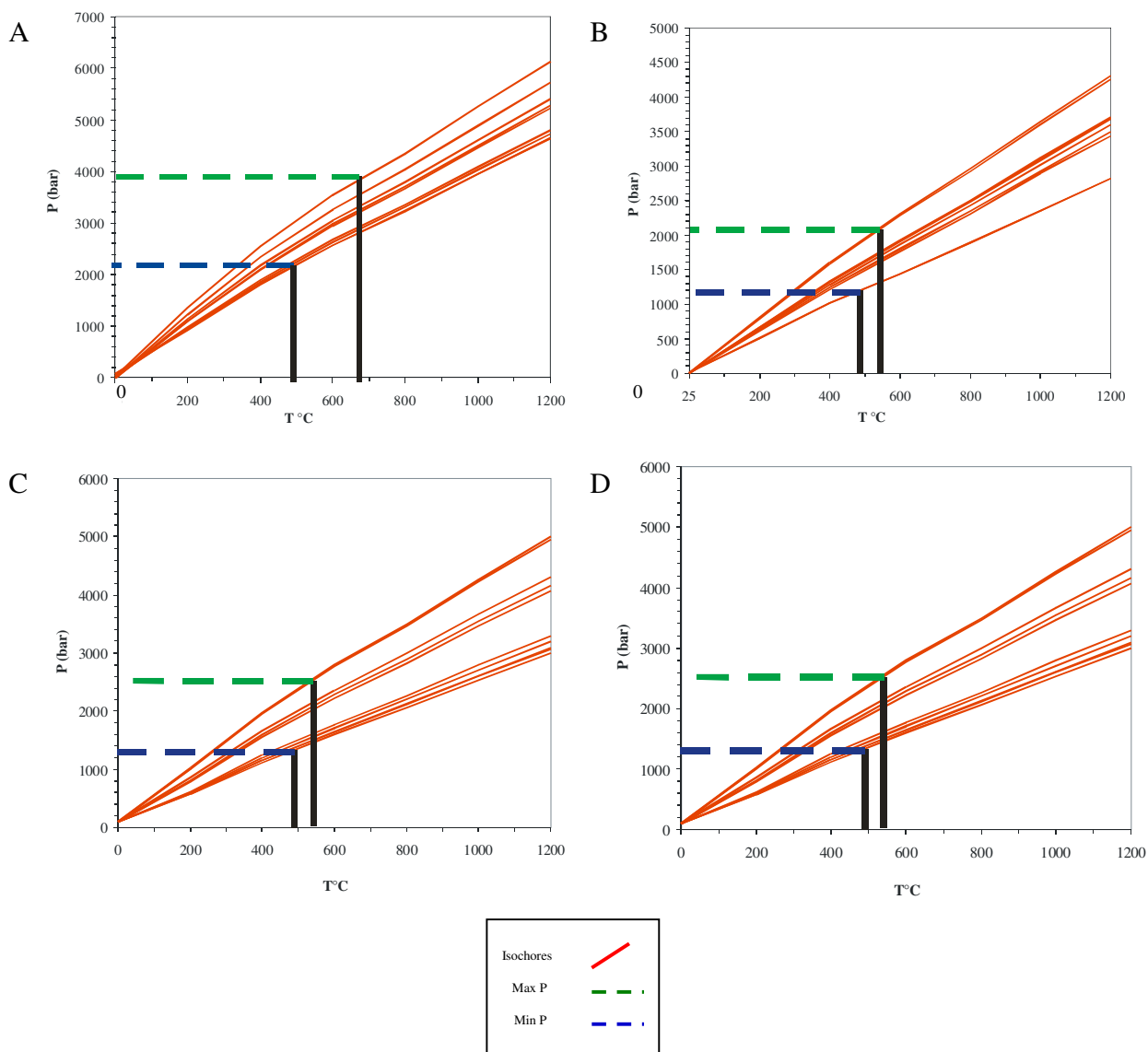
Fluid Inclusion Type	Origin	Description	Fluid properties
<b>Type I a: CO<sub>2</sub> (L)</b>	 P & PS	CO <sub>2</sub> rich inclusions with 1-2 phases at room temperature (<5 – 15) L (CO <sub>2</sub> )± V (CO <sub>2</sub> )	Th= -10.5- 30.1°C Density= 0.59- 0.99g/cc
<b>Type I b: CO<sub>2</sub>+H<sub>2</sub>O</b>	 P & PS	CO <sub>2</sub> rich inclusions with 1-3 phases at room temperature (<5 – 25) L (CO <sub>2</sub> )+L(H <sub>2</sub> O) ±V (CO <sub>2</sub> )	Th(CO <sub>2</sub> )= 26.9- 27.6°C Th= 256.7°C
<b>Type I c: CO<sub>2</sub>+H<sub>2</sub>O+S</b>	 P & PS	CO <sub>2</sub> rich inclusions with 1-4 phases at room temperature (<10 – 30) L (CO <sub>2</sub> )+L(H <sub>2</sub> O)+H±V (CO <sub>2</sub> )	Th(CO <sub>2</sub> )= 27.1- 29.2°C Th= 235.6°C
<b>Type II a: L+V</b>	 P	Liquid rich inclusions with 2 phases at room temperature (<5 – 20)	Moderate Th (240- 330°C) Saline (1-10 wt% NaCl equivalent) NaCl- KCl- CaCl <sub>2</sub>
<b>Type II b: L+V</b>	 S	Liquid rich inclusions with 2 phases at room temperature (<5 – 20)	Low- moderate Th (100- 230°C) Saline (1-30 wt% NaCl & NaCl+CaCl <sub>2</sub> equivalent) NaCl- KCl- CaCl <sub>2</sub>
<b>Type IIIa: L+V+S</b>	 P	Liquid rich inclusions with 3 phases at room temperature (<5 – 30) L+V+H	High Th (310- 390°C) Saline (40-46wt% NaCl+CaCl <sub>2</sub> equivalent) NaCl- KCl- CaCl <sub>2</sub> - FeCl <sub>2</sub> -MgCl <sub>2</sub>
<b>Type IIIb: L+V+S</b>	 S	Liquid rich inclusions with 3 phases at room temperature (<5 – 40) L+V+H	Moderate Th (150- 270°C) Saline (29-42wt% NaCl+CaCl <sub>2</sub> equivalent) NaCl- KCl- CaCl <sub>2</sub> - FeCl <sub>2</sub> -MgCl <sub>2</sub>
<b>Type IV: Multisolid</b>	 P	Multisolid inclusions with 2-8 phases at room temperature (<5 – 30) L+ V+ H± S±D	Moderate to high Th(220- 495°C and above) Hypersaline (38- 60wt% NaCl+CaCl <sub>2</sub> eq.) NaCl- KCl- CaCl <sub>2</sub> - FeCl <sub>2</sub> -MgCl <sub>2</sub>

**Table 6.4:** Summary of petrographic and microthermometric data for all fluid inclusion types. Abbreviations: P-Primary; S-Secondary; PS-Pseudo-secondary; L-Liquid; V-Vapor; S-Solid; H-Halite; S-Sylvite; D-Other salts; Th-Homogenization Temperature.

for the formation of younger granites in the district and is used to compare the inclusion trapping pressures for Mt. Angelay intrusions. When applying an isochoric temperature correction from 670°C to the maximum temperature of homogenization (495°C from type 4 inclusions), it indicates pressures between 2.2 kbar and 3.8 kbar (Fig. 6.12A). The maximum pressure (3.8 kbar) estimated from Mt. Angelay granite fluids is about 0.8 kbar higher than the pressure estimated from the Saxby contact aureole (3 kbar). It is difficult to judge how reliable this is because of uncertainty about the timing of development of the fluid inclusions in quartz relative to the timing of the peak contact metamorphism, and also because the two intrusions may have been emplaced at different pressures.

Independent geothermometers used for the isochores of type 1a fluid inclusions from pegmatites and Mt. Angelay brain rocks are the temperature estimates from oxygen isotope studies by Mark and Foster (2000), and the maximum temperature determined for type 4 fluid inclusions (495°C). Mark and Foster (2000) estimated a maximum temperature of 540°C for the oxygen isotope equilibrium of albite and quartz in the aplitic and pegmatitic components of albite-quartz-actinolite-apatite-rich rocks. These rocks form the carapace that caps a small dome-like intrusion of Roxmere pluton, which is part of the MAIC. These rocks are mineralogically and texturally similar to the brain rocks described in this study. Estimated pressures for type 1a inclusions from Mt. Angelay brain rocks using these two methods range from a maximum of about 2.1 kbar at 540°C to a minimum of approximately 1.3 kbar at 495°C (Fig.6.12B). Pegmatites,

aplitites and quartz veins from both MAIC and SIC show inclusion trapping pressures between 1.3 and 2.5 kbar (Fig.6.12C & D).



**Figure 6.12:** Pressure-temperature diagram for type 1a fluid inclusions from the SIC and MAIC. In each sample, the isochores were calculated from fluid inclusions of similar assemblages (In this thesis, the term fluid inclusion assemblage is used to represent a group of petrographically associated fluid inclusions that formed at about the same time or during the same geological process). Isochores were calculated based

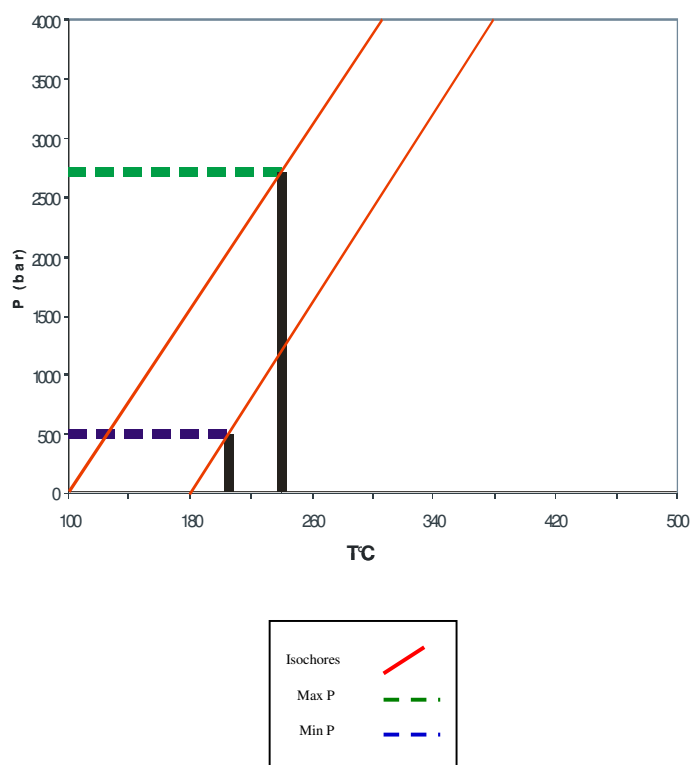
on the homogenization temperatures of the inclusions using the program ISOC (Bakker, 2003). **6.12A:** Isochores for type 1a inclusions from Mt. Angelay granites. Independent geothermometers used are the temperature of the contact aureole of the Saxby Granite (~670°C; Rubenach et al., 2008) and the maximum temperature determined for type 4 fluid inclusions (495°C); **6.12B:** Isochores for type 1a inclusions from Mt. Angelay brain rocks. Independent geothermometers used are the temperature of the calculated equilibrium of the quartz-albite assemblage (~540°C) in the aplitic and pegmatitic components of albite-actinolite-aplite-rich rocks determined by oxygen isotope studies (Mark and Foster, 2001) and the maximum temperature determined for type 4 fluid inclusions (495°C); **6.12C:** Isochores for type 1a inclusions from Mt. Angelay pegmatites. Independent geothermometers used are the temperature of the calculated equilibrium of the quartz-albite assemblage (~540°C) in the aplitic and pegmatitic components of albite-actinolite-aplite-rich rocks determined by oxygen isotope studies (Mark and Foster, 2001) and the maximum temperature determined for type 4 fluid inclusions (495°C); **6.12D:** Isochores for type 1a inclusions from Saxby late phases (pegmatites, aplite and quartz veins). Independent geothermometers used are the temperature of the calculated equilibrium of the quartz-albite assemblage (~540°C) in the aplitic and pegmatitic components of albite-actinolite-aplite-rich rocks determined by oxygen isotope studies (Mark and Foster, 2001) and the maximum temperature determined for type 4 fluid inclusions (495°C).

**b. Type 3b fluid inclusions**

It is also possible to obtain pressure estimates from secondary L+V+S inclusions using the data for the disappearance of halite crystals. The minimum trapping pressure of these inclusions was estimated by the method described by Roedder and Bodnar (1980). L+V+S inclusions totally homogenize by halite dissolution and this temperature provides a minimum pressure and temperature of trapping. The minimum trapping pressures were estimated by comparing the fluid inclusion isochores with the liquid- vapor- solid curve



for a pure H<sub>2</sub>O- NaCl fluid. The presence of CaCl<sub>2</sub> in the fluids, which is not accounted for in the equation, made the estimate artificially high (Stewart and Potter, 1979). However inclusions that homogenize in this manner could have been trapped at higher pressures than those calculated from homogenization (Roedder, 1984). The calculated minimum trapping pressures of secondary L+V+S inclusions are in a range between 0.5 and 2.5 kbar (Fig.6.13).



**Figure 6.13:** *P-T diagram for secondary L+V+S fluid inclusions. Isochores were calculated based on the vapor homogenization temperatures using the BULK- ISOC program (Bakker, 2003). The minimum trapping pressures for individual inclusions was estimated by the method described by Roedder and Bodnar (1980).*

### *6.6.2. Fluid evolution*

Of the four major fluid inclusion groups, type 1a, 2b and 3b inclusions are observed in all the samples from both the SIC and MAIC, and all other fluid inclusion types are typically observed in Mt. Angelay brain rocks. Interpretation of the magmatic fluid evolution of the SIC and MAIC requires studies on the mafic, intermediate and felsic intrusions, as the complexes contain all these rock types (Chapter 2) and the geochemical studies suggested different magma sources for their formation (Chapter 4). In fluid inclusion studies, only the felsic intrusions were studied due to the absence of fluid inclusions in mafic and intermediate rocks. Some interpretations about the total fluid evolution are presented by comparison of this data with field and geochemical studies on the more mafic rocks.

#### **6.6.2.1. Fluid compositions of the SIC and MAIC felsic intrusions-A comparison**

The fluid composition and evolution of the SIC and MAIC show both similarities and differences. In both the complexes, a CO<sub>2</sub>-rich fluid phase is commonly observed and the abundance of CO<sub>2</sub> inclusions in these rocks suggests that the SIC and MAIC intrusions are unusually rich in CO<sub>2</sub>. Absence of primary saline fluid inclusions in the SIC and MAIC granites probably suggests a less saline magmatic fluid compared to mafic rocks (which contain abundant halogen-bearing hydrous minerals, Chapter 5) or loss of salinity during the granitic magma evolution (see Chapter 8). The fluid inclusions in pegmatites from both the complexes also indicate primary CO<sub>2</sub> rich fluids. These similarities in observed primary fluid inclusion assemblages in the SIC and

MAIC granites and pegmatites suggest a single felsic magma source and similar general fluid evolution, confirming the geochemical observations (Chapter 4).

However, evidence for variation in the magmatic fluid composition and evolution in the SIC and MAIC are obtained from the distinct fluid inclusion assemblages of Mt. Angelay brain rocks (this study) and Saxby breccias (Bertelli 2007). These two sets of rocks represent the final release of magmatic fluids (Chapter 2 & 8) and their primary fluid inclusion assemblages include CO<sub>2</sub> only, CO<sub>2</sub>-H<sub>2</sub>O and CO<sub>2</sub>-H<sub>2</sub>O-brine types. The main difference in fluid inclusion populations between the SIC and the MAIC is the abundance of multi-solid inclusions at the Mt. Angelay brain rocks and their absence in the breccias from the SIC. Such high salinity brines in the MAIC may have formed from unmixing during cooling or gradual uplift (see below), and their absence in the SIC suggests different fluid release mechanisms (Chapter 8).

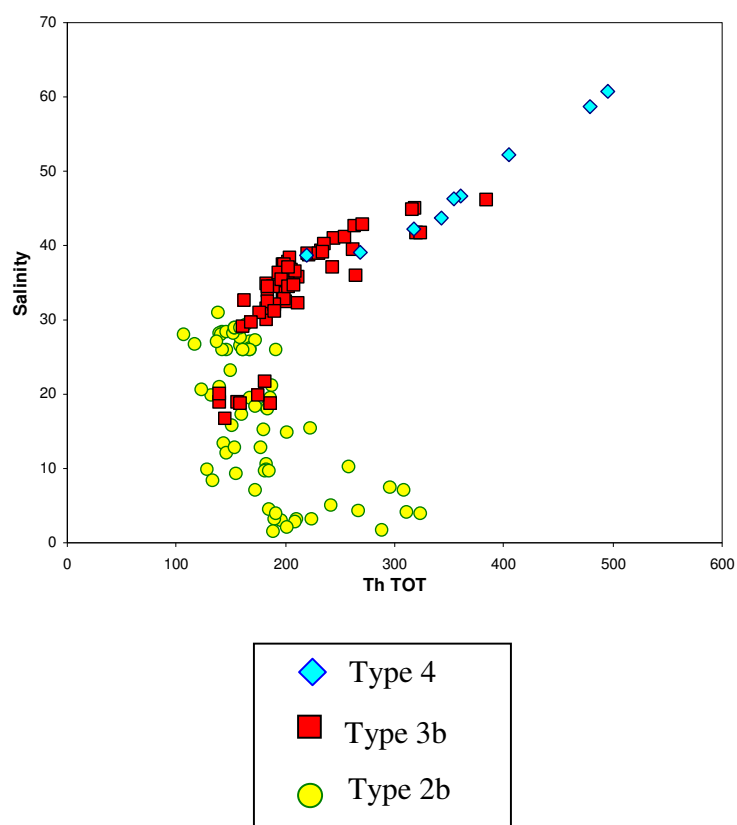
#### **6.6.2.2. Fluid Evolution in MAIC**

In the MAIC, other than granites, fewer mafic intrusions and more intermediate intrusions are reported than in the SIC (Chapter 2). The main evidence for fluid evolution in the MAIC is obtained from the various fluid inclusion assemblages observed in Mt. Angelay brain rocks. Brain rocks are felsic in composition and rich in albite and quartz; however, their typical occurrence within mafic and intermediate rocks suggests a fractional crystallization origin for their formation (Chapter 2 & 4).

The major difference between fluid inclusions of granites and brain rocks from the MAIC is the presence of CO<sub>2</sub>-H<sub>2</sub>O, CO<sub>2</sub>-H<sub>2</sub>O-brine and multisolid fluid inclusions in brain rocks. Some primary L+V and L+V+S inclusions were also observed exclusively in brain rocks. The occurrence of such a wide range of primary inclusions in these rocks principally suggest that they were either derived from unmixing of an original H<sub>2</sub>O-CO<sub>2</sub>-NaCl magmatic fluid (Beardsmore, 1992; Adshead, 1995; Perring et al., 2000; Pollard, 2001; Fu et al., 2003; Mustard et al., 2004) or by mixing of magmatic and external, non-magmatic sources. An unmixing model is strongly supported from the observation of coexistence of multisolid and mixed carbonic inclusions at three dimensional spaces and pseudo-secondary trails. Furthermore large pressure variations are observed in CO<sub>2</sub> fluid trapping pressure estimations of granites and brain rocks (up to 1.7 kbar; Fig.6.12A & B) and so fluid unmixing related to pressure drop is considered to be the ideal model for the typical fluid inclusion assemblage in brain rocks. The dominant magmatic component of these inclusions is also confirmed by fluid inclusion halogen studies (see Chapter 7).

However, the observation of rare primary L+V and L+V+S fluid inclusions and varying phase ratios of rare CO<sub>2</sub>-H<sub>2</sub>O and CO<sub>2</sub>-H<sub>2</sub>O-brine inclusions may suggest limited mixing with external fluids. The typical occurrence of brain rocks in the magmatic-hydrothermal transition location and the abundance of high salinity secondary fluids (type 3b) in these rocks may reflect some mixing of magmatic and non-magmatic fluids. This observation is supported by figure 6.14, which shows a mixing trend of magmatic (type 4) and non-magmatic fluids (type 2b). The halogen evidences for the

provenance of different fluids are more detailed in chapter 7; however, the halogen evidence for the sources of type 2a & 3a inclusions could not be studied due to their scarcity (Chapter 7).



**Figure 6.14:** Variations in salinity and total homogenisation temperatures in different fluid inclusion types from the SIC and MAIC. The figure supports the formation of type 3b inclusions by the mixing of magmatic (type 4) and non-magmatic (type 2b) fluids.

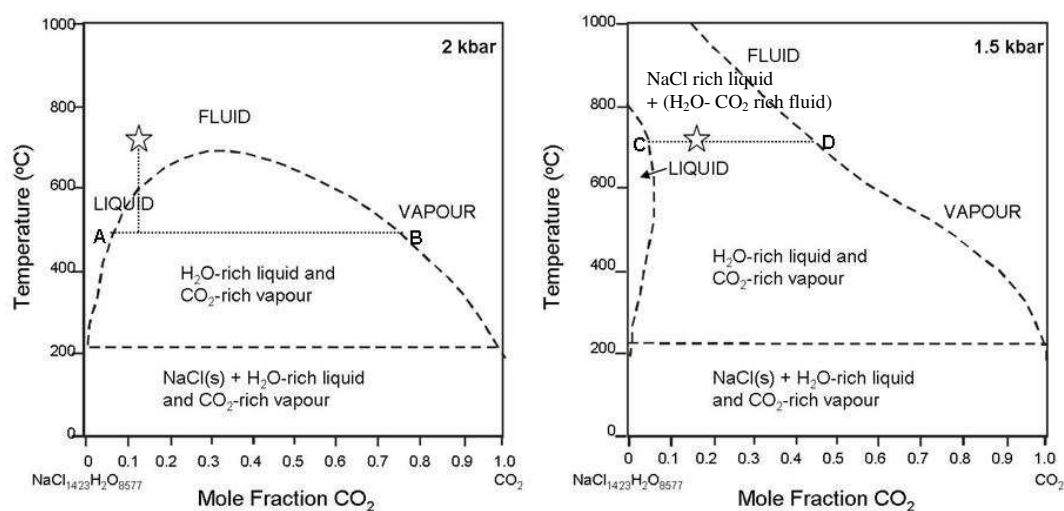
### 6.6.2.3. Fluid evolution in SIC

The fluid inclusion studies in the SIC during this research is limited to Saxby granites and pegmatites. In the SIC, breccias are considered to be the final mode of volatile release and the various fluid inclusion assemblages in these rocks were studied by

Bertelli (2007). The primary fluid inclusion types observed in these breccias include CO<sub>2</sub>-only, CO<sub>2</sub>-H<sub>2</sub>O and CO<sub>2</sub>-H<sub>2</sub>O-brine inclusions. Her research also revealed evidence for fluid overpressuring in the SIC and sudden pressure drop during the breccia formation. Bertelli's (2007) study recorded a fluid over-pressure of about 1.2 kbar in the trapped fluid densities of the primary CO<sub>2</sub> inclusions (4.2 kbar) and a sudden pressure drop of about 1.5 kbar in pseudo-secondary inclusion fluids (2.7 kbar). This sudden pressure drop is explained by explosive brecciation (see also Oliver et al., 2006). Such explosive nature of volatile release is quite different from the volatile release of the MAIC, where it is in the form of brain rocks.

The absence of multisolid inclusions in the breccias suggests various implications for the salinity sources of these inclusions. In Mt. Angelay brain rocks, the high salinity of multisolid inclusions may be influenced by a number of factors including fluid unmixing and external fluids. The T-X<sub>CO<sub>2</sub></sub> diagrams for the system H<sub>2</sub>O-CO<sub>2</sub>-NaCl by Bowers and Helgeson (1983) show that the presence or absence of multisolid inclusions is mainly a function of pressure (Figure 6.15). The pressures during brain rock formation vary from 1.3 to 2.1 kbar and such conditions most likely triggered phase separation forming both multisolid and mixed carbonic inclusions. The micro-analytical data also shows a purely magmatic origin for the salinity of multisolid inclusions (see Chapter 7), and so it is not likely that non-magmatic fluids contributed to multisolid inclusion formation.

In breccias of the SIC, the pressure variations recorded by CO<sub>2</sub> inclusions show higher ranges than in the MAIC, from 2.7 to 4.2 kbar. It is possible that these pressures were high enough in which phase separation did not occur during initial brecciation (Figure 6.15), or that unmixing occurred after the final crystallization of quartz.



**Figure 6.15:**  $T-X_{CO_2}$  diagrams for 35 wt% NaCl brine CO<sub>2</sub> fluids (from Bowers and Helgeson, 1983). The stars on each diagram denote the inferred compositions from the MAIC and show that a decrease in temperature would drive phase separation producing a brine with composition A and a vapour with composition B. The second diagram shows that a decrease in pressure would also trigger phase separation and form multisolid and CO<sub>2</sub> populations with compositions C and D respectively.

### 6.6.3. CO<sub>2</sub> abundance in Cloncurry intrusions

Relative to other granite fluid inclusion studies, the presence of abundant CO<sub>2</sub> bearing fluid inclusions in the SIC and MAIC rocks is notable. In granitic and intermediate

melts, the CO<sub>2</sub> solubility is normally very low (Holloway, 1976) and so this CO<sub>2</sub> abundance is assumed to be derived from some other sources. Previous studies on the CO<sub>2</sub> abundance in felsic intrusions suggest possibilities of crustal contamination by carbonates (Lowenstern, 2001; Iacono-Marziano et al., 2007) or contributions of mantle CO<sub>2</sub> (Kendrick et al., 2007).

In the Cloncurry district, a variation in the CO<sub>2</sub> content of the intrusions of the SIC and MAIC is inferred from the differences in the volatile release behaviour of these Complexes. The huge volume expansion of CO<sub>2</sub> upon exsolution from the magma and depressurization is thought to be one of the reasons for the formation of explosive breccia pipes in the SIC (Bertelli, 2007). The absence of explosive breccias in the MAIC preliminarily suggests that the CO<sub>2</sub> content of the SIC and MAIC are different. The details of these inferences will be discussed more in Chapter 8.

A number of previous studies in the district suggested a mafic source for this abundant CO<sub>2</sub> (Bertelli 2007; Oliver et al., 2006 & 2008) and a mantle source for mafic magmas (Mitchell 1993; Goleby et. al., 1996; Goncharov et. al., 1997; Pollard et. al., 1998; Mark, 1999). Furthermore, there are widespread calcite vein systems and gangue to ore components in the district, in which carbon isotopes suggest a magmatic or mantle origin for the CO<sub>2</sub> (Oliver et. al., 2004). Even though no quantitative studies have been done in the SIC and MAIC, the simultaneous emplacement of mafic and felsic intrusions during the Williams-Naraku batholith event with the presence of wide spread magma mixing and mingling zones supports the possibility of a mafic CO<sub>2</sub> source, that



may have been transferred into the granites during the mafic-felsic co-emplacement. Assuming this mechanism of CO<sub>2</sub> transfer, the abundance of mafic intrusions in the SIC compared to the MAIC is also consistent with a higher CO<sub>2</sub> concentration in the SIC, which may then have caused the explosive breccia formation in the SIC.

### 6.7. Conclusions

The various rock types of this study include granites, brain rocks, mixed-mingled rocks and late igneous phases of pegmatites, aplites and quartz veins from the SIC and MAIC. Four fluid inclusion types are identified; in which CO<sub>2</sub>-only inclusions, L+V inclusions and L+V+S inclusions are commonly observed in all these rocks. All CO<sub>2</sub> bearing inclusions are of primary origin and are subdivided into CO<sub>2</sub> only inclusions (type 1a), CO<sub>2</sub>-H<sub>2</sub>O inclusions (type 1b) and H<sub>2</sub>O-CO<sub>2</sub>-brine inclusions (type 1c). The latter two types were typically observed in Mt. Angelay brain rocks together with primary multisolid inclusions. The common secondary fluid inclusion types include L+V (type 2b) and L+V+S (type 3b) inclusions in which L+V inclusions represent the last fluid activity of the area.

All rock types contain large number of CO<sub>2</sub> only fluid inclusions showing the exceptional abundance of CO<sub>2</sub> in the intrusive phases of Cloncurry. This unusual CO<sub>2</sub> abundance is inferred to be sourced from mafic rocks, and the field studies during this research have noticed the presence of large number of mafic intrusives in the SIC compared to the MAIC. The difference in CO<sub>2</sub> contribution from mafic rocks is interpreted to be the major reason for the generation of explosive breccia pipes in the

SIC and brain rocks in the MAIC. Saxby explosive breccia pipes are considered to be derived from fluid overpressuring due to CO<sub>2</sub> volume expansion and release of volatiles during magma crystallization (Bertelli, 2007). The apparent absence of fluid overpressuring in Mt. Angelay granite is possibly related to the fewer mafic intrusions in the MAIC. The modest CO<sub>2</sub> input and cyclic accumulation and release of volatiles may have generated the brain rocks in the Mt. Angelay pluton instead of explosive breccia pipes.

Evidence for fluid unmixing is obtained from the fluid inclusion assemblages within brain rocks. The presence of a variety of primary fluid inclusions together with the assemblage of mixed carbonic and multisolid inclusions suggest fluid unmixing from an original H<sub>2</sub>O-CO<sub>2</sub>-NaCl (± other salts) fluid, which may have occurred as a result of pressure or temperature drops during magma evolution.

## Chapter 7: Fluid chemistry of Cloncurry intrusions-Micro-analytical study

### 7.1. Introduction

In the previous chapter the various fluid inclusion populations and their trapping conditions and salinity were investigated. In this chapter proton induced x-ray emission (PIXE) and laser ablation inductively coupled plasma mass spectrometry (LA-ICP-MS) are used to further investigate the composition of inclusions. Both these methods allow the individual analysis of fluid inclusions, enabling the comparison of inclusion populations. Moreover, the PIXE halogen analysis is used to understand the origin of fluids. The chapter also compares the fluid sources of intrusions and some Cloncurry IOCG deposits to determine the genetic connection between intrusions and ore deposits.

### 7.2. Inclusion selection and methodology

The fluid inclusions identified from the SIC and MAIC rocks include four different varieties with a number of sub-divisions (Chapter 6). However, the PIXE and LA-ICP-MS studies were focussed only on limited number of inclusions due to micro-analytical limitations and are described below.

#### 7.2.1. *PIXE*

PIXE analysis was conducted on the CSIRO-GEMOC Nuclear Microprobe at University of Melbourne. The analyses of individual fluid inclusions were performed prior to microthermometry to avoid decrepitation problems, but most of the inclusions used for PIXE decrepitated during later heating experiments, which is due to the

potential decrepitation observed in shallow fluid inclusions. Approximate microthermometric data of PIXE inclusions were obtained from adjacent similar fluid inclusion groups.

This non-destructive analysis was performed on carbon-coated doubly polished thin sections using a micro-focused proton beam of 3MeV under experimental conditions documented by Ryan et al. (1991). Details of the technique are reported in Ryan et al. (1993, 1995 & 2001). The inclusion sizes and depths were estimated with an optical microscope, based on focusing positions, prior to the PIXE analysis. Analysis is typically considered to be effective only in inclusions at depths of less than 20 $\mu$  below the sample surface as detection limits of some elements are depth dependent (e.g. K) (Ryan et al., 1993). Because only elements with atomic numbers >17 are detectable by PIXE, important elements such as Na and S cannot be determined. The calculation of fluid inclusion composition requires a number of parameters including the densities of the matrix and the fluid, their proton stopping powers, the detector sensitivity for each element, the X-ray production cross sections, and the X-ray absorption coefficients (e. g: Ryan et al., 1993; Kurusawa et al., 2003).

A distinct advantage of PIXE analysis is the imaging technique which allows easy discrimination of different phases within inclusions and to identify and exclude the nearby inclusions in the quartz that could otherwise contaminate the analysis. In PIXE analyses, the presence of Fe-rich solids may create 'pile ups' or elevated backgrounds in other element signals, most commonly on Cu peaks. Such pile ups can be observed as a 'wedge' on the spectra, which obscure the Cu peak and contributes artificially to the Cu signal. The removal of these 'wedges' lowers the measured concentration.

PIXE results are subject to a variety of errors including analytical error of 10-15%, and geometry related errors, which may occur due to uncertainties in the estimation of depth and thickness (may exceed up to 20%) or from deviations between natural inclusion shape and modelled ellipsoid. An uncertainty of ~30% has previously been reported in element concentrations, although inter-element ratios, particularly for elements with similar atomic numbers, are expected to be more accurate than individual element concentrations (Ryan et al 2001, Williams et al 2001).

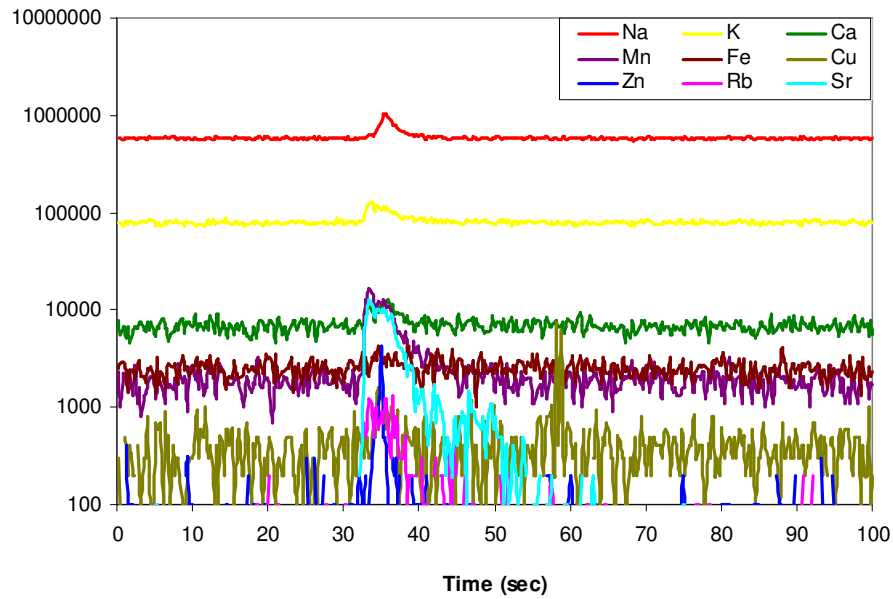
### 7.2.2. LA-ICP-MS

LA-ICP-MS studies were carried out using a Coherent GeolasPro 100 laser ablation unit coupled to a Varian 820-MS quadrupole ICP-MS at the Advanced Analytical Centre, James Cook University. The methodology is described thoroughly in Gunther et al. (1998) and Heinrich et al. (2003); details on the instrumentation and analytical procedures for the analyses presented in this study can be found in Allan et al. (2005). A mixing bulb which mixes the high purity Helium (LA carrier gas about 230 ml/minute) and Ar gas (ICP-MS carrier gas about 1 l/minute) was used to smooth the laser signal. The instrument was optimized to obtain highest sensitivity while keeping Th/U ratio to 1 and oxide low ( $\text{ThO}/\text{Th} < 0.5\%$ ). The laser repetition rate was 10 Hz with laser energy fluency of  $6.6 \text{ J}/\text{cm}^2$ . NIST 610 & 612 was used to calibrate the instrument and Na was used as the internal standard to correct for matrix effects. Laser beam aperture (spot size) was selected according to the size of the targeted fluid inclusion and 15  $\mu\text{m}$  and 23  $\mu\text{m}$  were mostly used, in order to ablate the entire fluid inclusion.

In LA-ICP-MS analysis, the concentrations, detection limits and sensitivities were calculated for each inclusion individually using the method of Longerich et al. (1996). Detection limits vary as a complex function of the mass of the element, the size and shape of the inclusion and the number of elements measured from a single inclusion, and must be determined for each element in each inclusion (Heinrich et al., 2003). The limits of detection normally decrease with decreasing size of the inclusion (Heinrich et al., 2003). The integrated intensities (counts/second) of the fluid inclusion signals from each analysis were background corrected and further corrected for matrix contributions, as even quartz, which is compositionally simple, may contain trace elements at high concentrations (Dennen, 1964; 1966; Flem et al., 2002; Müller et al., 2003; Götze et al., 2004). The data was processed off-line using SILLS (Guillong et al., 2008), a MATLAB-based data reduction software for LA-ICP-MS data. Analytical errors and matrix effects can be minimised since only well-ablated inclusions were chosen for the calculation and all signals are scanned for spikes (Fig. 7.1). LA-ICP-MS analyses of fluid inclusions were conducted subsequent to the microthermometric study as the density and salinity values were required for the analysis and the technique is destructive.

### *7.2.3. Comparison of micro analytical techniques*

For PIXE analysis, the depth of inclusions should be within 20 $\mu$  from the sample surface to get good results, but the LA-ICP-MS method needs slightly deeper inclusions as the shallow inclusions explode quickly which makes it hard to resolve the laser signal. Because of this difference in inclusion selection criteria, the same fluid inclusions could not easily be compared using the two techniques, however fluid inclusions from the same inclusion groups were analyzed for comparison purposes.



**Figure 7.1:** Representative LA-ICP-MS signal obtained from the ablation of a multisolid inclusion- Inclusion number JB 61\_MS1. The different spikes in this diagram correspond to different elements, which are used to measure the element concentrations in SILLS data reduction program.

Average detection limits of each element vary in PIXE and LA-ICP-MS techniques, and so the suite of commonly detected elements also varies in different methods. Some elements are only detectable by one method; in particular, Na was only analyzed by LA-ICP-MS. PIXE element maps help to understand the phase associations, but the lower detection limits of Sr, Ba, Rb and Pb in LA-ICP-MS method provided information about their concentrations, which are below the PIXE detection limits. Similarly, metal concentrations of fluid inclusions are better detected by PIXE analysis than LA-ICP-MS due to the lower detection limits of metals in PIXE.

Figures 7.2A & B show a comparison of common element concentrations measured by PIXE and LA-ICP-MS techniques in primary multisolid and secondary L+V+S inclusions. In both inclusion groups, the LA-ICP-MS analyses show comparatively

higher element concentrations than the PIXE. However, the element ratios show approximately similar values, suggesting that both techniques are reliable for interpreting fluid compositions and sources (e.g. Figure 7.3A-D).

### 7.3. Results

#### 7.3.1. *Chemistry of fluids*

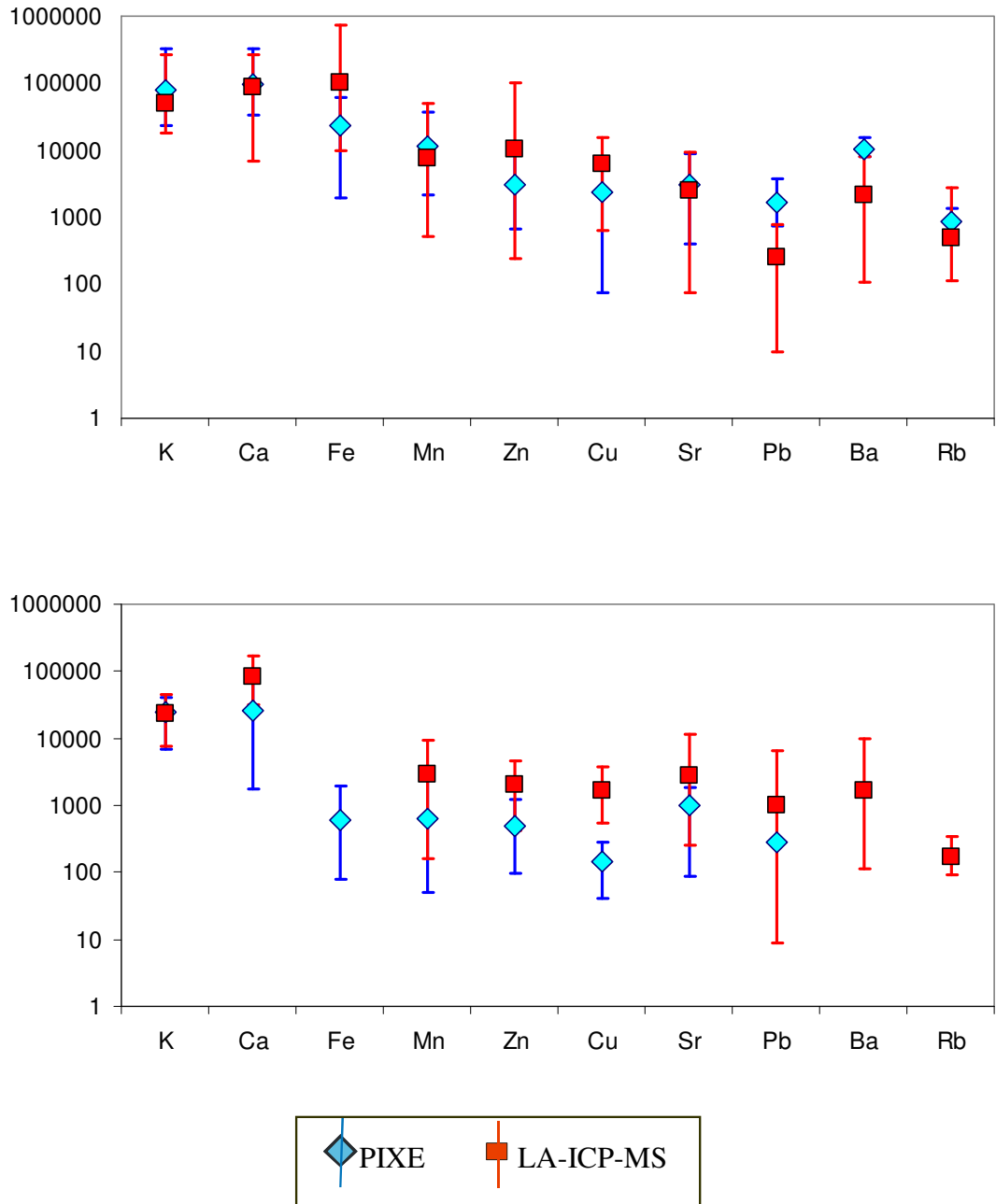
Both primary and secondary fluid inclusions were analysed by PIXE and LA-ICP-MS methods; in which the analyses particularly focused on multisolid inclusions (type 4) and L+V+S inclusions (type 3b). A limited number of L+V inclusions (type 2b) and CO<sub>2</sub>-H<sub>2</sub>O-brine inclusions (type 1c) were also analysed by PIXE. All the rock types were analysed for secondary fluid (type 2b & 3b) chemistry; however the primary inclusions (type 1c & 4) were exclusively studied from Mt. Angelay brain rocks.

The typical suite of elements detected by each method is tabulated in table 7.1 and the full data sets are attached in appendix 5.2 & 5.4.

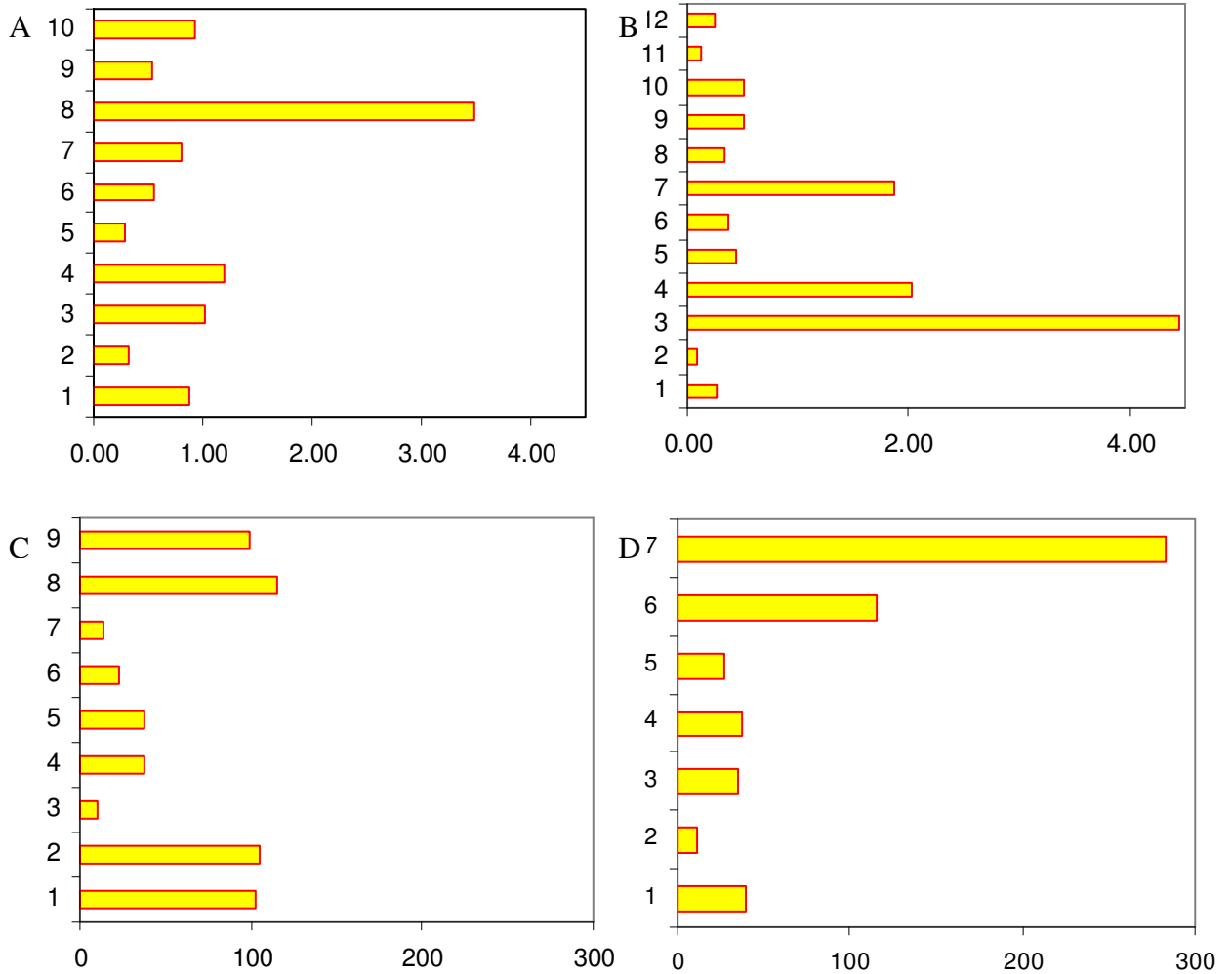
##### **7.3.1.1. Primary fluid inclusions**

In the SIC and MAIC, the most common primary fluid inclusion type is CO<sub>2</sub> only inclusions. However, these inclusions could not be analysed due to their non-saline nature. The primary fluid inclusions used for micro-analytical study are multisolid inclusions and CO<sub>2</sub>-H<sub>2</sub>O-brine inclusions, which were exclusively observed in Mt. Angelay brain rocks. These rocks represent the final phases of fractional crystallization and the primary origin of these inclusions was confirmed by microscopic studies and microthermometric estimations (Chapter 2 & 6).





**Figure 7.2:** Common elements measured by PIXE and LA-ICP-MS. **7.2A:** Elements measured in multisolid inclusions by PIXE and LA-ICP-MS methods. The inclusions are exclusively from the Mt. Angelay brain rocks; **7.2B:** Elements measured in secondary L+V+S inclusions by PIXE and LA-ICP-MS methods. The data is collected from the secondary L+V+S inclusions of all the samples. The error bars represent the maximum and minimum range of element concentrations. Most elements show enrichment in LA-ICP-MS compare to PIXE. Data is available in Appendix 5.2 & 5.4.



**Figure 7.3:** Examples for comparatively similar element ratios in PIXE and LA-ICP-MS analyses. **7.3A:** PIXE K/Ca values of 10 multisolid inclusions; **7.3B:** LA-ICP-MS K/Ca values of 12 multisolid inclusions; **7.3C:** PIXE Ca/Zn values of 9 secondary L+V+S inclusions; **7.3D:** LA-ICP-MS Ca/Zn values of 7 secondary L+V+S inclusions. Data is available in Appendix 5.2 & 5.4. Only values above the detection limits are used for calculation.

PIXE			LA-ICP-MS		
Routinely detected	Frequently detected	Rarely/never detected	Routinely detected	Frequently detected	Rarely/never detected
K	Cu	Mo	K	Ca	Li
Ca	Sr	Ag	Na	Fe	Co
Cl	Pb	Sn	Rb	Cu	Ni
Fe	Br	Cs	Sr	Mn	As
Mn		As	Pb	Zn	Mo
Zn		S	Ba		Ag
Ti		Ba			Sn
		Rb			W

**Table 7.1:** The suite of elements detected by PIXE and LA-ICP-MS analyses

**a. Multisolid inclusions (type 4)**

The maximum and minimum concentrations of major cations measured among all multisolid fluid inclusions by PIXE and LA-ICP-MS methods are tabulated in tables 7.2 & 7.3 and major element ratios are given in tables 7.4 & 7.5. A total of 11 type 4 inclusions were analysed by PIXE and 20 by LA-ICP-MS. Multisolid fluid inclusions contain the highest element concentrations of all inclusion types. PIXE element maps show considerable variation in the element phase association of multisolid inclusions (Fig. 7.4A & B); most commonly Ca and Cl are dissolved in the liquid phase. K is observed bound in the solid phases in the majority of inclusions; however it is dissolved in the liquid in some inclusions. In all multisolid inclusions, the majority of metals (Fe, Cu, Zn & Mn) appears to be in the solid phase and most of the elements show a general link to salinity (Fig. 7.5A-D).

K and Ca estimations by PIXE and LA-ICP-MS are mostly similar. The multisolid inclusions contain up to 33 wt % of K and Ca, with average concentrations generally range from 2 to approximately 8 wt% for both elements in most inclusions (Fig. 7.6;

tables 7.2 & 7.3). The average K/Ca ratio is ~1 in majority of analyses. Some exceptions were noticed in deep seated inclusions and may have occurred due to errors in depth estimation during PIXE analysis (tables 7.4 & 7.5). The Na and Cl contents of multisolid inclusions range from 7 to 16 wt% and from 25 to 60 wt % respectively (Fig. 7.6; table 7.2 & 7.3). The average Na/K and Na/Ca ratios vary from 0.2 to 4.7 and from 0.02 to 4 (tables 7.4 & 7.5).

Metal concentrations are routinely detected by PIXE method and in LA-ICP-MS analysis, many inclusions show Fe, Cu, Mn and Zn values below detection due to the high detection limits for metals in LA-ICP-MS analysis (Table 7.1). Fe and Mn concentrations of type 4 inclusions vary from 1000 to 77000 ppm and from 2000 to 50000 ppm respectively (Fig. 7.6; table 7.2 & 7.3). Fe is commonly observed in the solid phase (Fig. 7.4). Mn is also present as a solid phase, sometimes as a separate solid or in the Fe-bearing solid phase, but it is also observed as a dissolved phase in the inclusion liquid (Fig. 7.4). The Mn/Fe ratios are variable, but are mostly <1; however some PIXE analyses show values up to 4.5 (tables 7.4 & 7.5). Ti is frequently detected in multisolid inclusions and they appear to be in the liquid phase and a number of inclusions reported a Ti solid. However, the concentrations are not very reliable as the background value of Ti is very high in most inclusions.

		Cl	K	Ca	Fe	Mn	Zn	Cu	Sr	Pb	Ba	Br	Rb
<b>Type 4</b>	<b>Min</b>	243179	23523	33528	1975	2089	657	<116	<139	<130	<2064	<162	<117
	<b>Max</b>	599631	332680	326783	62652	37269	10590	5397	8750	3806	15727	603	1352
	<b>Avg</b>	363715	80342	96679	23455	11666	3121	2400	3009	1697	10160	420	875
<b>Type 1c</b>	<b>Min</b>	262645	9118	11529	810	364	329	1237	<157	147	<2802	<141	<154
	<b>Max</b>	308942	28800	22705	12038	698	689	4595	476	862	<6437	<243	<177
	<b>Avg</b>	285794	18959	17117	6424	531	509	2916	b.d	505	b.d	b.d	b.d
<b>Type 3b</b>	<b>Min</b>	36266	7018	1759	79	49	99	<35	<52	<65	<1703	<96	<76
	<b>Max</b>	542809	39973	100478	1891	2532	1210	281	1811	<497	<11264	<444	<494
	<b>Avg</b>	244227	23971	26342	615	620	486	148	980	281	b.d	220	b.d
<b>Type 2b</b>	<b>Min</b>	2698	1889	844	60	<38	80	43	<59	<70	<2184	<112	<74
	<b>Max</b>	352197	15226	47483	1641	403	744	323	1147	<469	<17244	1468	<417
	<b>Avg</b>	103721	6572	12351	527	206	330	138	436	b.d	b.d	1097	b.d

*Table 7.2: Minimum, maximum and average concentrations of selected major and trace elements measured by PIXE in fluid inclusions. Full data set is in Appendix 5.2 & 5.4.*

		Na	K	Ca	Fe	Mn	Zn	Cu	Sr	Pb	Ba	Rb
<b>Type 4</b>	<b>Min</b>	5371	18168	<8158	<9803	510	<95	<63	75	10	107	112
	<b>Max</b>	165921	272040	140230	77490	50842	100374	15215	9380	765	7877	2754
	<b>Avg</b>	104397	48770	71771	45560	7464	10126	6080	2536	251	2194	503
<b>Type 3b</b>	<b>Min</b>	47240	7556	<27292	<9169	<221	<133	<136	250	<5	114	<31
	<b>Max</b>	154442	45742	170222	<109741	9166	4522	3675	11437	6525	9892	350
	<b>Avg</b>	105501	23446	81726	b.d	2893	2032	1697	2754	940	1682	173

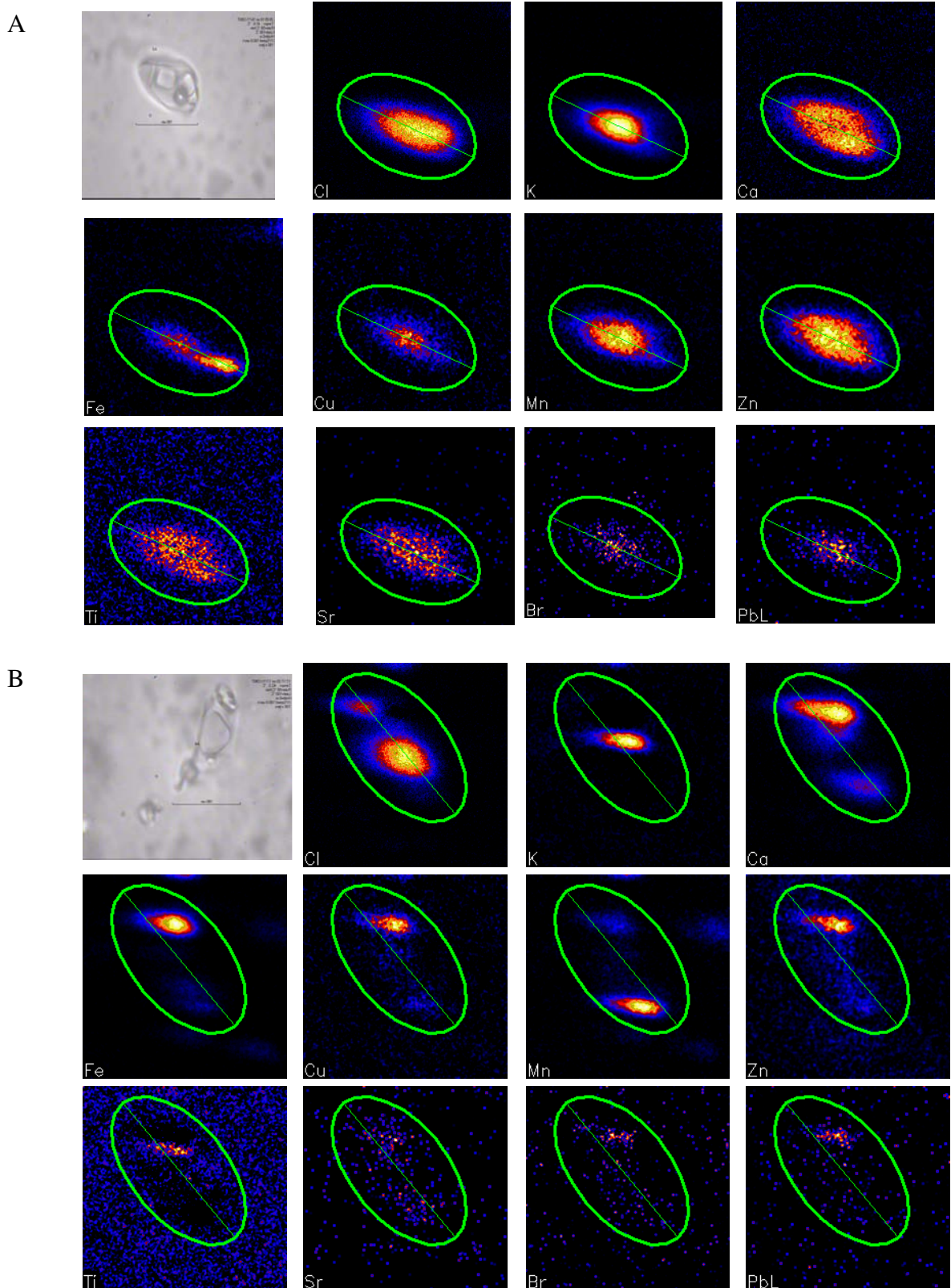
*Table 7.3: Minimum, maximum and average concentrations of selected major and trace elements measured by LA-ICP-MS analysis in fluid inclusions. Full data set is in Appendix 5.2 & 5.4.*

		K/Ca	Mn/Fe	Zn/Pb	Br/Cl*1000
<b>Type 4</b>	<b>Min</b>	0.29	0.03	0.22	0.58
	<b>Max</b>	3.49	4.26	8.88	1.19
	<b>Avg</b>	1	1.52	4.1	0.89
<b>Type 1c</b>	<b>Min</b>	0.79	0.45	2.24	b.d
	<b>Max</b>	1.27	0.06	0.8	b.d
	<b>Avg</b>	1.03	0.25	1.52	b.d
<b>Type 3b</b>	<b>Min</b>	0.39	0.16	1.96	0
	<b>Max</b>	3.99	5.89	1.96	0
	<b>Avg</b>	1.79	1.29	1.96	0
<b>Type 2b</b>	<b>Min</b>	0.18	0.1	b.d	4.17
	<b>Max</b>	15.42	1.73	b.d	8.85
	<b>Avg</b>	2.28	0.56	b.d	6.51

**Table 7.4:** Minimum, maximum and average values of selected element ratios measured by PIXE analysis in fluid inclusions. Values are derived from analyses above detection limit. Full data set is in Appendix 5.2 & 5.4.

		K/Ca	Na/K	Na/Ca	Mn/Fe	Zn/Pb
<b>Type 4</b>	<b>Min</b>	0.09	0.2	0.02	0.01	1.85
	<b>Max</b>	4.45	8.14	20.94	0.98	193.6
	<b>Avg</b>	0.94	3.5	4.1	0.26	29.28
<b>Type 3b</b>	<b>Min</b>	0.1	2.68	0.34	b.d	0.72
	<b>Max</b>	1.42	19.87	4.05	b.d	497.41
	<b>Avg</b>	0.57	6.4	1.94	b.d	60.49

**Table 7.5:** Minimum, maximum and average values of selected element ratios measured by LA-ICP-MS analysis in fluid inclusions. Values are derived from analyses above detection limit. Full data set is in Appendix 5.2 & 5.4.



**Figure: 7.4:** Representative PIXE element maps showing phase associations in multisolid inclusions from Mt. Angelay brain rocks. **7.4A:** Inclusion No. JB 64A\_MS3; **7.4B:** Inclusion No. JB61\_MS2. Full data set is in Appendix 5.3.

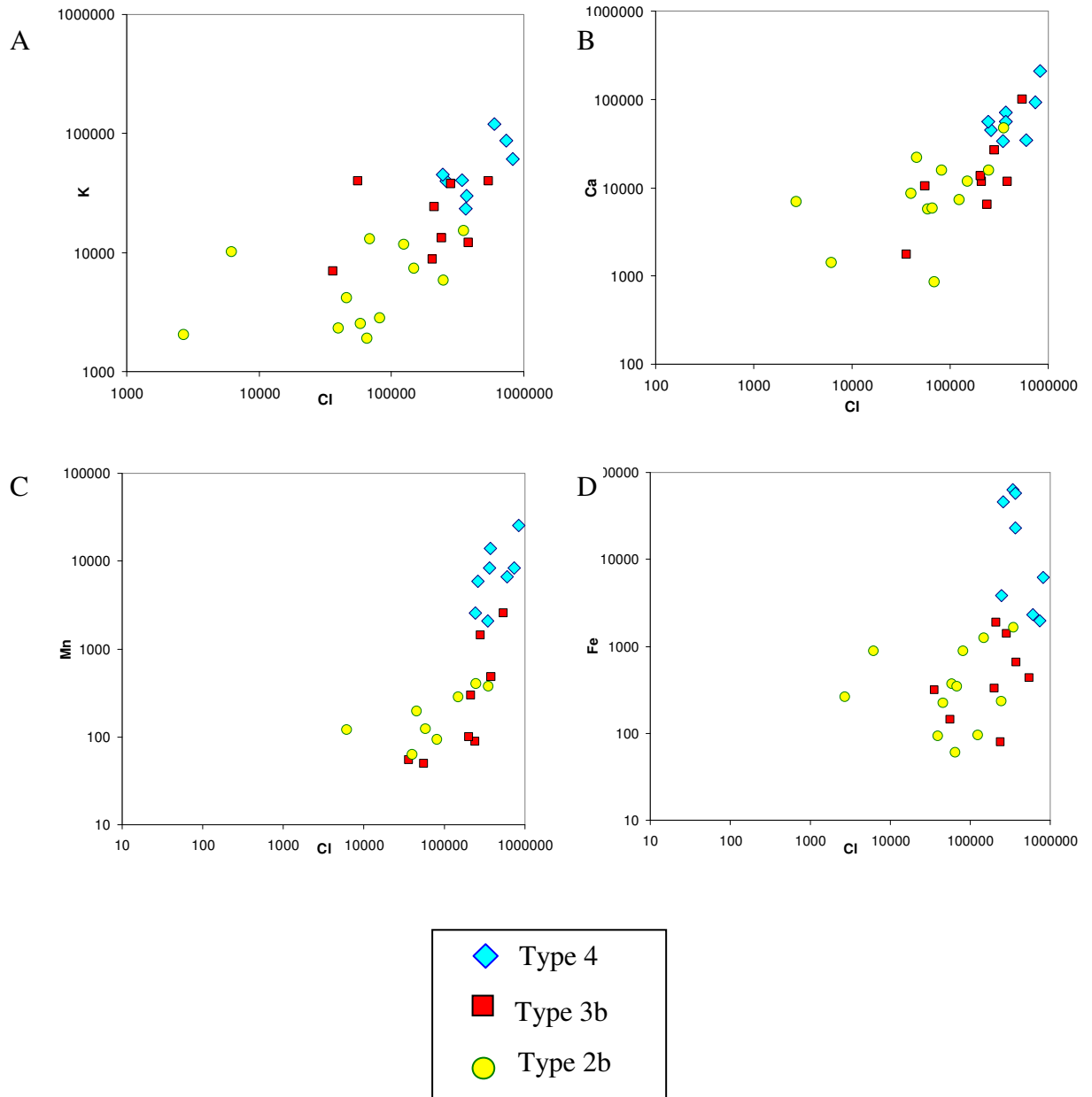
Cu is mostly present in the Fe-bearing solid (Fig.7.4) and is occasionally exaggerated by Fe pile-up that artificially contributed to the measured Cu values. However, many multisolid inclusions show high Cu concentrations even after this effect is removed. In PIXE studies, the Cu concentrations generally range from a few hundreds to thousands of ppm, and the highest Cu concentration detected from multisolid inclusions is 5397 ppm (Fig. 7.6A; table 7.2 & 7.3). The high Cu contents of these fluids were later confirmed by the LA-ICP-MS analysis and some inclusions show Cu contents up to 1.5 wt% (Fig. 7.6B; table 7.2 & 7.3).

In element maps, Zn is commonly observed in the Fe-bearing solid; however it is also observed as a dissolved liquid phase in one multisolid inclusion (Fig.7.4). Zn and Pb contents are detected by both the micro-analytical methods and the values range from 650ppm to 1 wt% and from 10ppm to 1700ppm respectively (Fig. 7.6; table 7.2 & 7.3). Rb concentrations by LA-ICP-MS analyses commonly vary from 100ppm to 500ppm and are rarely detected by PIXE (Fig. 7.6; table 7.2 & 7.3). Pb and Rb also show an association with Fe-bearing solids, which may either be Fe carbonates or halides or sulphates, or artificial signals caused by high Fe concentrations, as these elements would not be expected to substitute into Fe silicates.

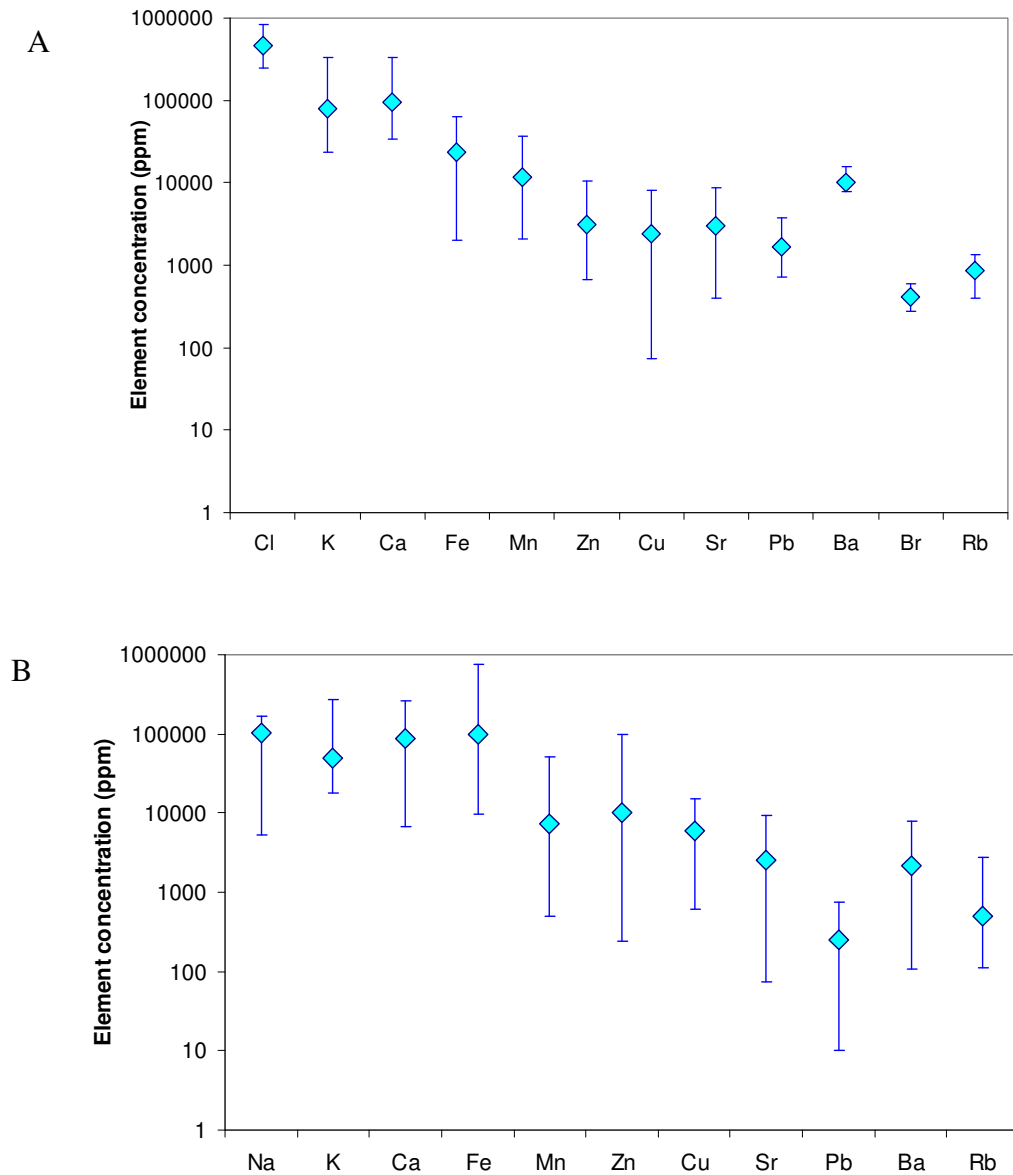
Ba in multisolid inclusions varies from 100ppm to 1.5 wt% and is usually detected in LA-ICP-MS analysis (Fig. 7.6; table 7.2 & 7.3). Ba detection by PIXE method is limited due to the high Ba detection limits. Sr is a dissolved phase in all multisolid inclusions and mostly ranges from few hundreds to thousands ppm in both the micro-analytical methods (Fig. 7.6; table 7.2 & 7.3). Br is analysed by PIXE and the results



show 280 to 600ppm of Br in multisolid inclusions (Fig. 7.6; table 7.2 & 7.3). It is commonly observed in the liquid phase.



**Figure: 7.5A-D:** PIXE analyses of various fluid inclusions showing positive correlations between Cl and elements. Type 4 fluid inclusions plotted are exclusively from Mt. Angelay brain rocks and type 2b and 3b are collected from all the samples. The full data set is tabulated in Appendix 5.2.



**Figure: 7.6:** Diagram displaying minimum, maximum and average concentrations of major and trace elements in multisolid fluid inclusions. The inclusions are exclusively analysed from Mt. Angelay brain rocks; **7.6A:** PIXE results; **7.6B:** LA-ICP-MS results. Bars represent the range of concentrations of each element in the fluid. The concentrations used are tabulated in tables 7.2 & 7.3 and the full data set is available in Appendix 5.2 & 5.4.

***b. CO<sub>2</sub>-H<sub>2</sub>O-brine inclusions (type 1c)***

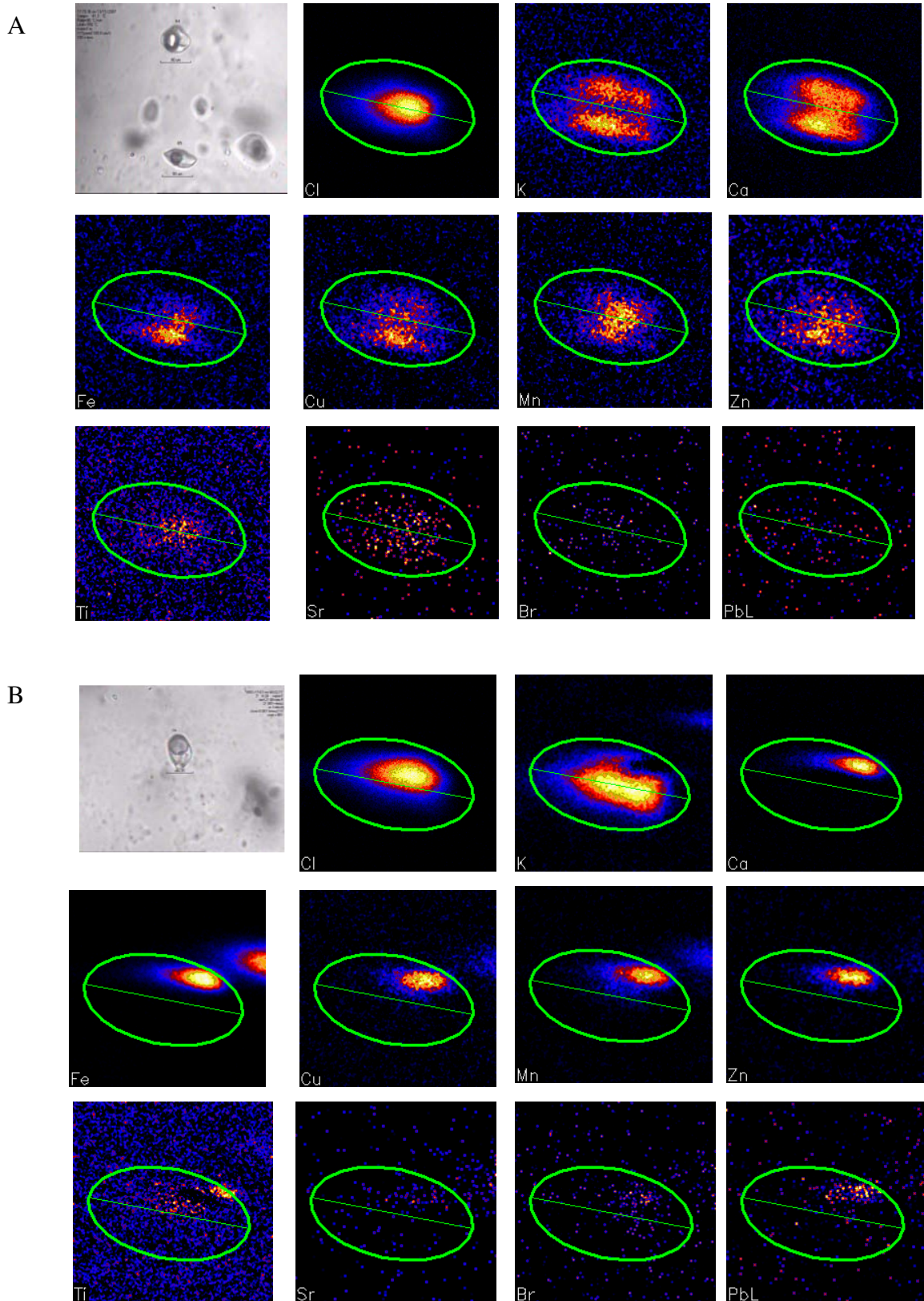
Two CO<sub>2</sub>-H<sub>2</sub>O-brine (type 1c) inclusions were analysed by PIXE method. The results are tabulated in table 7.2 with element ratios calculated in table 7.4.

PIXE element maps show considerable variation in the element phase associations between these two inclusions (Fig.7.7). In both the inclusions, K appears to be dissolved in the liquid phase with Cl being bound within the solid phase. Ca is dissolved in the liquid in one inclusion, but is associated with the solid phase in the other. Both K and Ca concentrations vary up to 2 wt % (Fig.7.8; table 7.2) and the K/Ca ratios are 0.4 and 2.5 (table 7.4). The Cl contents are 26 wt% and 30 wt% (Fig.7.8; table 7.2).

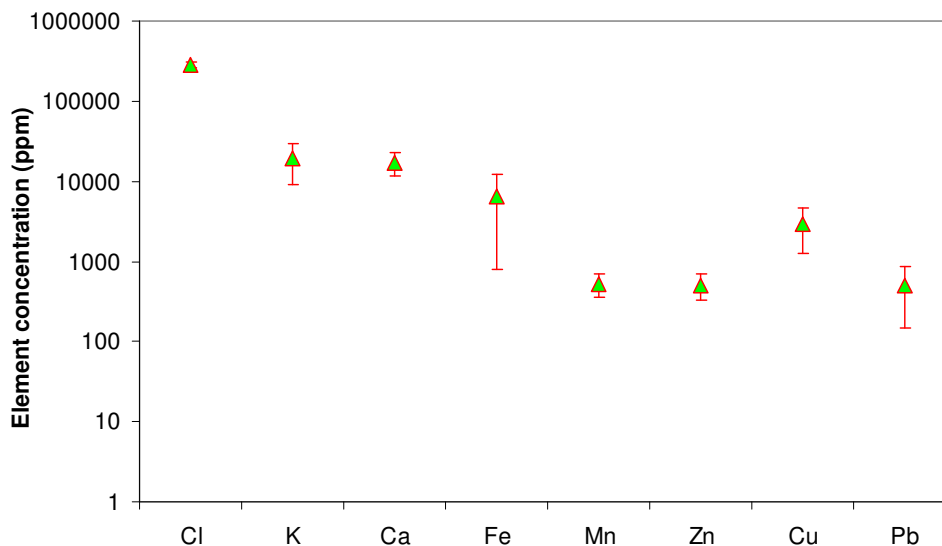
The element phase associations of Fe, Mn, Cu and Zn vary and are associated with the liquid phase in one fluid inclusion and with the solid phase in the other (Fig.7.7). Their concentrations vary by a few hundred ppm; however the Cu concentrations are quite high (1237ppm and 4595ppm) and higher than the Fe content in one inclusion (Fig.7.8; table 7.2). The PIXE element maps also show a substantial enrichment of Cu in CO<sub>2</sub>-H<sub>2</sub>O-brine inclusions. Most other elements including Br, Sr, Ba and Rb are not detected in type 1c inclusions; however the Pb values are between 147 and 862 ppm (Fig.7.8; table 7.2).

**7.3.1.2. Secondary fluid inclusions**

The secondary fluid inclusions analysed by micro-analytical techniques include L+V+S inclusions (type 3b) and L+V inclusions (type 2b). These inclusions were observed in all the intrusive rock types and they cross cut all other inclusion types and



**Figure 7.7:** Representative PIXE element maps showing phase associations in  $\text{CO}_2$ - $\text{H}_2\text{O}$ -brine inclusions from Mt. Angelay brain rocks. **7.7A:** Inclusion No. JB61\_CB1; **7.7B:** Inclusion No. JB61\_CB2. Full data set in Appendix 5.3.



**Figure: 7.8:** PIXE results of minimum, maximum and average concentrations of major and trace elements in  $\text{CO}_2\text{-H}_2\text{O}$ -brine (Type 1c) inclusions; Bars represent the range of concentrations of each element in the fluid. The data is tabulated in table 7.2 and in Appendix 5.2.

mineral boundaries. They are confirmed as of secondary origin and type 2b represents the last fluid activity in the study area (Chapter 6). These inclusions were likely trapped in between 140-250°C and 600-2600 kbar pressures (this study, Bertelli, 2007).

#### **a. L+V+S inclusions (type 3b)**

A total of 11 inclusions were studied by PIXE and 5 by LA-ICP-MS and the maximum, minimum and average values of major cations measured are listed in tables 7.2 & 7.3. The calculated element ratios are given in tables 7.4 & 7.5.

In type 3b inclusions, most elements, including metals, appeared to be dissolved in the liquid phase; however K and Ca are bound with the solid phase in some inclusions (Fig. 7.9). The Cl concentrations commonly vary between 20 and 30 wt% and Na

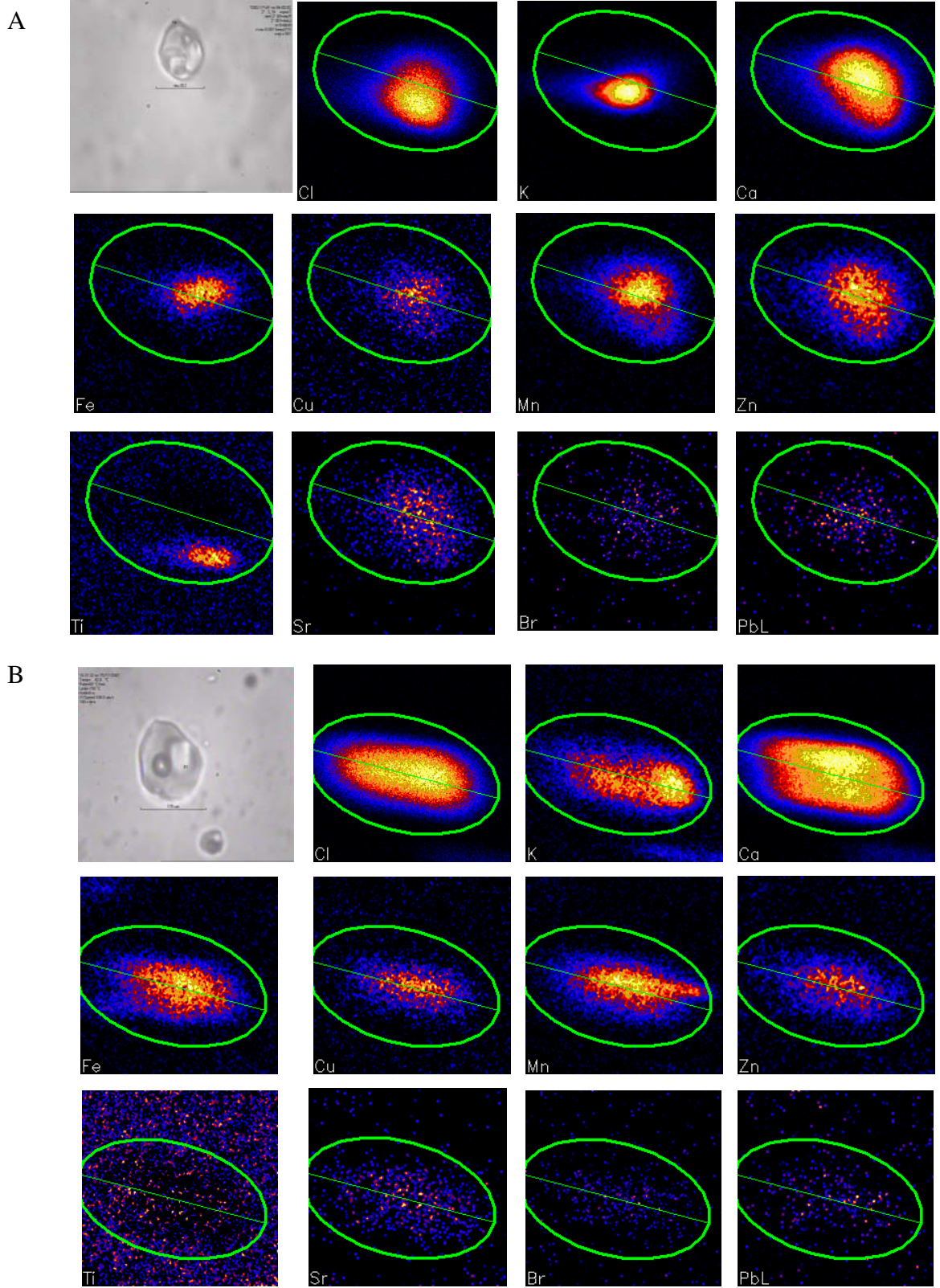
from 5 to 13 wt% (Fig. 7.10; tables 7.2 & 7.3). In addition to Na and Cl, L+V+S inclusions are dominated by K and Ca with concentrations from about 7000 ppm to 46000 ppm and from 6000 ppm to 10 wt% respectively (Fig.7.10; tables 7.2 & 7.3). Average concentrations generally range from 1 to approximately 4 wt% for both elements in both micro-analyses (Fig.7.10; tables 7.2 & 7.3). The K/Ca ratio is variable from 0.1 to 4 and the average Na/K and Na/Ca ratios range from 2.7 to 4.6 and from 0.34 to 4 respectively (tables 7.4 & 7.5).

Fe, Mn and Zn are detected by PIXE method than LA-ICP-MS and commonly vary between 50ppm and 1000ppm (Fig.7.10; tables 7.2 & 7.3). Cu is detected only in seven inclusions and LA-ICP-MS analyses show comparatively high values range from 550 to 3675 ppm (Fig.7.10; table 7.3). The PIXE values of Cu vary from 41ppm to 281ppm (Fig.7.10; table 7.2). Ti varies from few hundred to thousand ppm; however the values are not dependable as the Ti background is very high.

Ba, Rb, Pb and Sr are detected by LA-ICP-MS method and these elements are below detection in PIXE. They commonly vary in a few hundred ppm. Br is detected only in two inclusions.

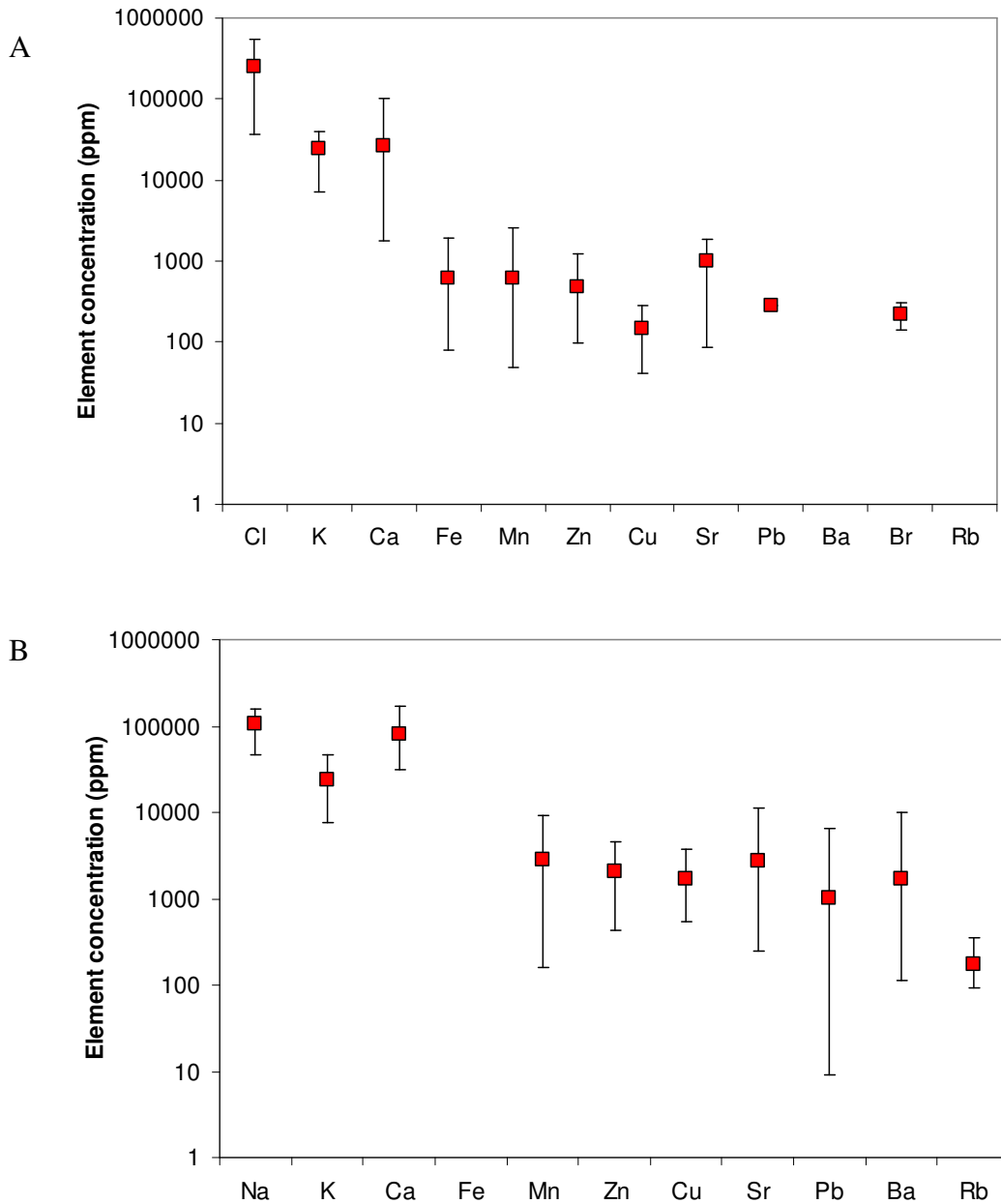
***b. L+V inclusions (type 2b)***

Type 2b fluid inclusions contain the least element abundance. They were studied by PIXE method only and the major cations are listed in table 7.2 with calculated element ratios.



**Figure 7.9:** Representative PIXE element maps showing phase associations in L+V+S fluid inclusions. **7.9A:** Inclusion No. JB88C\_A1; **7.9B:** Inclusion No. JB6D\_B1. Full data set in Appendix 5.3.





**Figure: 7.10:** Diagram displaying minimum, maximum and average concentrations of major and trace elements in L+V+S (Type 3b) fluid inclusions; **7.10A:** PIXE results; **7.10B:** LA-ICP-MS results. Bars represent the range of concentrations of each element in the fluid. The data is tabulated in table 7.2 & 7.3 and the full data is present in Appendix 5.2 & 5.4.



Ca, K and Cl are the only element signals observed in the PIXE element maps of L+V inclusions (Fig.7.11A); however elements like Fe and Zn were also widely measured by the analyses. The Cl contents approximately vary from 2000 ppm to 15 wt% (Fig.7.11B; table 7.2). K and Ca are the major elements in type 2b inclusions in addition to Cl and their concentrations generally range from 2000 to 10000 ppm and from 1000 to 15000 ppm respectively (Fig.7.11B; table 7.2). The K/Ca ratio is highly variable from values 0.2 to some inclusions with exceptionally high values like 15.4 (table 7.4). Fe ranges from 60 ppm to 1250 ppm and Zn from 80 ppm to 750 ppm (Fig.7.11B; table 7.2). Mn, Cu and Sr concentrations range in a few hundred ppm; however two inclusions show Br contents of 726 ppm and 1468 ppm.

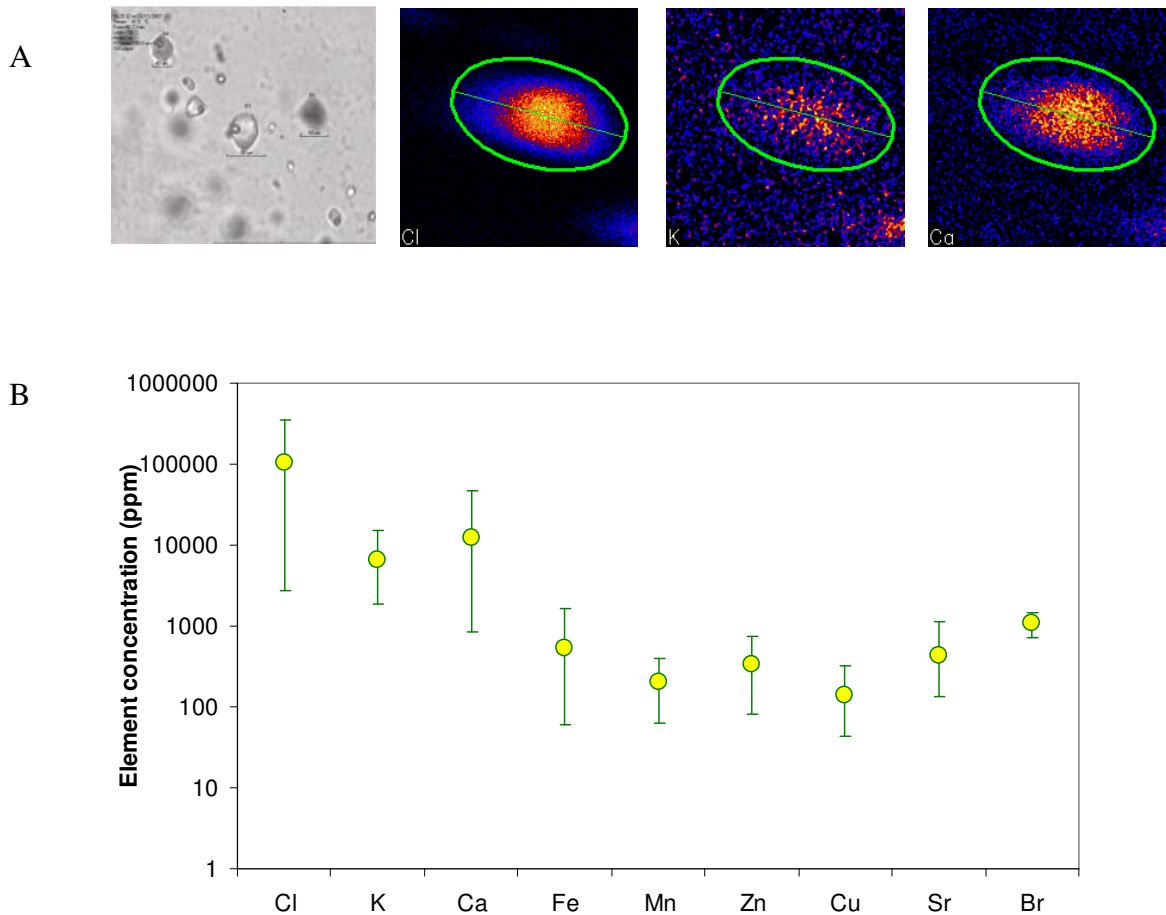
## 7.4. Discussion

### 7.4.1. *Fluid compositions*

Micro-analytical studies confirm different compositions for the primary and secondary fluid inclusions of the SIC and MAIC. The suite of elements detected in the inclusions is similar; however, significant distinctions are observed in the cation concentrations and element ratios between primary and secondary fluids.

In general, fluids trapped in the inclusions of the SIC and MAIC rocks are enriched in Cl, K and Ca; however their concentrations vary according to the inclusion type. Compared to secondary inclusions in all the rock types, the salinity of fluids trapped in multisolid inclusions of Mt. Angelay brain rocks is very high with very high concentrations of several elements (Fig.7.12). Ideally, magmatic fluids contain high Fe, Mn and Zn concentrations (Yardley et al., 2000) and in brain rocks, the metal concentrations, especially Fe, Mn, Zn and Cu of primary inclusions are very high

(Fig.7.12). The Cl, K and Ca concentrations of multisolid inclusions also show a marked increase from the secondary fluids of type 2b & 3b (Fig.7.12; table 7.2 & 7.3). However, the Na concentrations detected from the primary multisolid inclusions and secondary L+V+S inclusions are almost similar.



**Figure: 7.11A:** Representative PIXE element maps showing phase associations in L+V fluid inclusions. Inclusion number JB4\_B3. The full data set in Appendix 5.3; **7.11B:** PIXE results of minimum, maximum and average concentrations of major and trace elements in L+V fluid inclusions. Bars represent the range of concentrations of each element in the fluid. The values used are tabulated in table 7.2 and the whole data is in Appendix 5.2.

The major element ratios of primary and secondary fluid inclusions suggest magmatic and non-magmatic origins for those inclusions respectively. High temperature fluids of magmatic origin are often K-rich with low Na/K ratios, ranging between 0.5 and 7 with a mean of ~2.5 (Yardley et al., 2000; Rusk et al., 2004). They also show high Na concentrations compared to Ca and high Na/Ca ratios (4 – 25) (Yardley et al., 2000). The primary fluids of brain rocks are dominated by Na compared to Ca, with Na/K values ranging between 0.2 and 8.14 and high Na/Ca ratios between 0.02 and 20.94 (Table 7.5), which suggest a magmatic origin. In non-magmatic fluids, the Na/K values may show large ranges from 0.5 to 71.55; however most Na/Ca values are in between 0.3 and 7.52 (Yardley et al., 2000). These fluids are commonly enriched in Ca. In Cloncurry, the secondary L+V+S inclusions from different intrusive rocks of the SIC and MAIC show Na/K values between 2.68 and 19.87 and Na/Ca from 0.34 to 4.05 (Table 7.5). Although these values show much overlap between magmatic and non- magmatic signatures, these ratios suggest possible non- magmatic origin for secondary L+V+S inclusions, which can also be inferred from K/Ca ratios and halogen values (see below).

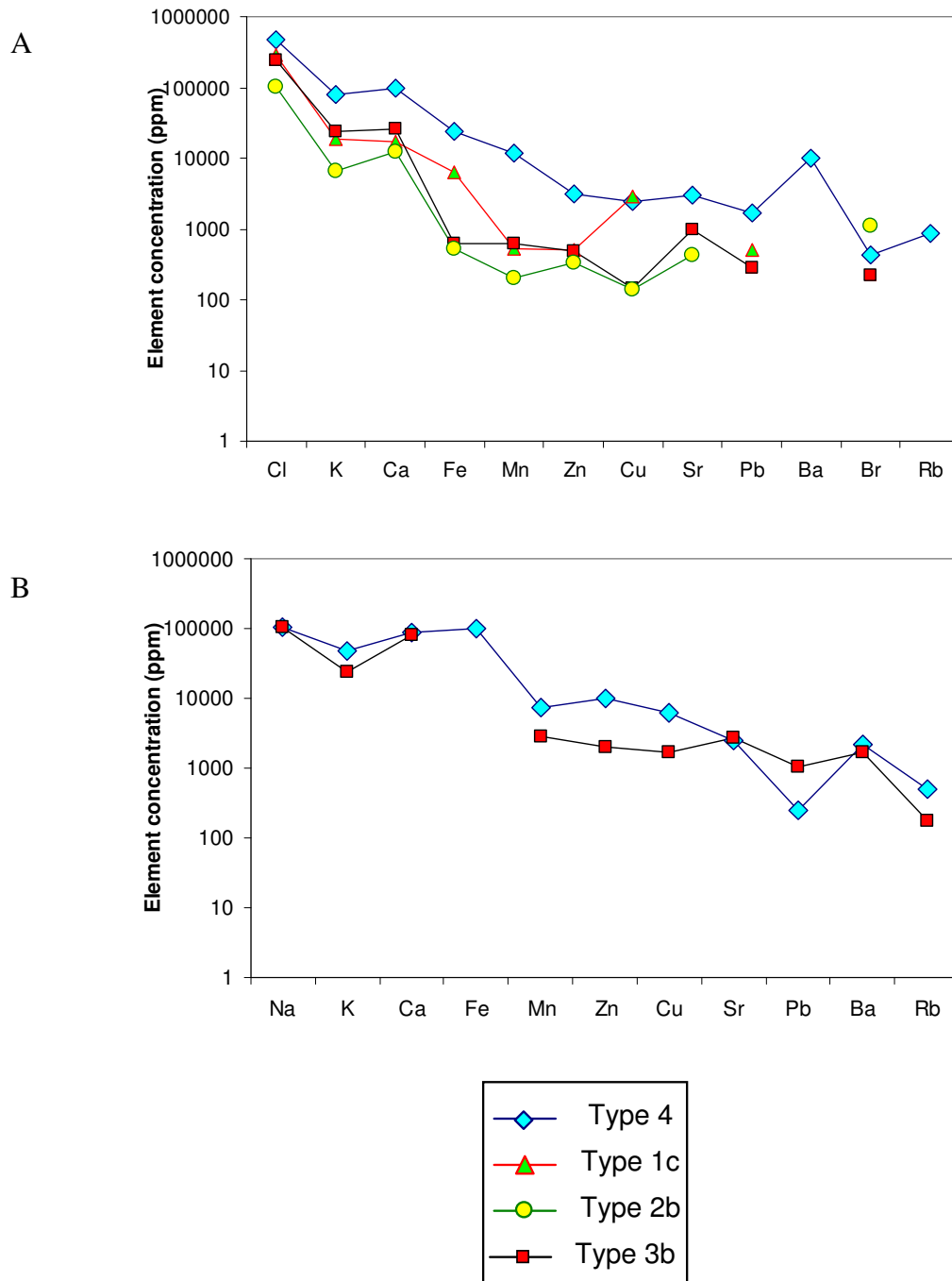
The K/Ca ratios of primary and secondary fluids are very different, in which the primary multisolid inclusions show K/Ca values mostly < 1 and secondary fluids show highly variable numbers ranging from 0.1 to 15.4 (Table 7.4 & 7.5). This may indicate variable degrees of wall rock interaction and/or different sources of secondary fluid generation (see below).

#### 7.4.2. *Halogens and fluid sources*

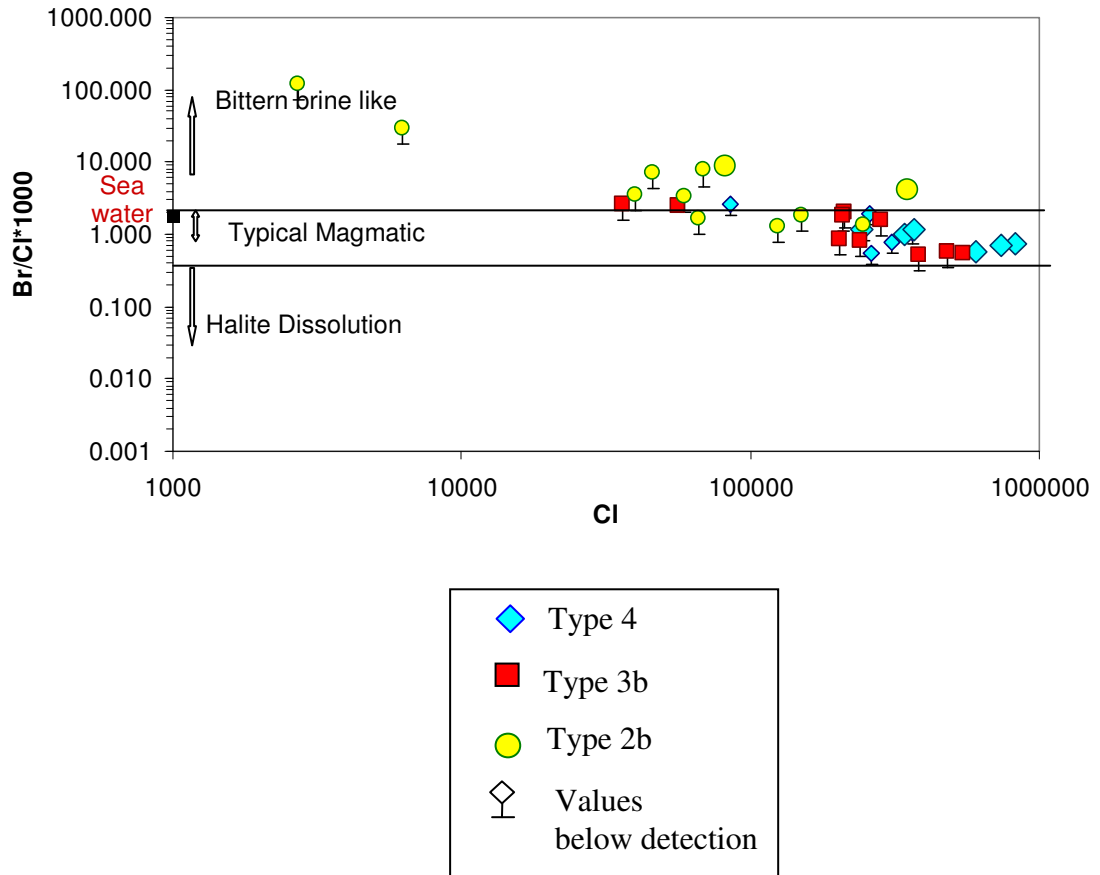
An important advantage of PIXE method is its ability to analyze halogens, especially bromine and chlorine, which are widely used as tracers for salinity source (Bohlke and Irwin 1992, Yardley et al., 1992, 2000; Fontes and Matray, 1993; Banks et al., 2000; Gleeson et al., 2000, 2003; Rusk et al., 2004; Yardley, 2005; Chiaradia et al., 2006, Kendrick et al., 2001, 2002, 2007 & 2008; Fisher and Kendrick 2008; Baker et al., 2008). Primary multisolid inclusions of brain rocks contain 280-600ppm of Br, commonly found associated with liquid phase. Their Br/Cl\*1000 values vary from 0.58 to 1.19 and these low values are broadly consistent with magmatic origin ((Williams et al., 1999; Baker et al., 2008; Williams et al., in press) Fig.7.13; Table 7.4).

Secondary fluids of L+V and L+V+S are observed in all the analyzed rocks, but their origin is not clear. Previous researchers have different opinions about secondary fluid sources. Pollard (2001) has suggested a magmatic origin for these fluids and he related them with the wide spread Na-Ca alteration of Cloncurry area based on fluid inclusion and stable isotope data; however, a bittern brine like origin is also supported by others (e.g. Bertelli, 2007-based on fluid inclusion crush leach studies). Secondary inclusions were not studied thoroughly during this research, but the field evidences, especially the presence of explosive breccia pipes and brain rocks (Chapter 2, 4 & 6) indicate that magmatic fluids may have dispersed during the batholith evolution. These high salinity fluids may have increased the rate of Na-Ca alteration by mixing with basinal/ metamorphic fluids. The halogen studies of secondary inclusions also suggest a magmatic component in the formation of high salinity secondary fluids; however the low salinity inclusions are purely non-magmatic in origin. The halogen

ratios (4.17 and 8.85 from 2 inclusions) from PIXE analyses support a bittern brine like origin for the L+V fluids and a bittern brine like and/or magmatic origin for L+V+S fluids (0.56 and 2.46 from 2 inclusions) (Fig. 7.13).



**Figure 7.12:** Average concentration of major cations in different fluid inclusion groups; **7.12A:** PIXE results; **7.12B:** LA-ICP-MS results. Both analyses show higher element enrichment in primary inclusions than secondary inclusions. The data is available in Appendix 5.2 & 5.4.



**Figure 7.13:** Halogen ratios of different fluid inclusion groups, measured by PIXE. Type 4 inclusions show primary magmatic signatures and type 2b bittern brine like compositions. Type 3b mainly falls in magmatic field; however, one value is noted at the bittern brine like field. The Br values in secondary inclusions are mostly below detection limit, and the values suggest chances of more magmatic involvement in their formation. Fluid source Br/Cl ranges from Bohlke and Irwin (1992) and Kendrick et al. (2001).

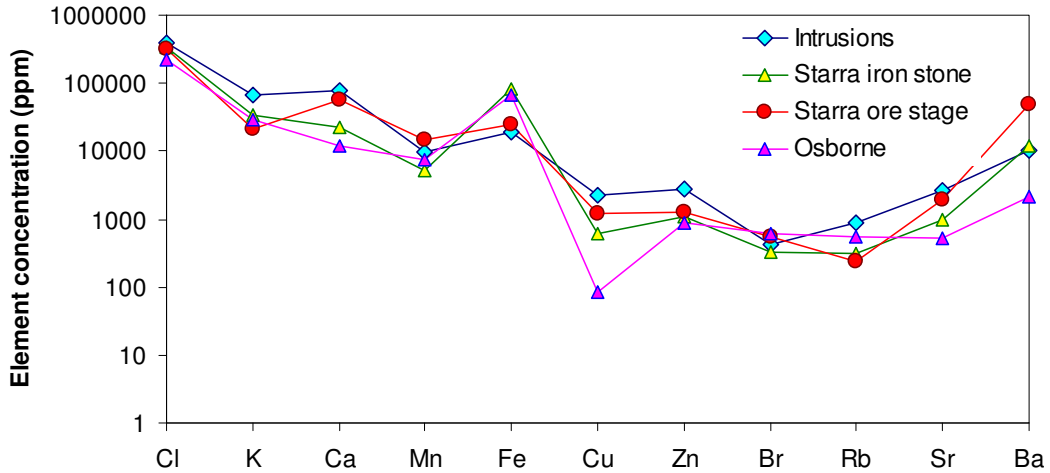
#### 7.4.3. Intrusions and ore deposits

The fluid inclusion populations in the various rock types of the SIC and MAIC appeared to be consistent except in Mt. Angelay brain rocks (Chapter 6). All the rocks including Saxby and Mt. Angelay granites contain abundant primary CO<sub>2</sub> only fluid inclusions and secondary L+V and L+V+S inclusions. However, the fluid inclusion assemblage in brain rocks is distinct with a variety of primary inclusions including

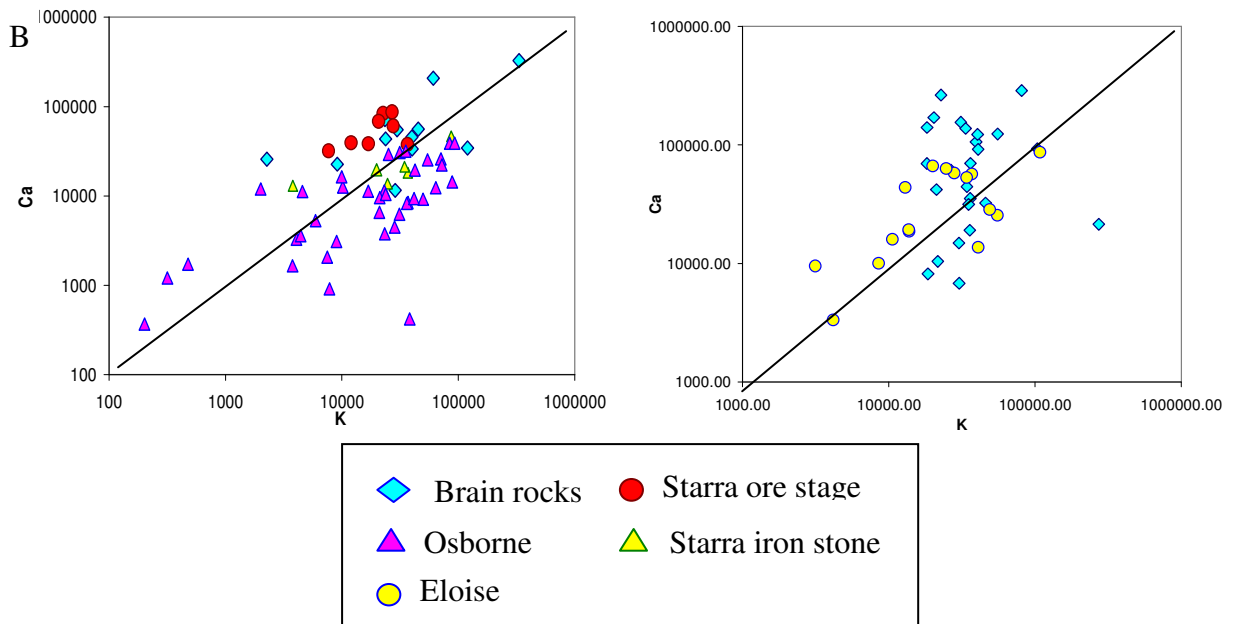
CO<sub>2</sub>-only inclusions, mixed carbonic types, L+V, L+V+S and multisolid inclusions. The coexistence of primary multisolid and carbonic inclusions is the typical fluid inclusion assemblage observed in many IOCG deposits of Cloncurry (Mark et al 1999, Williams et al 2001, Baker 1998; Fisher 2008, Baker et al 2008). The presence of multi-solid inclusions in brain rocks, which have been interpreted as magmatic (Baker et al., 2008; this study), together with their high element concentrations and consistent ratios suggest a possibility of magmatic fluids in ore deposit formation (Baker et al., 2008).

PIXE and LA-ICP-MS trace element analyses of multisolid inclusions from brain rocks show that they are highly saline with high concentrations of metals, nearly similar to some of the Cloncurry ore deposits (Eloise-Baker, 1998; Lightning Creek-Perring et al., 2000; Ernest Henry-Mark et al., 2000; Starra-Williams et al., 2001; Osborne-Fisher, 2008) (Fig.7.14, 7.15 & 7.16). However, element ratios suggest variations between fluids from intrusions and some ore deposits. PIXE K/Ca ratios of primary brain rock fluids and Starra primary fluids show similar range ( $\geq 1$ ), with considerable variations in Osborne fluids ( $\leq 1$ ) (Fig. 7.15A). The different signatures of Osborne fluids are also obvious in Fe/Cu ratios. Figure 7.15C shows a comparison of Fe/Cu PIXE data from various settings of Cloncurry (Baker, 2006) and the multisolid inclusions from Mt. Angelay brain rocks shows significant connection with Ernest Henry and Starra inclusions, but they are clearly distinct from Osborne fluids. This suggests the possible involvement of magmatic fluids in ore deposits like Ernest Henry. However, the important variations in element ratios between Osborne fluids and brain rock fluids support the origin of Osborne ore fluids from non-magmatic source.

LA-ICP-MS values of multisolids and Eloise fluids mimic the PIXE trends from brain rocks (Fig. 7.15B).



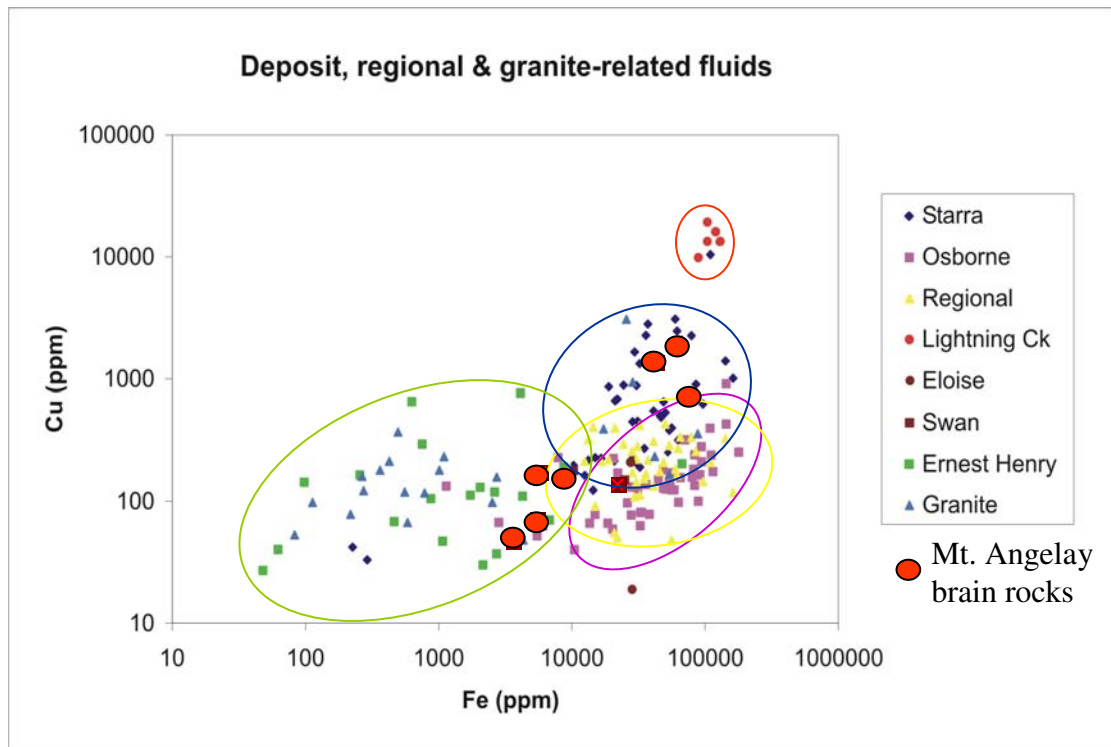
**Figure 7.14:** Average PIXE element concentrations in multisolid inclusions from Mt. Angelay brain rocks (this study), Starra (Williams et al., 2001) and Osborne (Fisher, 2008) IOCG deposits. Multisolid inclusions from the intrusions contain metal and major element concentrations similar to or higher than the deposits.



**Figure 7.15A:** PIXE K/Ca ratios in multisolid inclusions of brain rocks (this study), Starra (Williams et al., 2001) and Osborne (Fisher, 2008) IOCG deposits; **7.15B:** LA-ICP-MS K/Ca ratios in multisolid inclusions of brain rocks and Eloise (Baker,



1998) deposit. The values show similar ranges in deposits and brain rocks, but Osborne fluids show different ratios.



**Figure 7.15C:** PIXE Fe/Cu ratios in multisolid inclusions from Mt. Angelay brain rocks, various Cloncurry ore deposits and regional systems. The brain rock inclusions show similarities to Ernest Henry and Starra fluids, but are distinct to Osborne fluids. This suggests the presence of magmatic and non-magmatic fluids in Cloncurry ore genesis. Brain rock data is collected during this study and tabulated in Appendix 5.2. Data from ore deposits and regional systems are present in Baker, 2006.

Cu concentrations in primary multisolid inclusions from brain rocks show large variations ranging from values below detection to ~1.5 wt% and two primary halite bearing carbonic fluid inclusions recorded Cu concentrations of 1237ppm and 4595ppm. Baker et al., 2008 also reported high Cu concentrations of up to ~3000ppm from multisolid inclusions within Mt. Angelay brain rocks (Fig.7.16A). Much higher Cu concentrations are documented from Lightning Creek magnetite prospect in the

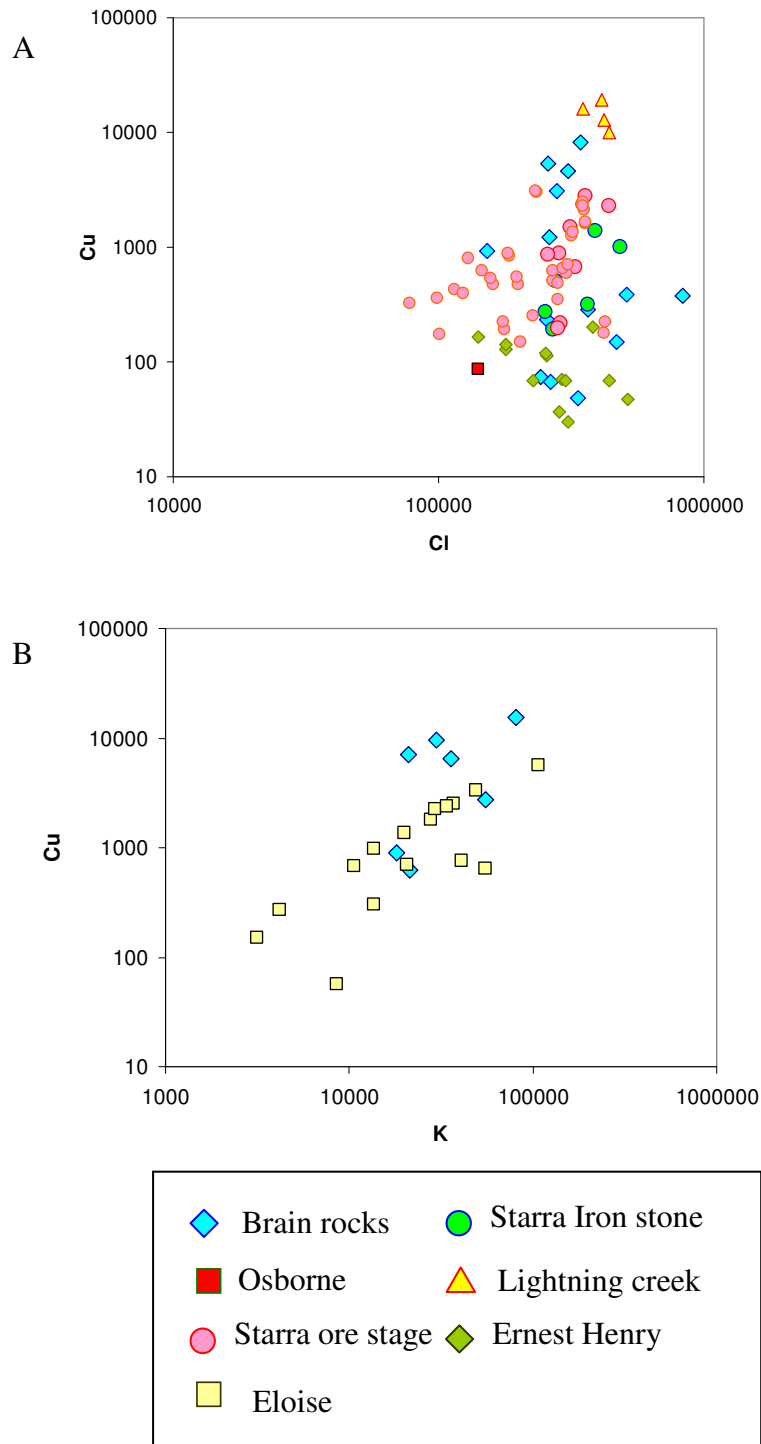
Squirrel Hills granite (Perring et al., 2000), where the multisolid fluid inclusions contain up to 2 wt% Cu (Fig.7.16A). The Cu concentrations of Ernest Henry (Mark et al., 1999), Starra (Williams et al., 2001) and Osborne (Fisher, 2008) IOCG deposits show wide variations with ore fluids recorded average Cu concentrations of 160ppm (max ~203ppm), >1000ppm (max ~2800ppm), <100ppm respectively (Fig.7.16A). Baker (1998) documented average Cu concentrations of >1000ppm from near by Eloise Cu-Au deposit with a maximum of ~5600ppm (Fig.7.16B).

#### *7.4.4. IOCG fluid sources*

Halogen ratios of multisolid inclusions from various ore deposits (Ernest Henry-Mark et al., 2000; Starra-Williams et al., 2001; Osborne-Fisher, 2008) show both magmatic and non-magmatic signatures (Fig. 7.17) and in Cloncurry district, a fluid mixing model is suggested by various researchers for the formation of individual deposits (Mark et al., 2000; Williams et al., 2001; Kendrick et al., 2007; Fisher, 2008).

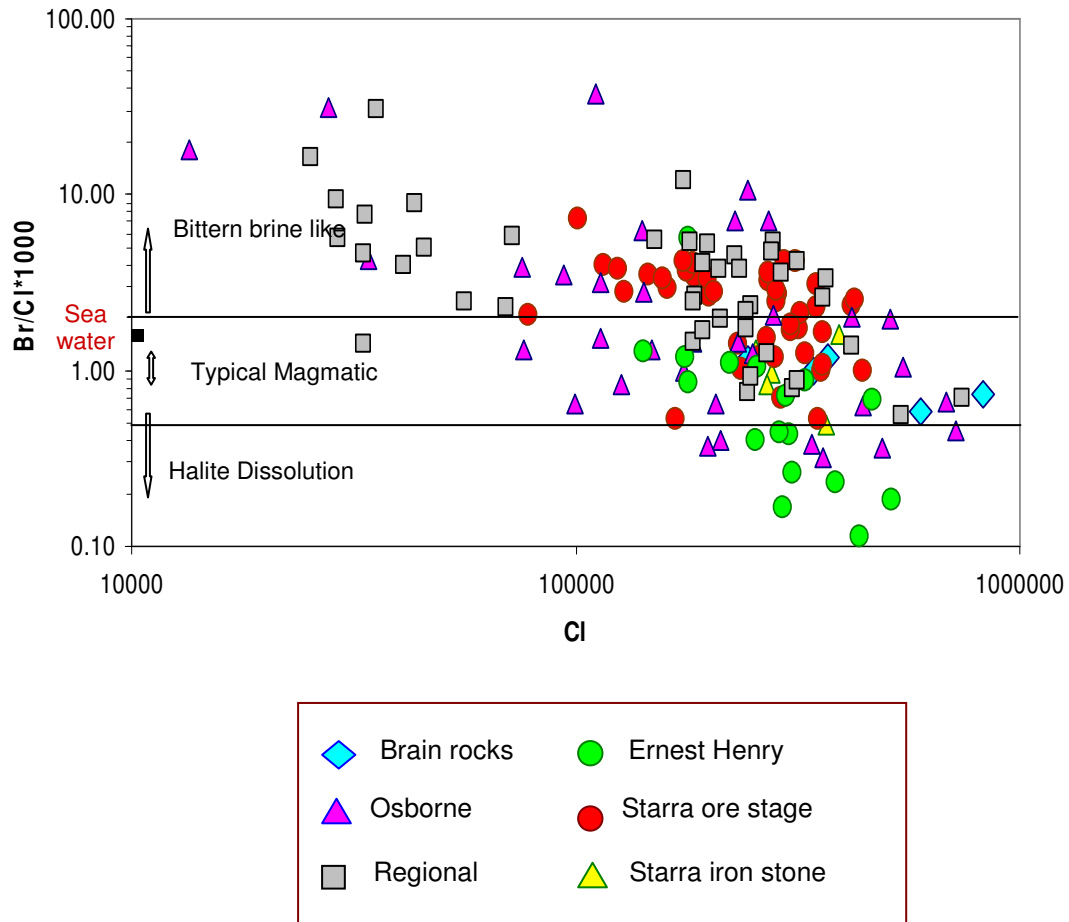
Figure 7.17 shows a comparison of halogen ratios of multisolid inclusions from Mt. Angelay brain rocks and that of different Cloncurry IOCG deposits. The Br/Cl ratios from Ernest Henry and Starra deposits fall mainly within magmatic category with a number of Ernest Henry samples show halite dissolution compositions and Starra samples, bittern brine like trends (Fig. 7.17). Osborne ore fluids span from halite dissolution to bittern brine like compositions (Fig. 7.17) and recent research suggest that mixing of those two end member fluids is responsible for the formation of this deposit (Fisher, 2008). Age relations also confirm a different origin for Osborne deposit as it formed before all other deposits and before any recognized igneous activity. However, it is suggested that an extra metal input from magmatic process

has contributed to the metal budget of large ore deposits like Ernest Henry (Fisher, 2008; Baker et al., 2008).



**Figure 7.16A:** PIXE Cu concentrations in multisolid inclusions of brain rocks (this study), Ernest Henry (Mark et al., 2000), Starra (Williams et al., 2001), Lightning Creek (Perring et al., 2000) and Osborne (Fisher, 2008) deposits; **7.16B:** LA-ICP-

*MS Cu concentrations in multisolid inclusions of brain rocks (this study) and Eloise (Baker, 1998) deposit. The Cu contents in brain rocks are nearly similar to deposits.*



**Figure 7.17:** Halogen values from multisolid inclusions of Mt. Angelay brain rocks (this study), regional fluids (compiled by Baker et al., 2008), and Ernest Henry (Mark et al., 2000), Starra (Williams et al., 2001) and Osborne (Fisher, 2008) deposits. The brain rocks show magmatic origin, Ernest Henry falls in both magmatic and halite dissolution range and Starra at the magmatic and bittern brine area. The regional fluids and Osborn fluids show large ranges.

## 7.5. Conclusions

The primary fluid inclusions studied by PIXE and LA-ICP-MS techniques are multisolid inclusions (type 4) and CO<sub>2</sub>-H<sub>2</sub>O-brine (type 1c) inclusions and both of them were observed exclusively in Mt. Angelay brain rocks. They have very high

salinities (~40 wt% Cl) and higher dissolved metal contents (up to 1.5 wt% Cu) than the secondary inclusions and their magmatic origin is confirmed by various element ratios, in particular from low Br/Cl\* 1000 ratios. The primary fluid inclusions are enriched in K, Ca, Na, Cl, Fe, Mn, Cu and Zn.

Type 2b (L+V) and type 3b (L+V+S) are the secondary fluid inclusions analysed by microanalyses, which are widely observed in all the intrusions of Cloncurry. The suite of elements identified in secondary inclusions are the same as that of primary inclusions, however the concentrations are much lower. Of the secondary fluid inclusions, type 2b inclusions contain the least element abundance. The halogen ratios suggest bittern brine like origin for the L+V fluids and bittern brine like and/or magmatic origin for L+V+S fluids. The non-magmatic signature of these inclusions was also confirmed by various element ratios.

Mt. Angelay brain rocks show a combination of multisolid inclusions and CO<sub>2</sub> bearing inclusions, which is the typical fluid inclusion assemblage observed in Cloncurry IOCG deposits. More over, the high element concentrations of primary inclusions from brain rocks together with the element ratios and halogen results suggest a possible involvement of magmatic fluids in some ore deposits. More discussions on the magmatic input in IOCG ore genesis will be explained in the following chapter and the results of various fluid inclusion analyses will be compiled with the geochemical and mineral chemical data to better understand the magma evolution of SIC and MAIC intrusions.

## Chapter 8: Discussion

### 8.1. Introduction

This chapter discusses the findings of this research, which mainly deals with the chemical and volatile evolution of the younger (1530-1500 Ma) intrusions of Cloncurry district and their possible role in IOCG ore genesis. In previous chapters, various techniques were used to identify the processes which control the magma crystallization and formation of various rock types (Chapters 2, 3 & 4). The halogens in both minerals and fluid inclusions were used to track the fluid evolution of intrusions and in particular to understand volatile release from the Saxby (SIC) and Mt. Angelay (MAIC) Igneous Complexes (Chapter 5 & 6). The chemistry of various primary and secondary fluid inclusions and their trapping conditions were estimated, with implications for their source regions and migration history (Chapter 6 & 7). Here, this study of various intrusions of the SIC and MAIC is integrated to propose new ideas regarding the connection between magmatic evolution of these complexes and IOCG ore genesis.

### 8.2. Chemistry and source of SIC and MAIC intrusions

Field studies (Chapter 2), geochemical observations (Chapter 4) and mineral halogen variations (Chapter 5) are indicative of two distinct magma sources for the mafic (to intermediate) and felsic intrusions of the SIC and MAIC (Mitchell, 1993; Pollard et al., 1998; Wyborn, 1998; Mark 1999). The extent of mafic rocks in the SIC and MAIC is small compared with the abundant felsic intrusions. At the current exposure level, the small proportion of mafic rocks is not apparently enough to have produced the voluminous felsic rocks by fractional crystallization. Although the possibility of a large volume of mafic rocks at depth cannot be completely ignored, mixing and

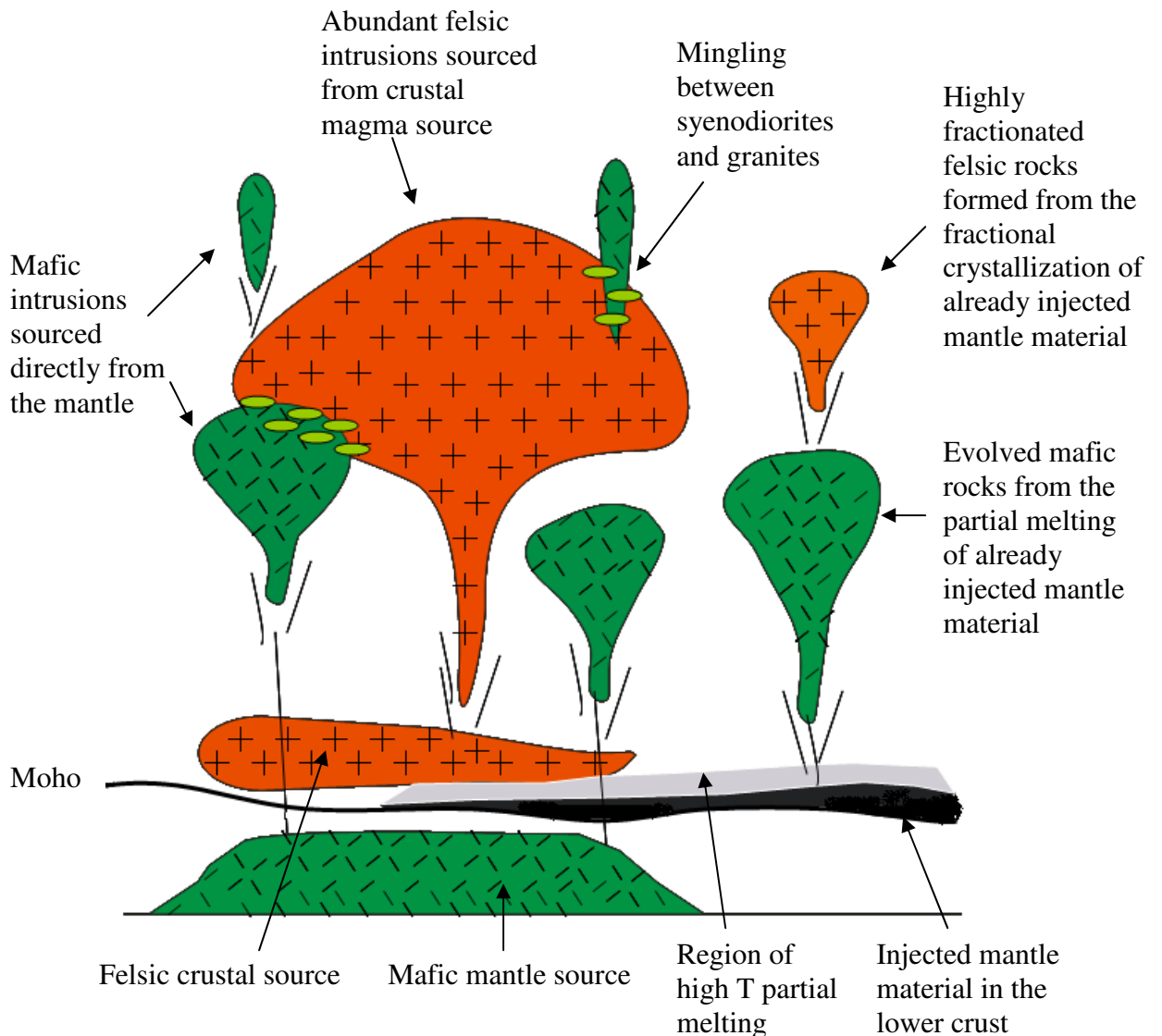
mingling between the intermediate and felsic magma in many parts of the complexes suggests coeval emplacement of mafic and felsic intrusions (Blake, 1987; Mitchell, 1993; Pollard et. al., 1998; Mark, 2001). Moreover, the Harker variation plots of elements show a continuous fractionation trend from gabbros to syenodiorite, with a prominent gap to the granites.

The rare earth and multi-element patterns also show different signatures for mafic and felsic rocks (Chapter 4). A mafic, mantle derived source, enriched in ferro-magnesian minerals, plagioclase and apatite is suggested for the generation of mafic intrusions, from which the intermediate intrusions evolved by fractional crystallization. The magma source for the granites and alkali granites was enriched in plagioclase and minor ferro-magnesian minerals without any apatite. Their REE patterns and strong negative Nb anomalies also support a crustal origin. Previous studies detected a mantle component in Cloncurry granites, however no such evidences were obtained during this study. Figure 8.1 summarizes the formation and emplacement history of various intrusions of the SIC and MAIC.

### 8.3. CO<sub>2</sub> in Cloncurry intrusions

An abundance of CO<sub>2</sub> fluid inclusions is observed in the SIC and MAIC rocks, which suggest the amount of CO<sub>2</sub> in Cloncurry granites is unusually high (Oliver et al., 2006, 2008; Bertelli, 2007), contrary to the low CO<sub>2</sub> solubility in intermediate to felsic silicate melts (Holloway, 1976). Generally the volatile concentration in magma is considered to be inherited from mantle melting; however, a few studies report high CO<sub>2</sub> contents in magmas, generated by contamination from carbonate sedimentary rocks (Lowenstern, 2001; Iacono-Marziano et al., 2007). In the Cloncurry district,

evidence for the presence of non-magmatic CO<sub>2</sub> has been suggested from noble gas analyses in Ernest Henry deposit and the devolatilization of calcite-rich, calc-silicate rocks were considered to be the preferred source (Kendrick et al., 2007). More over, the contact aureole of the SIC has abundant clinopyroxene-rich calc-silicate rocks which may have released CO<sub>2</sub>.



**Figure 8.1:** Schematic diagram for the formation of mafic and felsic intrusions in the Cloncurry. The mafic intrusions formed either from a direct mantle source or from the already injected mantle material at the lower crust. The abundant granites are derived from a crustal felsic source and small amounts of highly fractionated felsic material are also formed from the mafic magma fractionation. Magma mingling is present at the contact zones of mafic and felsic intrusions.



However, all of the veins, breccias and carbonate-bearing alteration systems lying above the intrusions show very distinctive stable isotope signals that are dominated by magmatic values, despite the large metacarbonate reservoir represented by the Corella Formation. Marshall and Oliver (2006) carefully documented the carbon, oxygen and strontium isotope ratios of calcite from many vein and ore systems in the district. They showed that veins and ores that formed at the time of the Williams Batholith were dominated by magmatic signals, conforming earlier work on specific parts of the system (Oliver et al., 2004, 2006 & 2008; Bertelli 2007).

CO<sub>2</sub> abundance and its degassing behaviour in igneous intrusions have been studied by many researchers (Holloway, 1976; Wyllie and Huang, 1976; Edwards, 1992; Blank and Brooker, 1994; Lowenstern, 2000 & 2001; Stix et. al., 2003 and references therein; Behrens et. al., 2009 and many others) and it is observed that the pressure and volatile composition have much stronger impacts on CO<sub>2</sub> solubility than temperature (Blank and Brooker, 1994; Lowenstern, 2000; Lowenstern, 2001). Previous studies suggested that ascending mafic magmas with more than 0.4 wt% CO<sub>2</sub> will exsolve CO<sub>2</sub> rich fluid or will degas CO<sub>2</sub> in shallow magma chambers due to the low CO<sub>2</sub> solubility at shallow levels (Edwards, 1992). Given the stable isotope data of regional calcite vein systems related to intrusions, the low solubility of CO<sub>2</sub> in felsic magmas (Lowenstern, 2001), and the mingling of mafic and felsic intrusions in the study area, a mafic magma source is suggested for the abundant CO<sub>2</sub> found in more felsic Cloncurry intrusions and related magmatic-hydrothermal products (breccias and brain rocks; see below).

## 8.4. Evolution of SIC and MAIC

Because the most felsic rocks have few halogen-bearing minerals, and the mafic to intermediate rocks do not contain fluid inclusions representing a component of their volatile evolution, this study has not been able to demonstrate a clear connection between the volatile evolutions of the two igneous suites (mafic to intermediate, and felsic). Felsic intrusions of the SIC and MAIC show high variations in their mineral halogen contents, which may be due to the interaction with country rocks or by degassing of felsic magma; however no clear trends are evident due to the small sample set. However, it is observed that the felsic magma has played a major role in the formation of different rock types in the complexes through mixing with mafic magma, and this may have influenced the mineral volatile compositional variability (see below).

### 8.4.1. *Saxby Igneous Complex (SIC)*

#### **8.4.1.1. Lithology and distribution**

The major intrusive rocks in the SIC include granites, gabbros and syenodiorites, however, their proportions vary widely. Granite is the most abundant rock type and individual smaller bodies of gabbros were observed at many locations. Syenodiorites are scarce in the SIC and they are exclusively observed in magma mingling zones. Magma mingling is a common feature, located at many outcrops, where granitic magma mingled and occasionally mixed with syenodioritic magma (Chapter 2). Other than these major plutonic rock types, a number of magmatic-hydrothermal breccias, pegmatites and aplites are also present in the SIC, and their occurrence and distribution are described in detail in chapter 2.

#### **8.4.1.2. Magma evolution**

In the SIC, fractional crystallization is the best explanation for the relationship between the chemistry of mafic and intermediate rocks. A decrease in the abundance of mafic minerals with increasing fractional crystallization is observed (Chapter 3) as predicted by Bowen's reaction series. The gabbros show abundant mafic minerals including clinopyroxene, amphibole and biotite, whereas the intermediate rocks have fewer total mafic minerals, and no pyroxenes. The Harker plots and multi-element (spider) diagrams confirm that these gabbros have undergone fractional crystallization and generated more fractionated syenodiorites.

Mineral halogen studies also support a fractional crystallization history for the generation of syenodiorites (Chapter 5). The systematic variations in F and Cl contents of hornblende, biotite and apatite from gabbros and syenodiorites suggest closed system halogen exchange between minerals and remaining melt within the mafic magma chamber; however this systematic variation does not reveal how and when halogens were contributed to the finally exsolved magmatic-hydrothermal fluid. With fractionation, chlorine appears to have become more incompatible, and fluorine became highly compatible, which may have influenced halogen concentration and ratios (high Cl & low F) in the final hydrothermal fluid. Unfortunately, because the most fractionated rocks (brain rocks, pegmatites) contained no mafic phases that potentially would contain halogens, the transfer of halogens from evolving magma to fluid during volatile saturation processes had to be inferred using different techniques. The albite-quartz rich pegmatites observed in the breccia pipes are considered to be

the final phases of fractional crystallization within the SIC, but their fluid chemistry and halogen enrichment was studied from the fluid inclusions (see below).

Because quartz is usually the last mineral to crystallize in a magma, fluid inclusions from magmatic quartz most likely represent some point along the path between the chemistry of the final magma and chemistry of the fluid as the magma saturates. In the SIC, the chemistry of late-stage magmatic-hydrothermal fluids was studied indirectly by Bertelli (2007) by analysis of quartz from pegmatite clasts in the discordant breccias extending outwards from the contact aureole. She reported the presence of a major CO<sub>2</sub> component in the breccia fluids. Because CO<sub>2</sub>-rich primary inclusions are also predominant in the main body of granites in the SIC (this study), this suggests that the magmatic to hydrothermal transition of the SIC was flushed or dominated by CO<sub>2</sub> with a common source.

#### **8.4.1.3. Genesis of breccia pipes**

Explosive breccias are suggestive of a rapid release of magmatic-hydrothermal fluid and an intrusion related origin is suggested for their formation, caused by fluid overpressuring due to CO<sub>2</sub> volume expansion upon exsolution (Oliver et al., 2006; Bertelli 2007). Because of the low solubility of CO<sub>2</sub> in granite, and the occurrence of widespread magma mingling and mixing zones particularly in the SIC, it appears that the CO<sub>2</sub> may ultimately have been derived from gabbro and transferred into granite prior to final crystallisation (Fig.8.4). Mafic magma generally forms at greater depths compared to felsic magma and when it ascends into shallower depths, it exsolves CO<sub>2</sub>, because of low CO<sub>2</sub> solubility at low pressures. In magmas, CO<sub>2</sub> is approximately ten times less soluble than H<sub>2</sub>O (Webster and Holloway, 1988; Fogel

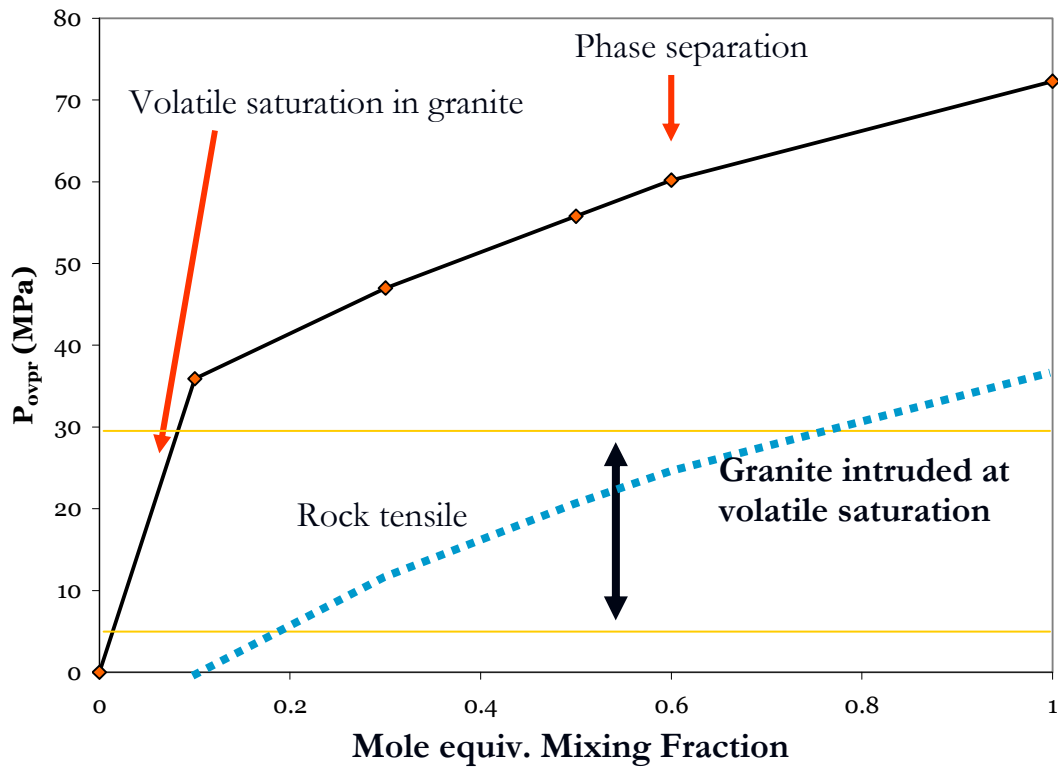
and Rutherford, 1990; Blank et al., 1993), which also supports the idea that during volatile saturation, the first fluid phase exsolved from a magma must be CO<sub>2</sub> (Nabelek and Ternes, 1997). The solubility of CO<sub>2</sub> strongly depends on the composition of the volatile phase, and presence of additional components such as H<sub>2</sub>O and NaCl decreases the CO<sub>2</sub> solubility (Lowenstern, 2000 & 2001).

In the SIC, the fractional crystallization of high volume of gabbros may have produced large quantity of volatiles and CO<sub>2</sub> at the final stages of crystallization, which resulted in volatile saturation in the mafic magma chamber. Moreover, the presence of clasts of intrusive rocks within the hydrothermal pipes, and the brecciated and lobate margins observed between the granite and breccia at its base in the carapace of the SIC, suggest that volatile saturation was reached and overpressures achieved in the SIC prior to final crystallisation of the granite (Marshall, 2003; Oliver et al., 2006; Bertelli, 2007). Furthermore, the presence of abundant CO<sub>2</sub> inclusions in granitic quartz suggest that the CO<sub>2</sub> input from the mafic magma during mingling has occurred before the complete crystallization of quartz.

In a highly saturated magma chamber rich in volatiles and CO<sub>2</sub>, degassing of CO<sub>2</sub> can take place under closed or open system conditions (Eichelberger et. al., 1986) with important consequences for the amount of over pressure, which develops within the magma chamber (Fischer et al. 1994; Stix & Layne 1996; Stix et al. 1997 & 2003). In volcanic environments, some volcanoes can be considered as leaky systems, whereas others appear to be sealed (Stix et. al., 2003). In the SIC, there is clear evidence for CO<sub>2</sub>-driven overpressures because of the explosive breccia pipes extending from the upper contact aureole, features not readily apparent in the MAIC.

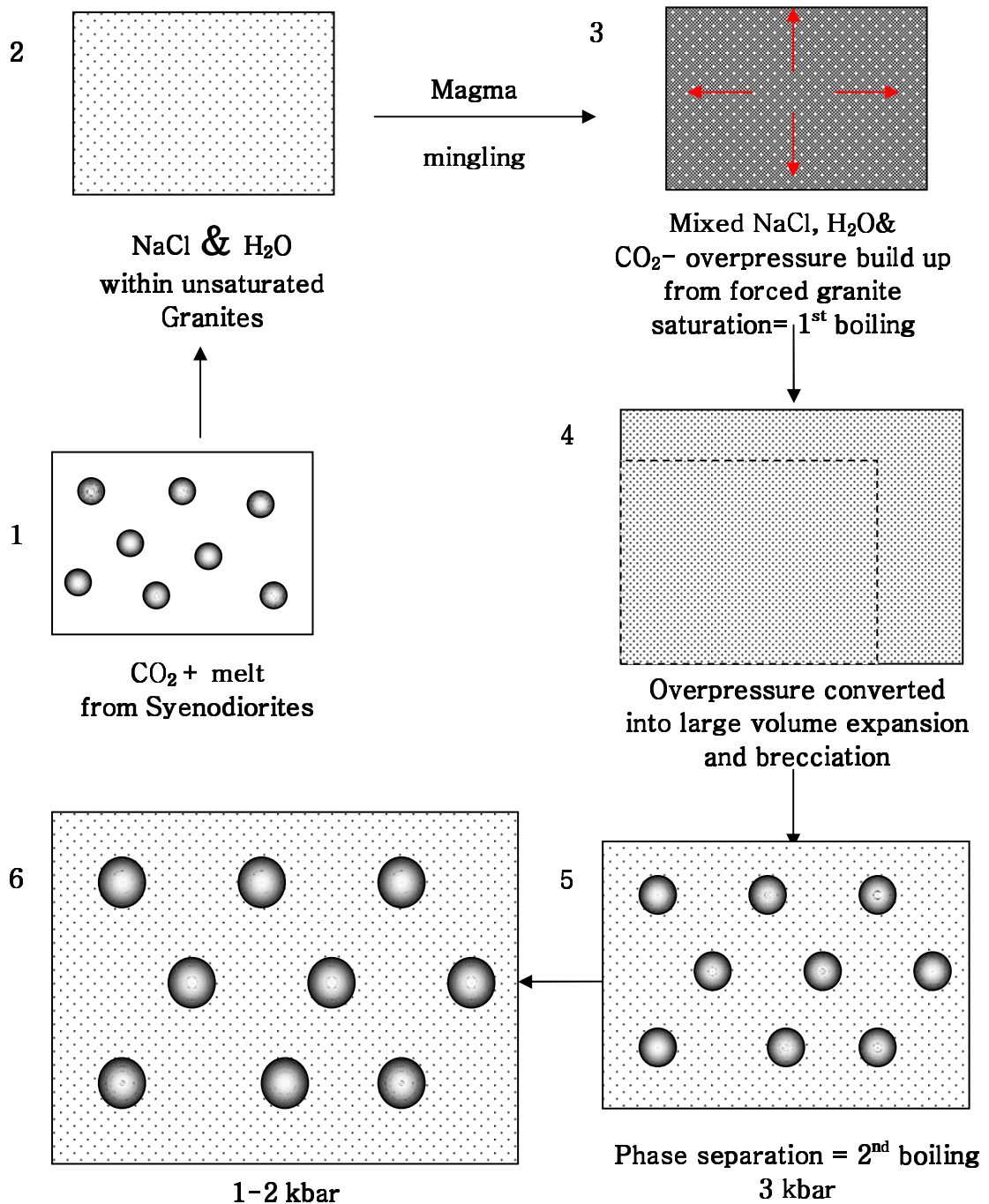
It is suggested here that the generation of very high CO<sub>2</sub> overpressures and subsequent explosive brecciation was triggered by widespread mixing and mingling between the more CO<sub>2</sub>-rich syenodioritic magma and water-rich granites, with a complex interplay between saturation states of the two magmas. In any magma chamber, fluid overpressuring can be produced by the interaction of magma and an external source of water, in which the magma may directly interact with fluid or solely act as a heat source (Sillitoe, 1985). Alternatively, high fluid pressure gradients may be generated during the emplacement and crystallization of hydrous magma in subvolcanic environments by exsolution and subsequent decompression of an aqueous fluid phase – the so-called first boiling process (H<sub>2</sub>O-saturated melt → crystals + H<sub>2</sub>O vapor), and also by later phase separation or ‘second boiling’ into gas and liquid (Burnham, 1985). In the SIC, the external fluid source (CO<sub>2</sub>+ melt) interacted with the partly saturated felsic magma (crystals + undersaturated melt) during mingling, and produced forced granite saturation and volume expansion accompanied by first boiling (Fig.8.3). Because the granite had also produced a contact aureole during emplacement, the accumulated volatiles quickly built up overpressure under the impermeable, hornfelsed carapace. This was followed by second boiling process synchronous with release of the overpressure during brecciation, probably accentuating the rapid transport of fragments outwards and upwards from the granite. At the start of the process, it is also possible that the mingling process also triggered the initial saturation of the mafic magma, by rapid cooling as it came into contact with the cooler felsic melt.

Cleverley (2008) modelled the process of over pressuring and phase separation in granitic magma due to the addition of extra CO<sub>2</sub> (Fig.8.2). Using predicted volatile concentrations in gabbroic and granitic magma at 3 MPa (3 kbar, calculated by Rubenach et al. 2008 for Saxby granite emplacement), he modelled progressive addition of CO<sub>2</sub> into both saturated and unsaturated granitic magma at constant total system volume (Fig. 8.2). For a granite that has already reached volatile saturation, the model suggests only a gradual increase in potential overpressure consistent with the extra volume of CO<sub>2</sub> added. The point at which the two-phase field for the system H<sub>2</sub>O-CO<sub>2</sub>-NaCl was reached (second boiling) did not produce a great change in volume. However, for the model in which granite was previously unsaturated, even a small amount of CO<sub>2</sub> addition produces a huge volume expansion due to rapid forcing of granite volatile saturation, followed by CO<sub>2</sub> phase separation and rock failure. The fluid inclusion pressure estimates within albite-quartz rich rocks from the breccia pipes (Bertelli, 2007) suggest an overpressure of about 1.2 kbar (P= 4.2 kbar) followed by a pressure drop of at least 1.5 kbar upon pressure release during brecciation, and similar large pressure changes were recorded by Oliver et al. (2006) for a location away from the intrusions.



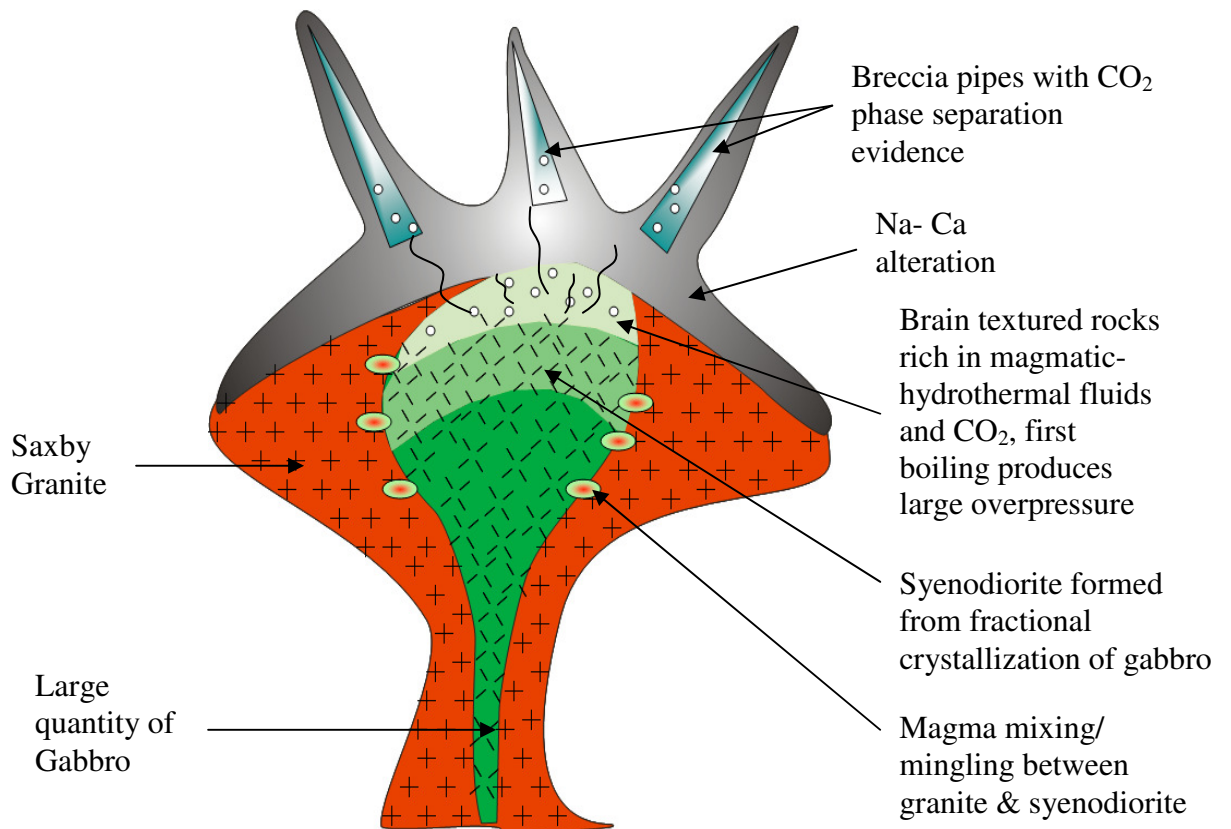
**Figure 8.2:** Calculated overpressures within a granitic magma chamber for the modelled volatile mixing and volume changes (Cleverley, 2008)). The black, left curve represents the overpressuring for an initially volatile under-saturated granite and the right, blue curve represents an initially volatile saturated granite. Depending on the initial saturation state of granite, the  $\text{CO}_2$  addition during magma mixing can produce overpressuring and phase separation in the granitic magma chamber at different stages. A small  $\text{CO}_2$  addition can create huge overpressuring in an unsaturated granite followed by phase separation and volume decrease, and in saturated granite, the overpressuring is a slow process.





**Figure 8.3:** Recommended model for the formation of Saxby breccias. Box 1 represents the syenodioritic magma enriched in CO<sub>2</sub> and other volatiles, and that intruded into the granitic magma chamber (box 2), which is initially unsaturated. The mingling of those two produces forced granite saturation accompanied by 1<sup>st</sup> boiling, which builds up huge overpressure in the granite magma chamber (box 3). This overpressure is later converted into volume expansion and rock failure that cause explosive brecciation. The 2<sup>nd</sup> boiling occurs with phase separation at the time of

*brecciation (box 5), with modest volume change at fixed pressure; however this would produce a volume increase if this occurs at pressures lower than 3 kbars due to volume expansion of the CO<sub>2</sub> (Cleverley, 2008).*



**Figure 8.4:** *Magma evolution and volatile release of the SIC. The fractional crystallization of large number of gabbros produced syenodiorites, which mixed/ mingled with Saxby granite at many locations. This mingling process triggered the CO<sub>2</sub> phase separation in the magma chamber and formation of explosive breccia pipes with evidence of phase separation. Vast Na-Ca alteration zones are observed in the SIC, which may have related to the magmatic-hydrothermal fluid release through the breccia pipes.*

The role of both felsic and mafic magma in the breccia pipe formation is also evident from the presence of granites, gabbros and albite-quartz rich rocks as breccia clasts. The granite fragments within the breccia pipes represent the partly solidified nature of felsic magma during brecciation. The albite-quartz rich rocks are thought to be formed from the residual hydrothermal fluid after the fractional crystallization of mafic minerals in the magma chamber. Evidence for their formation at saturated conditions during the final stages of magma evolution is obtained from the MAIC (see below). The gabbroic intrusions point to physical incorporation of both granite and gabbro in the top of the magma chamber during and after magma saturation and release of overpressured fluids.

#### *8.4.2. Mt. Angelay Igneous Complex (MAIC)*

##### **8.4.2.1. Lithology and distribution**

Like the SIC, granites, gabbros and syenodiorites are the major intrusive rocks present in the MAIC. The most notable differences between the SIC and MAIC are the relative scarcity of gabbros and zones of magma mixing and mingling in the MAIC. Discordant magmatic hydrothermal breccias were also not found anywhere within or around the MAIC. However, the MAIC contains a prominent body of albite-quartz-rich rocks showing distinctive textures (“brain rocks”), which are absent in the SIC (except for small occurrences in breccia pipe clasts).

##### **8.4.2.2. Magma evolution**

Even though the quantity of gabbros varies between the complexes, the gabbro compositions from both the SIC and MAIC are very similar, suggesting the same parental source. Like the SIC, fractional crystallization of mafic magma is the major

controlling factor in the chemistry of Mt. Angelay intermediate intrusions, and compared to the SIC, the most fractionated syenodiorites are observed in the MAIC. In the MAIC, the mineral proportions and bulk rock geochemistry also suggest that more evolved magmas were derived from gabbroic parents by fractional crystallisation. Similar to the SIC, mineral halogen contents in the MAIC also confirm similar magma types and fractionation history in both the complexes, with incompatible behaviour of Cl and compatible behaviour of F with ongoing fractional crystallization.

In the MAIC, the last products of fractional crystallization are represented by brain rocks (Fig.8.6). The only analytical evidence for the hydrothermal connection between parent (syenodiorite) magma and brain rock is the fluid inclusion assemblages in the latter, which shows magmatic halogen signatures and evidence for phase separation of magma fluid (Chapter 6 & 7). Furthermore, the typical occurrence of these rocks within syenodiorites, surrounded by gabbros, suggests their formation from the final magmatic fluids at the end of a continuous fractional crystallization process (Chapter 2; also see Mark and Foster, 2000; Perring et al., 2001). Mark and Foster (2000) regarded these rocks as representative of a magmatic-hydrothermal transition, which is supported by the results from this study.

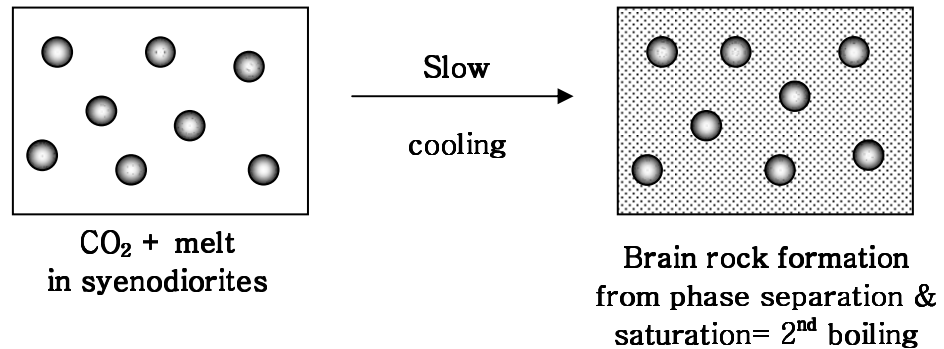
#### **8.4.2.3. Genesis of brain rocks**

Figure 8.6 illustrates the formation of Mt. Angelay brain rocks. Due to the absence of a high volume of mafic rocks in the MAIC, the potential CO<sub>2</sub> contribution from mafic magmas into the surrounding granites was less than in the SIC. Even though some evidence of magma mixing was reported from the MAIC (Tolman, 1998), the smaller

volume of observed gabbro suggests that the released CO<sub>2</sub> may not have been enough to produce huge volume expansion like that observed in the SIC. Alternatively, the magma mixing/mingling may have happened at a different stage of magma evolution in the MAIC, perhaps due to different volatile concentrations or emplacement levels. In the SIC, the mingling has occurred at the final stages of mafic magma fractionation and the mafic magma became fully saturated at that stage; but in the MAIC, the presence of brain rocks without any direct evidence of magma mingling or granite association at the outcrop level suggest that the magma mingling in the MAIC may have happened at the earlier stages or elsewhere, or the mafic magma may not have reached CO<sub>2</sub> saturation.

In any case, it is clear from the brain rock appearance that they represent the pooling of magmatic fluids as a result of fractional crystallization and the typical textures of brain rocks show their formation in saturated conditions. Formation of complex textures like brain textures require higher degrees of under-cooling ( $\Delta T$ ) and cooling rates ( $\Delta T/\Delta t$ ), much larger than those needed to produce euhedral crystals (Lofgren and Donaldson, 1975; Fenn, 1977; Swanson and Fenn, 1986; London, 1992). Under-cooling conditions may normally be linked to the rapid cooling following the emplacement of a magmatic body (Drever and Johnston, 1957; Lofgren and Donaldson, 1975) or by increasing the liquidus temperature of a water-bearing magma above its actual temperature. The increase in liquidus temperature can either be caused by a change in the water content or by a change in the confining pressure (Jahns and Tuttle, 1963; Jahns and Burnham, 1969; Lofgren and Donaldson, 1975). In the MAIC, separation of CO<sub>2</sub> fluid phase may have created water saturated conditions

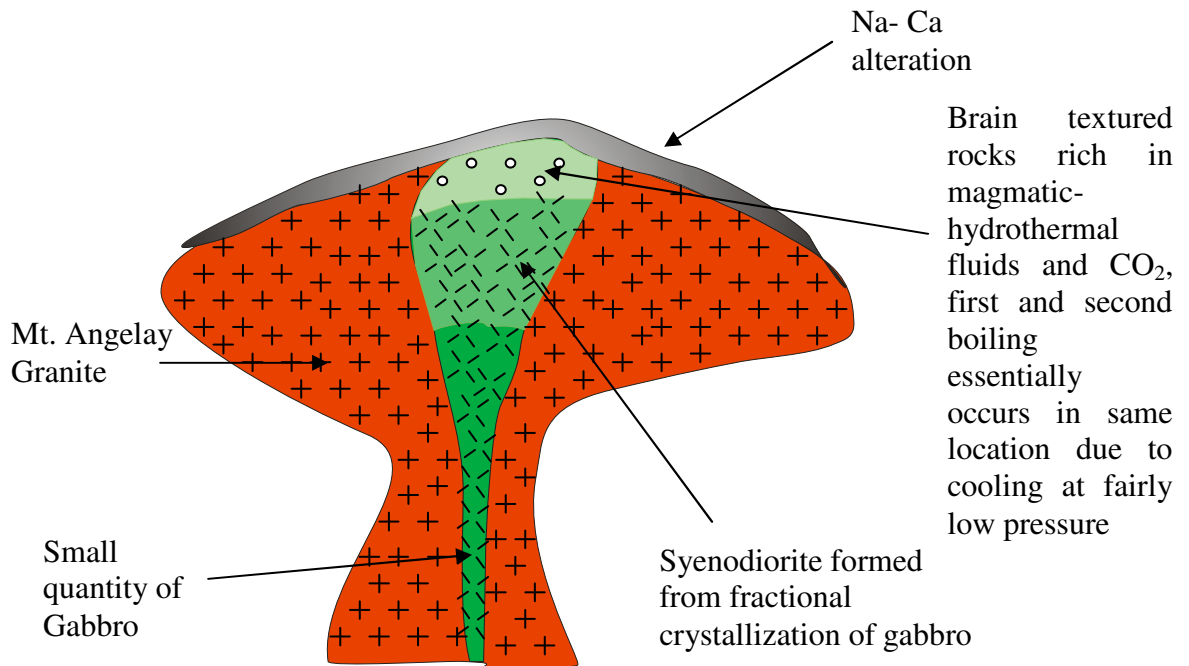
in the magma chamber, which raised the liquidus temperature of the magma (Nabelek and Ternes, 1997) and created under cooling conditions (Fig.8.5).



**Figure 8.5:** Recommended model for the formation of Mt. Angelay brain rocks. The crystallization of syenodiorites in the MAIC occurs without any direct involvement of granites. The separation of small volume of CO<sub>2</sub> rich volatile phase during the final stages of crystallization creates saturated conditions followed by phase separation (2<sup>nd</sup> boiling) and brain rock formation.

In Mt. Angelay brain rocks, the coexistence of CO<sub>2</sub> bearing inclusions and multisolid inclusions suggest unmixing of a single magmatic-hydrothermal fluid (CO<sub>2</sub>-H<sub>2</sub>O-NaCl-other salts), as suggested elsewhere around the Williams Batholith (Perring et al., 2000; Pollard, 2001; Fu et al., 2003; Mustard et al., 2004). However, the absence of explosive brecciation suggests that the fluid volumes or CO<sub>2</sub>-content within that fluid may have been smaller than in the SIC. This is consistent with the proposed abundance of CO<sub>2</sub> in the SIC due to larger volumes of gabbroic melt. However, the phase separation itself (first boiling) may have created second boiling conditions in the melt and generated water saturated conditions, which cause the crystallization of brain textures within them. A similar process is suggested for the brain textures

within granitic inclusions in the Saxby breccia pipes, even though the multisolid inclusions are absent in breccia pipes and may have been lost during the brecciation process or simply not recorded.



**Figure 8.6:** *Lithology, magma evolution and volatile release in the MAIC. In the MAIC, only small proportions of gabbros are observed, which underwent fractional crystallization and produced syenodiorites. The absence of magma mixing/mingling evidence between syenodiorites and granites suggest that in the MAIC, volatile saturation was triggered gently in syenodioritic magma after considerable fractionation and cooling, with formation of brain rocks. The Na-Ca altered zones in and around the magmatic-hydrothermal location may have caused from the release of separated fluids from the brain rocks.*

### 8.5. Chemistry of magmatic fluids

In a magma chamber, the chemistry of magmatic fluids is primarily related to the composition of the magma source region; however, a number of processes including fractional crystallization, magma mixing, coupled substitution reactions in minerals,

magma degassing and wall rock interaction may influence the fluid chemistry during the upward journey of magma. During this research, the halogen chemistry of mafic intrusions was partly studied from the fluorine and chlorine contents of igneous minerals and the results suggest a possible enrichment of Cl and depletion of F in the final melt (Chapter 5). This is inferred from the halogen chemistry of minerals as they show an increase in F and decrease in Cl with fractional crystallization.

Fluid inclusions were used as the major medium to understand the chemistry of hydrothermal fluids in the SIC and MAIC, and a CO<sub>2</sub> rich fluid phase was commonly observed in both the complexes. Gabbros and granites were analysed but no inclusions were found in gabbros due to the absence of quartz, which is the only mineral in which the inclusions were observed. However, the fluid composition of mafic magma was inferred from fluid inclusions within Mt. Angelay brain rocks and those from the Saxby breccia pipes as they represent the most fractionated equivalents of mafic magma (see previous section).

A variety of primary fluid inclusions was observed in the Mt. Angelay brain rocks and in the brain textured rocks observed within the Saxby breccia pipes. The common primary inclusion types present in both these rocks include CO<sub>2</sub>-only, CO<sub>2</sub>-H<sub>2</sub>O mixed and CO<sub>2</sub>-H<sub>2</sub>O-brine inclusions. The major difference between the fluid chemistry of brain rocks and breccias is the presence of multisolid inclusions in Mt. Angelay brain rocks, which are absent in Saxby breccias. The element populations in multisolid inclusions from Mt. Angelay brain rocks make them distinct as they contain two to eight solid phases and very high element concentrations (Cu up to 1.5 wt%), nearly similar to some of the Cloncurry ore deposits (Chapter 7). If the brain



textures in both the complexes were products of the fractional crystallization process, then the fluid inclusions in those rocks would ideally represent similar chemistry. However, based on the CO<sub>2</sub> trapping pressure estimations, the Saxby breccias record much higher pressure ranges (2.7 – 4.2 kbar) than Mt. Angelay brain rocks (1.3-2.1 kbar), and at such higher pressures, the multisolid inclusions may not have been generated as fluid immiscibility was suppressed (Fig.6.13, Chapter 6). Immiscibility most likely did occur as the breccias released pressure on the upwards path – perhaps represented by calcite (CO<sub>2</sub>) and albite (NaCl) breccia matrix, but this may have occurred after all quartz crystallized, so the information was not trapped in fluid inclusions.

The only CO<sub>2</sub>-bearing inclusions studied by micro-analytical techniques were CO<sub>2</sub>-H<sub>2</sub>O -brine inclusions. They show high concentrations of several elements particularly K, Ca and Cl, nearly similar to some multisolid inclusions. The Fe, Mn and Zn concentrations of CO<sub>2</sub>-H<sub>2</sub>O -brine inclusions commonly range from a few hundred to thousand ppm and the Cu values range up to 4595 ppm (Chapter 7).

## 8.6. Origin of sodic-calcic alteration

Widespread sodic-calcic alteration is considered as a distinguishing feature of IOCG terrains. Different models suggest that the intrusions either act as heat sources which induce hydrothermal fluid circulation of surrounding formation waters (Carten, 1986; Dilles et al., 1995; Barton and Johnson, 1996) or the intrusions directly provided saline fluids as they crystallized (Hildebrand, 1986; Menard, 1995; Perring et al. 2000; Pollard, 2001).

Many previous studies in the Cloncurry area suggested that the fluids released from the felsic intrusions were responsible for the widespread sodic-calcic alteration in the district (Pollard, 2001; Mark et. al., 2004a; Oliver et. al., 2004). In this study, abundant secondary fluid inclusions of L+V+S were observed in the SIC and MAIC rocks, which are cross-cut by less abundant L+V inclusions. Alteration studies were not an objective of this research; however, the observations during this study support the presence of magmatic, halite dissolution and bittern brine like fluids in the secondary fluid inclusions (Chapter 7). The PIXE halogen ratios suggest a halite dissolution and/or magmatic origin ( $\text{Br/Cl}^* 1000 = 0.56\text{-}2.46$ ) for the secondary L+V+S inclusions. The L+V inclusions show high  $\text{Br/Cl}^* 1000$  values ranging from 4.17 to 8.85, which correspond to bittern brine like sources.

The volatile saturated conditions inferred for the formation of Mt. Angelay brain rocks, and the presence of single veins with both magmatic and hydrothermal minerals (Mark and Foster, 2000) support a model for release of saline fluids during magma crystallization. In addition, the observations of sodic-calcic altered granite carapaces (SIC) in conjunction with discordant, explosive breccia pipes provides direct evidence that these magmas released saline,  $\text{CO}_2$ -bearing fluids into the surrounding country rocks. The magmatic signatures observed in the secondary L+V+S inclusions may indicate these represent the final magmatic fluids.

### 8.7. Relationship between Cloncurry intrusions and IOCG deposits

In Proterozoic IOCG terrains, the close spatial and temporal association of granitoid intrusion and widespread sodic-calcic alteration is common, and the intrusions and alteration features are contemporaneous with mineralization. In the Cloncurry district,

many ore deposits (e.g. Ernest Henry) were formed broadly synchronous with the younger phases of Williams and Naraku Batholiths (Perkins & Wyborn, 1996) and the intrusions are postulated as the possible sources for ore fluids (Rotherham *et al.* 1996; Perkins & Wyborn 1996; Twyerould, 1997; Meyer, 1988; Pollard, 2000; Perring *et al.*, 2000; Sillitoe, 2003; Mark *et al.*, 2004a; Pollard, 2006). In other districts, circulation of regional fluids has been proposed (Barton and Johnson, 1996; Haynes., 2000), and at least some ore bodies in the Cloncurry District did not form the same time as the Williams Batholith (e.g. Osborne, Oliver *et al.*, 2008). Some isotopic and fluid inclusion studies from the Cloncurry District suggest mixing of magmatic and evaporitic fluids (Williams *et al.*, 2001; Kendrick *et al.*, 2007; Baker *et al.*, 2008). However, even though the Corella Formation represents a former evaporate sequence, it had undergone greenschist to amphibolite-facies metamorphism at the time of emplacement of the Williams Batholith, so the possible origin of evaporitic fluids at ~ 1530 Ma is not clear as all salt in the Corella Formation would have been contained in scapolite (and fluid inclusions) at this stage, not as readily available halite (e.g. Oliver *et al.*, 2008).

During this research, various bulk and micro-analytical studies were used to reveal the intrusion characteristics and the results were compared with the available ore deposit data. This study infers that the younger Cloncurry intrusions (1530 to 1500 Ma) made an an important contribution of metals, CO<sub>2</sub> (as carbonates) and/or sulfur to some of the ore deposits. However, it is proposed that the mafic magma may have played more important roles in ore formation than felsic magma, even though most previous studies refer to an igneous mass and fluid contribution mostly from 'granite'. Evidence for mantle signatures in deposits were derived from halogen

studies in the Ernest Henry deposit (Kendrick et al., 2007) and some researchers also suggested the involvement of mafic rocks in ore formation (Wyborn et al., 1987; Pollard et al., 1998; Mark, 1999).

In this thesis, the suggestion of mafic magma involvement in ore genesis is primarily based on three aspects:

1. The continuous partitioning of chlorine and metals into magma fluid phase with fractional crystallization and the potential of Cl bearing fluids to carry ore components;
2. The presence of high salinity and metal concentrations in primary multisolid inclusions from brain rocks evolved from mafic rocks, which show similarity in fluid inclusion types and element association to some of the Cloncurry IOCG deposits; and
3. The occurrence of some Cloncurry ore deposits in milled hydrothermal breccias (e.g. Ernest Henry, Mark et al., 2006) and the role of mafic magma in explosive brecciation emanating from some igneous complexes (e.g. Oliver et al., 2006).

The geochemistry of mafic and felsic intrusions show that the highest metal concentrations are associated with mafic intrusions. Elements such as Fe, Cu, Zn and Ni broadly decrease with fractional crystallization (Chapter 4), suggesting continuous metal enrichment in the residual fluid phase. Similarly, the whole rock chlorine contents show progressive depletion from gabbros to syenodiorites, consistent with mineral halogen analyses, although the extent to which this reflects subsequent accumulation of metals into hydrothermal fluids is poorly understood due to lack of partitioning studies between all three of magma, fluid and minerals for key elements

(e.g. Cu, Cl, F). The potential of Cl to transport ore components and form ore deposits is demonstrated by many workers (Crerar & Barnes 1976; Mutschler et al. 1981; Boudreau et al. 1986; Brookins 1989; Coulson et al 2001) and it is suggested that in the SIC and MAIC, the final magmatic-hydrothermal fluid produced by the continuous fractionation of mafic intrusions was enriched in chlorine and metals.

The element enrichment of mafic magma was also determined from the PIXE and LA-ICP-MS analyses of primary multisolid fluid inclusions from Mt. Angelay brain rocks. The multisolid inclusions were generated by saturation in the magma after protracted fractional crystallization from mafic to intermediate compositions, and the separation of fluids during the final phases of magma crystallization. These inclusions are commonly observed associated with primary CO<sub>2</sub>-only inclusions and their magmatic origin is again confirmed from PIXE halogen studies.

The coexistence of primary multisolid and carbonic inclusions is the typical fluid inclusion assemblage observed in many Cloncurry IOCG deposits (Baker 1998; Mark et al 1999, Williams et al 2001; Fisher, 2008). The similarities between the fluid inclusion assemblages observed in brain rocks and ore deposits suggest that the mafic intrusions may have provided fluids and metals to the deposits. Both PIXE and LA-ICP-MS analyses detected high Cu, Fe, Mn and Zn concentrations in primary magmatic fluids with high K/Ca ratios, apparently similar to Starra, Ernest Henry and Eloise deposits (Baker 1998; Mark et al., 1999; Perring et al., 2000; Williams et al., 2001; Baker et al., 2008). Cu concentrations in brain rock multisolid inclusions show values ranging up to 1.5 wt%, suggesting the high Cu potential of mafic magma (Chapter 7).

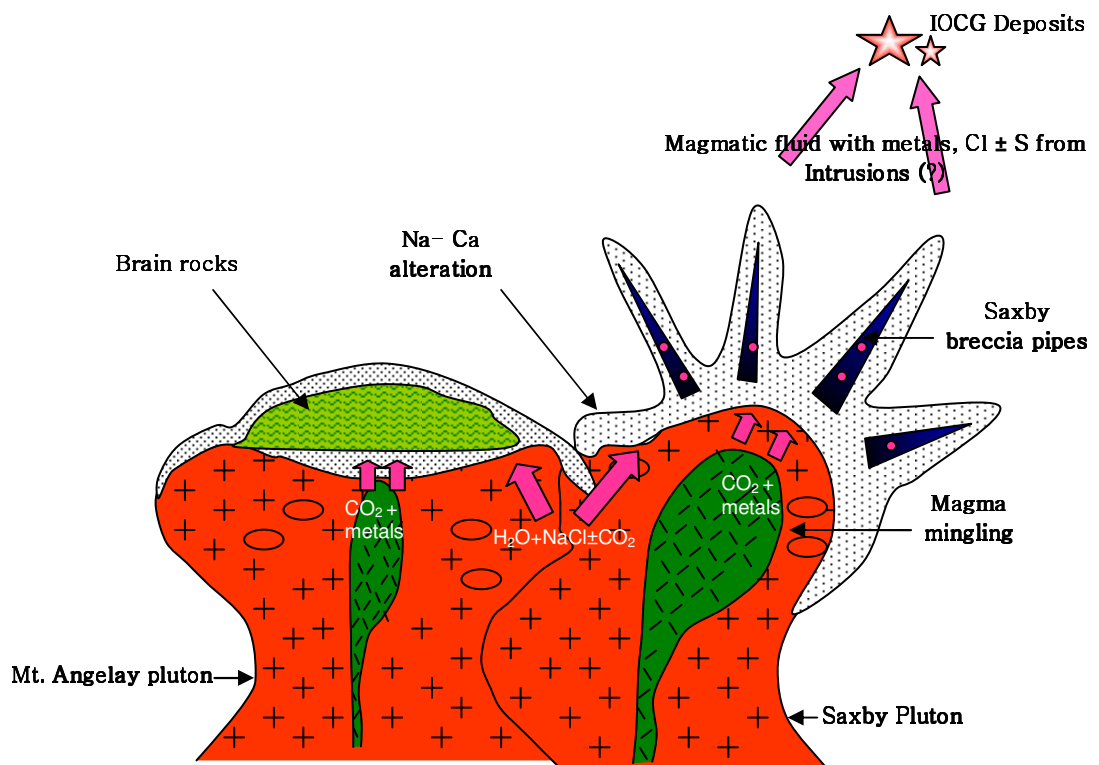
In Cloncurry, the intrusions do not host any ore deposits; however, minor occurrences of Fe-rich (Lightning Creek) and small Cu and Ag deposits (Wimberu Granite) are hosted within some of them.

Figure 8.6 shows the proposed model for the formation of Cloncurry IOCG deposits. Breccias of the SIC indicate rapid emplacement of fluidized breccias and the emission and dispersion of high T, magmatic Cl and metal rich fluids into structural gaps. However, in the MAIC, the brain textures were observed as isolated, small scale features at the top of many intermediate plutons with multisolid inclusions in them. These inclusions represent the remnants of unmixed, Cl and metal rich magmatic fluids, which did not explode as pipes due to the low CO<sub>2</sub> contribution from mafic magma and from the inferred low amounts of magma mingling.

In the Cloncurry district, Ernest Henry is the main ore deposit hosted in breccias of the same timing as the Williams Batholith. The observations during this study suggest that the breccias in this deposit may represent a giant version of the Saxby breccia pipes. The occurrence of ores in breccia host rocks of large Australian IOCG deposits like Olympic Dam and Ernest Henry supports the connection between breccia formation and ore genesis, which may have occurred over very short geological time periods due to the rapid breccia emplacement.

The transportation of ore fluids from intrusions to the deposits is also important as some IOCG deposits (e.g. Starra) occur several kilometres away from the intrusions without any direct evidences of breccia involvement in their generation. The

observations during this research suggest that the metal rich, highly saline fluids from the Williams and Naraku intrusions, which dispersed in an eruptive manner with the formation of breccia pipes, might have channelled through structural sites (e.g. Cloncurry fault) to ideal locations (where a change in P-T conditions and/or mixing of fluids and/or wall rock interaction) to precipitate the ores.



**Figure 8.7:** Saxby and Mt. Angelay intrusions and their connection with distal ore deposits. The magmatic fluids released from the intrusions channelled through structural sites and precipitated at suitable conditions to form ore deposits.

However, the fluid inclusion halogen studies indicate that magmatic fluids were not the only source of IOCG components. The halogen studies on the origin of various IOCG deposits in the Cloncurry district are consistent with the fluid mixing model suggested by various researchers on individual deposits (Williams et al., 2001; Mark

et al., 2006; Kendrick et al., 2007). The comparison of halogen ratios on multisolid fluid inclusions from the ore deposits and brain rocks show that the larger deposits like Ernest Henry have a predominant magmatic component. The observation that the most magmatic signals are found in the deposit hosted in the most obviously brecciated rocks, along with the breccia pipes emanating from the SIC, also suggests a strong link between Ernest Henry and the processes of fluid release from the SIC. It is suggested that the magmatic fluids have mixed with non magmatic fluids of various origins and a combination of fluid mixing, P-T variations and wall rock interaction may have resulted in ore deposition.



## Chapter 9: Conclusions and Recommendations

### 9.1. Conclusions

#### *9.1.1. Key findings on the chemistry & evolution of the SIC and MAIC*

##### ➤ **Rock types and distribution**

- The major intrusive rocks in the SIC and MAIC are granites, gabbros and syenodiorites; however, they show significant variations in abundance between the complexes.
- The SIC contains abundant granites and a few isolated outcrops of gabbros. The syenodiorites in the SIC occur only at the magma mixing/mingling locations, where the granitic magma mingles and apparently mixes with syenodioritic magma.
- The MAIC includes abundant granites and large number of syenodiorites with very rare gabbros.
- Explosive breccia pipes are typical features of the SIC, which cross cut the country rocks and granites, and are suggestive of a magmatic-hydrothermal origin. The pipes contain albite-quartz rich rocks and fragments of granites, gabbros and country rocks.
- Brain rocks are observed in the MAIC, which are albite-quartz rich rocks with complex magmatic-hydrothermal transition textures.
- Pegmatites, aplites and quartz veins are the late igneous phases in the SIC and MAIC.

➤ **Mineralogy of intrusions**

- The granites from the SIC and MAIC dominantly consist of medium to coarse grains of microcline, quartz and plagioclase with minor biotite and hornblende. These are coarse to medium grained rocks and they show myrmekite, perthite and graphic textures.
- The gabbros show fine to coarse and equigranular to porphyritic varieties, with ophitic and subophitic inter granular textures. The gabbro mineralogy is dominated by hornblende, biotite and plagioclase with local occurrences of quartz, K-feldspars and clinopyroxenes. Gabbros that occur close to the country rocks contain secondary amphiboles in the form of edenite. Apatite and magnetite are common accessory minerals in gabbros.
- Syenodiorites mainly contain hornblende, biotite and plagioclases with small percentages of clinopyroxenes, feldspars and quartz. Apatite, magnetite and titanite are present as accessory with presence of zoned zircons typically in the Mt. Angelay samples. Recrystallization textures are observed in syenodiorites from the SIC and they contain quartz, hornblende and augite with triple junction boundaries. The igneous clinopyroxene observed in the MAIC are typically diopside.

➤ **Geochemistry and magma sources**

- The intrusive rocks of the SIC and MAIC are I-type, rich in potassium with Y-undepleted and Sr-depleted signatures, and some of them show A-type geochemical affinities.

- Various studies during this research are indicative of two different magma sources for the felsic and mafic-intermediate rocks of the SIC and MAIC. The key evidences for the different magma sources are:-
  - Mixing and mingling of felsic and intermediate magma at many locations in the SIC suggests coeval emplacement of mafic and felsic intrusions.
  - The prominent gap in the geochemical diagrams (Harker plots) that separates the linear trend of gabbros to syenodiorites from cluster of granites.
  - The REE and multi-element patterns suggest a mafic, mantle derived source, enriched in ferro-magnesian minerals, plagioclase and apatite for the generation of mafic intrusions, from which the intermediate intrusions evolved by fractional crystallization. The strong negative anomalies in the multi-element patterns of felsic rocks are suggestive of a crustal origin. They show different REE patterns to gabbros and syenodiorites with evidences for the presence of plagioclase and minor ferro-magnesian minerals at the source region without any apatite.
  - Fluorine and chlorine trends of gabbros and syenodiorites are continuous, suggesting a fractional crystallization origin, but that of granites are very different.

➤ **Volatile evolution and release of fluids**

- The fluorine and chlorine contents of biotite, hornblende and apatite from the gabbros and syenodiorites in the SIC and MAIC were studied to understand the evolution of magmatic volatiles, but those of granites could not be analysed due

to the rare occurrence of these minerals in granites. Halogen and geochemical trends suggest that the evolution of mafic magma from gabbros to syenodiorites was consistent being fractional crystallization as the main process that controls the chemistry of intrusions.

- With fractional crystallization, the fluorine content of biotite, hornblende and apatite increases and chlorine content decreases. This would alternatively suggest a consistent enrichment of chlorine and loss of fluorine in the magma fluid phase during mineral crystallization, which may end up in a final magmatic fluid, which has more chlorine compared to fluorine. Uncertainties in halogen partitioning behaviour between coexisting magma, minerals and fluid at the point of volatile saturation are a major limit to how far this interpretation can be extended.
- The release of magmatic fluids is different in the SIC and MAIC, in which the SIC shows a violent, eruptive type fluid release that generated discordant breccia pipes and in MAIC the fluid release is represented by brain rocks, which show pooling of magmatic-hydrothermal fluids in a more silent manner.
- The typical, distinct magma fluid release and formation of different rock types in the SIC and MAIC is primarily caused by two reasons:-
  - *Variable CO<sub>2</sub> release*-CO<sub>2</sub> is considered to be one of the major causes for the formation of Saxby breccia pipes. In the Saxby and Mt. Angelay granites, abundant CO<sub>2</sub> is noticed from the fluid inclusion studies. Due to the low CO<sub>2</sub> solubility in felsic magmas (Holloway, 1976), the occurrence of magma mingling process in the area and the magmatic stable isotope signals observed in the previous studies (Marshall et al.,

2006), the high CO<sub>2</sub> in Cloncurry intrusions most likely was sourced from mafic magmas in the complex. This study has noticed the presence of different proportions of mafic rocks in the complexes and it is suggested that the abundant mafic rocks in the SIC compared to the MAIC have introduced higher volumes of CO<sub>2</sub> in the Saxby felsic magma chamber.

- *Magma mixing/mingling*-Magma mixing/mingling, particularly observed in the SIC, is considered to be another major reason that introduced CO<sub>2</sub> in to the unsaturated Saxby granites and caused forced volatile saturation in it, which created overpressuring and large volume expansion in the felsic magma chamber and produced breccia pipes in an eruptive way. Fluid immiscibility is also reported from the breccia pipes (Bertelli, 2007), which happened due to the sudden pressure release at the time of brecciation. However, in the MAIC, absence of magma mingling and possible shallower levels of emplacement allowed continued fractional crystallization of mafic to intermediate magma and at some point, either a temperature drop, or the contribution of small volumes of CO<sub>2</sub> (sourced from the less abundant mafic rocks at the MAIC) caused saturation conditions in the evolved intermediate melt and generated magmatic-hydrothermal rocks with brain textures.

➤ **Causes of Na-Ca alteration**

- Widespread Na-Ca alteration is common in the SIC and MAIC; however this aspect was not thoroughly studied during this research. However, from the

magmatic-hydrothermal fluid release histories of the SIC and MAIC, it is suggested that these fluids may have altered the intrusion carapaces and surrounding country rocks by mixing with regional fluids. The fluid inclusion PIXE halogen studies also suggest the presence of magmatic fluids in the generation of high salinity secondary fluid inclusions. However, halite dissolution and bittern brine like components are also observed in the inclusions, so the presence of magmatic and non-magmatic fluids is suggested in the generation of alteration assemblages.

*9.1.2. Key findings on the connection between intrusions and ore deposits*

The observations during this study suggest a magmatic, specifically a mafic magma involvement in the formation of some Cloncurry IOCG ore deposits, which are listed below:-

- ***Similarities in the fluid inclusion assemblages of Mt. Angelay brain rocks and ore deposits, which are rich in CO<sub>2</sub> and multisolid inclusions***-Mt. Angelay brain rocks are considered to be the final products of fractional crystallization of mafic magma. The multisolid inclusions observed in these rocks are confirmed as primary and formed by fluid release from magma crystallization, based on petrographic observations and PIXE halogen signatures. However, the primary fluid inclusions in granites are CO<sub>2</sub> only inclusions, which is different from the fluid inclusion assemblage of the ore deposits. On the other hand, Ernest Henry has a large calcite matrix component to the ore matrix, which may represent the CO<sub>2</sub> released from the intrusions below.

- *High concentration of elements and metals in the multisolid inclusions of brain rocks, similar to ore deposits.*
- *The continuous partitioning of chlorine and metals into magma fluid phase with fractional crystallization and the potential of Cl bearing fluids to carry ore components.*
- *Breccia pipes and role of mafic magma in their formation*-Ernest Henry IOCG deposit was formed within a magmatic-hydrothermal breccia similar to that in the SIC. This also suggests the chance of mafic magma (and its ore element budget) involvement in Ernest Henry breccia formation. Alternatively, the magmatic fluids released through the breccia pipes may have transported some (magmatic) ore components through structural sites (faults) and formed ore deposits by mixing with non-magmatic and evaporitic fluids at ideal conditions.

## 9.2. Recommendations for future work

- The study on fluid sources during this research used PIXE halogen analyses, which only general distinguish magmatic and non-magmatic components in fluid inclusions using Br/Cl ratios in particular. He and Ne isotopes could be used to identify mantle derived components in these fluid inclusions, and a study on the various fluid inclusions in Mt. Angelay brain rocks and various ore deposits will provide a good understanding of the exact sources of ore fluids.
- In this study, the source of high CO<sub>2</sub> contents of Cloncurry intrusions is inferred as mafic magmas from various field observations and previous works. A detailed study to model the CO<sub>2</sub> budget of mafic intrusions and the mechanisms of CO<sub>2</sub> injection in the Cloncurry district will give a better idea on the formation of breccia pipes and

which can also be used to better understand the ore deposition conditions at magmatic-hydrothermal breccia hosted deposits.

- This study suggests an important role for mafic magmas in ore deposit formation; however, the isotopic studies to understand the sources of mafic intrusions are outside the scope of this study. A geochemical and isotopic study to compare various mafic intrusions in the Cloncurry district would be very useful to understand the role of potential of mafic magmas in ore generation.